RSC Advances

REVIEW

Published on 08 July 2026

Cite this: DOI: 10.1039/d6ra02856j

Bismuth-based metal–organic materials: lone-pair-driven structures, single-crystal-mediated synthetic strategies, and emerging applications

Aliyu M. Hamisu,[a] Esraa Al-Adawi,[b] Iman Al-Yahyai,[b] Sanobar Naaz,[b] Laila Al-Maqbali,[b] Haider A. J. Al Lawati [b] and Arief C. Wibowo *[b]

Bismuth-based metal–organic materials (MOMs), including coordination polymers and metal–organic frameworks (MOFs), are gaining momentum in terms of their popularity in the field of materials chemistry. Their biocompatibility and potentially abundant and tunable structures and properties are some of their eye-catching features. The $6s^2$ lone pair of Bi^{3+} gives rise to both hemidirected and holodirected coordination environments, which strongly influence the dimensionality, topology, crystallinity, and porosity. This review summarizes the recent progress in Bi-based MOMs with emphasis on their synthetic methods, structural modification strategies, modulating agents, solvent and reaction effects, and the relationship between coordination geometry and framework formation. The review surveys representative dense and porous Bi-MOMs, inclusive of their oxide and sulfide derivatives, highlighting emerging applications in catalysis, sensing, photoluminescence, gas adsorption/separation, energy storage, and biomedicine. Finally, current challenges and future opportunities are outlined, foreseeing Bi-based MOMs with holodirected building units to follow in the footsteps of reticular chemistry-guided transition-metal MOFs. Further developments are required to improve strategies to directly synthesize hemi- and holo-directed building units, balance the degree of connectivity and net's interpenetration, thereby controlling porosity and stability, and develop greener routes for high-quality crystalline materials.

Received 5th April 2026
Accepted 29th May 2026

DOI: 10.1039/d6ra02856j

rsc.li/rsc-advances

1. Introduction

The realm of materials chemistry and crystal engineering has, in the past few decades, garnered unprecedented attention from academics and industries. In particular, a subclass of metal–organic materials (MOMs), known as metal–organic coordination polymers (MOCPs), is gaining attention owing to their potential to combine the distinctive properties of the individual building blocks into one material for obtaining the target functionality for a particular application. MOCPs are polymeric materials built from a synergistic self-assembly of metal moieties and organic ligands coordinatively extending into one-, two-, or three-dimensional structures.[1] An emerging second generation of MOCPs that are characterized by highly ordered, three-dimensional extended structures featuring permanent porosity with astonishing structure-driven functionalities is popularly known as metal–organic frameworks (MOFs), a term coined by Prof. Omar Yaghi,[2,3] or otherwise porous coordination polymer (PCP), as proposed by Prof. Susumu Kitagawa, for which they share the 2025 Nobel Prize in Chemistry, together with Prof. Richard Robson.[4,5] Historically, Yaghi and O'Keeffe developed the so-called reticular chemistry,[6,7] in which the use of a secondary building unit (SBU) is exploited as molecular polyhedra for the construction of unlimited numbers of well-designed MOFs with intriguing structures (network topologies), diverse sizes (pore size, surface area, and resulting particle size), as well as outstanding physical and chemical properties (multifunctional MOFs). In a similar way, the concept of nodes and spacers was introduced by A. F. Wells[8–10] to form regular and somewhat predictable network topologies, such as cubic diamondoid, hexagonal diamondoid, square grid, and octahedral network topologies.

1.1 Uniqueness of bismuth MOMs

Unfortunately, the aforesaid concepts are predominantly observed in the transition-metal (TM) and late-TM-based MOCPs that form regular SBUs. This is not the case, however, for heavy, lone-pair-containing groups 14 and 15 cations, such as Sb^{3+}, Sn^{2+}, Pb^{2+} or Bi^{3+}, possessing an ns^2 lone pair of electrons that can be stereochemically active or inactive. Their network topologies are not as regular and predictable as those of the commonly used TM and late-TM MOCPs, such as Cu^{2+}

[a]Department of Polymer Chemistry and Technology, Kaunas University of Technology, K. Barsausko 59, LT-51423 Kaunas, Lithuania
[b]Department of Chemistry, College of Sciences, Sultan Qaboos University, Muscat PC 123, Oman. E-mail: a.wibowo@squ.edu.om

and Zn^{2+}, respectively. However, several materials of technological interest are observed to have asymmetric electronic densities[11] typically associated with the main group metals owing to the presence of a nonbonding lone electron pair.

Among the heavy lone pair electron-containing cations, Bi^{3+} is the heaviest nonradioactive, abundant and inexpensive element. It was found to have not only fascinating applications but also unusual and complex structural topology.[12] Bi^{3+} and its compounds are gaining prominence in multivarious applications, especially in the medical field, owing to their biomedical safety and biocompatibility. They are considered noncarcinogenic and nontoxic, attributable to their low solubility in neutral aqueous solution.[13–15] For decades, bismuth-based compounds have been used as antimicrobial and antitumor agents and for the treatment of ulcers and dyspepsia.[16] Recently, CAU-7, a Bi^{3+}-based MOF, has been successfully applied as an efficient drug-delivery system owing to its high biocompatibility and low accumulation in cells.[17]

Although the network topology in bismuth-based MOCPs is commonly irregular and unpredictable, both the hemidirected and holodirected geometries produce the corresponding primary building unit (PBU) or SBU, which may translate into the respective library of MOCPs. Interestingly, the holodirected coordination geometry forms less distorted and relatively regular polyhedra, with stereochemically inactive lone electron pairs, similar to those of the rich TM-based ones. Notable examples include the formation of Bi carboxylate-based Kagomé Lattice,[18] paddle wheel,[19–22] and ionic layer compounds.[23] Carboxylate-based bismuth complexes and extended networks have demonstrated rich and intriguing structural diversity and have drawn substantial attention recently, and we observe an increased interest in this less explored area, in particular, Bi^{3+} carboxylate-based compounds, showing potentially rich structural chemistry comparable to those of TM-based compounds. Further details on the effects of Bi^{3+} lone pairs can be found in Section 2.4.

Based on the generalized concept of the hard-soft acid-base (HSAB) principle, Bi^{3+} is classified as a borderline acid, with an affinity for ligands containing either or both hard donor atoms (*e.g.* O-atom) and soft donor atoms (*e.g.* N-atom).[24–26] Thus, one can envisage Bi^{3+} forming a stable structure with aromatic and heteroaromatic polycarboxylic acid based ligands.[27,28] Although most of the discussion will deal with bismuth compounds containing O- and N-donor atoms originating from aromatic and heterocyclic carboxylate-based ligands, occasional references will also be presented on chalcogen-, halogen- or mixed-donors where appropriate (see the ligand definitions in Tables 1 and 2). Based on the current reports pertaining to bismuth coordination compounds, a large number of these compounds form dimeric units or extended 1D chains/ladders, 2D layers/sheets or 3D polymeric compounds.[29–31] However, examples of monomeric or discrete multinuclear bismuth-based compounds are also common.[32–35]

A previous review by Whitmire and co-workers examined the general binding motifs of numerous Bi^{3+}-carboxylates, focusing on amino-polycarboxylate and polyamino-carboxylate ligands.[31] The readers are also referred to a comprehensive structural review on thio- and seleno-coordination compounds of bismuth halides,[36] more specifically on porous Bi-based MOFs and more generally on MOCPs based on $6s^2$ Pb^{2+} and Bi^{3+}.[37] Moreover, Kai Wang and co-workers systematically reviewed the synthesis and modification strategies of Bi-based MOFs, highlighting advances in their catalytic performance and photocatalytic applications.[38] Yankun *et al.* also reviewed photocatalytic applications of Bi-based MOFs.[39] Qing *et al.* and Wenjing *et al.* published review papers in 2021 and 2022, respectively, also focusing on photocatalytic applications.[40,41] There is no review, to our knowledge, that delineates the role of modulating agents in Bi MOM syntheses and the resulting structural porosity and crystallinity in connection to bismuth's hemidirected and holodirected coordination environments, which strongly influence dimensionality, topology, crystallinity, and porosity. With such a unique structural feature, a clear structure *vs.* property relationship needs to be revealed, covering emerging applications, such as sensing, photoluminescence, gas adsorption/separation, energy storage, and biomedicine. In this review, we highlight the Bi-based MOMs synthetic methods and strategies, *i.e.*, the use of modulating agents in combination with (various) synthetic methods, with the optimum recipe of selected solvent(s), starting materials ratio, and reaction conditions (mainly time and temperature control and indirect control of pressure) to produce high-quality single crystals. We further describe the effects of lone pair stereochemical activity, which form two types of PBU (hemi- or holo-directed), leading to their corresponding structure and dimensionality (from 0D discrete to 3D extended MOCPs and MOFs). A brief section on Bi MOM derivatives (oxide and sulfide) geared toward applications is also included. We conclude with the potential, emerging applications, and a summary, inclusive of critical insights and analysis, coupled with remaining questions to be addressed in future work.

2. Synthesis strategies

2.1 Synthetic methods

The partial solubility of bismuth precursors, such as $Bi(NO_3)_3 \cdot 5H_2O$ or Bi_2O_3, in aqueous or common organic solvents is one of the stumbling blocks in the synthesis of bismuth-based MOMs. To ease the solubility issues, chemists resort to using other synthetic routes, including solvo/hydrothermal, branch tube, or reflux methods. A new reaction pathway that is not accessible in ambient water due to the high energy barrier, lack of solubility, and/or low molecular diffusion rate, becomes accessible at hydro- (or in a similar manner, solvo-) thermal conditions, mainly due to the high temperature and autogenous pressure.[42] It is known that hydrothermal *vs.* conventional aqueous reactions can favor the formation of kinetic over thermodynamic products, giving MOMs with many interesting structure types.[43] These facts motivate us and others to explore the potential of hydro- or solvo-thermal methods to access bismuth-based MOMs. We have successfully isolated several bismuth carboxylate-based coordination polymers using a combination of hydro- or solvo-thermal methods with or without the addition of a base.[18,23,44–58] Other mono- and hetero-

Table 1 Summary of the Bi-based hemidirected MOMs, based on their ad hoc name, corresponding formula, synthetic conditions, structures, surface area and stability

Ad hoc name	Formula	Synthesis conditions	Modulating agent	PBU type	Dimension	Topology	Surface area and stability	Ref.
L-MOF-401	K[Bi(tcbpe)(DMF)$_2$]·xDMF; (tcbpe = 4′,4‴,4⁗,4⁗′–(ethene-1,1,2,2-tetrayl)tetrakis(([1,1′-biphenyl]-4-carboxylate)))	Solvothermal, DMF, 100 °C, and 3 days	Benzoic acid	9-Coordinated hemidirected distorted polyhedra BiO_9	3D	**sql**	Thermally stable up to 170 °C	100
—	[Bi(1,4-BDC)$_2$]·(DMA)(DMF); (BDC = 1,4-benzenedicarboxylate)	Solvothermal, DMF, 100 °C, and 3 days	LiOH H_2O	8-Coordinated hemidirected distorted polyhedra BiO_8	3D	**dia**	Thermally stable up to 450 °C	90
Bi-BDC	[NaBi(1,4-BDC)$_2$(DMF)$_2$] (BDC = 1,4-benzenedicarboxylate)	Solvothermal, DMF, 100 °C, and 3 days	NaOH	8-Coordinated and hemidirected polyhedra BiO_8	3D	—	—	59
—	Bi(pydc)(Hpydc)(H_2O) (pydc = pyridine-2,5-dicarboxylate)	Hydrothermal, H_2O, 140 °C, and 3 days	4,4′-Bipyridine/KOH	7-Coordinated and hemidirected polyhedra BiO_5N_2 with single Bi-center	3D	—	Water unstable	23
CAU-33	[$Bi_4(O)_2(OH)_2(H_2TCPB)(TCPB)(H_2O)_2$]·$x$$H_2O$ (TCPB = 1,2,4,5-tetrakis-(4-carboxyphenyl)benzene)	Solvothermal, DMF/toluene, 80–140 °C, and 12 h	—	5-Coordinated hemidirected geometry BiO_5, dimeric oxo rod	3D	—	Thermally stable up to 400 °C, chemically stable in DMF, acetone, ethanol, THF, ethyl acetate, and water between pH 3–11, and surface area is 450 m^2 g^{-1}	123
CAU-35	[$Bi_2(O)(OH)(TATB)$]·H_2O (H_3TATB = triazine-2,4,6-triyl-tribenzoic acid)	Solvothermal, H_2O/DMF, ramp to 120 °C, in 12 h, maintained for 36 h and cooled to r.t. in 60 h	—	Linear IBU, 7-coordinated, and hemidirected polyhedra BiO_7	3D	—	Surface area 77 m^2 g^{-1}	122
SU-100	Bi(BPT)·2MeOH (BPT = biphenyl-3,4′,5-tricarboxylate)	Solvothermal, MeOH, 160 °C, and 1 h	—	Bi_2O_{12} dimer with 7-coordinated hemidirected polyhedra BiO_7	3D	**esg**	Thermally stable up to 350 °C and surface area is 473 m^2 g^{-1}	104
SU-101	$Bi_2O(H_2O)_2(C_{14}H_2O_8)$·$2H_2O$ ($C_{14}H_2O_8$ = ellagate)	Solution chemistry, H_2O, R.T, and 48 h	Acetic acid	6-Coordinated hemidirected polyhedra, BiO_6 rods	3D	**svd**	Thermally stable up to 250 °C and the surface area is 412 m^2 g^{-1}	47
—	Bi_2O_2(HBPT) (BPT = biphenyl-3,4′,5-tricarboxylate)	Hydrothermal, H_2O, 160 °C, 1 h, and stirring	—	6- and 7-coordinated Bi dimer ($Bi(1)O_6$/$Bi(2)O_7$) with hemidirected polyhedra	3D	—	—	104
—	Bi_2(HBPT)$_3$(H_2O)$_3$·H_3BPT (BPT = biphenyl-3,4′,5-tricarboxylaye)	Hydrothermal, H_2O, 120 °C, and 7 days	—	6- and 7-coordinated Bi-hemidirected $Bi(1)O_6$/$Bi(2)O_7$ polyhedra	3D	**tfz-d**	—	104
—	Bi_6O_4(H_2TPTC)$_5$ (H_2TPTC = [1,1′:4′,1″] terphenyl-3,3″,5,5″-tetracarboxylic acid)	Hydrothermal, H_2O, 160 °C, 1 h, and stirring	—	6- and 7-coordinated Bi-hemidirected polyhedra Bi(1)O_6/Bi(2)O_7 of Bi hexamer	3D	—	—	104
NOTT-220 (α/β)	[$C_4N_2H_{10}$][Bi($C_7H_4NO_4$)($C_7H_3NO_4$)]·H_2O ($C_4N_2H_{10}$ = piperazine and $C_7H_3NO_4$ = pyridine-2,6-dicarboxylate)	Hydrothermal, H_2O, 180 °C, and 3 days	Piperazine	7-Coordinated hemidirected and distorted polyhedra BiO_5N_2-based layer	1D	—	Thermally stable up to 380 °C	93
—	[Bi(μ_2-OH)($C_7H_3NO_4$)] (3,4-pyridinedicarboxylate)	Hydrothermal, H_2O, 150 °C, and 3 days	Piperazine	7-Coordinated hemidirected and distorted polyhedra ($Bi(OH)_2O_4N$), Bi_2O_2-dimer	3D	**Fluorite**, **kgm** or **fcu**	Thermally stable up to 380 °C	93
—			4,4′-bipyridine		1D	—	Thermally stable up to 290 °C	96

Table 1 (*Contd.*)

Ad hoc name	Formula	Synthesis conditions	Modulating agent	PBU type	Dimension	Topology	Surface area and stability	Ref.
	[Hbpe][Bi(Hpydc)$_2$(pydc)]·H_2O (H_2pydc = pyridine-2,5-dicarboxylic acid, bpe = *trans*-bis(4-pyridyl) ethylene)	Hydrothermal, H_2O, 140 °C, and 3 days		7-Coordinated hemidirected distorted polyhedra (BiO_4N_3)				
—	$Bi_3O_2Cu(OH)(pdc)_2$ (pdc = 3,5-pyrazoledicarboxylate)	Hydrothermal, H_2O, 200 °C, and 3 days	4,4′-bipyridine	Trinuclear 6- and 7-coordinated hemidirected distorted polyhedra. Bi(1) O_4N_2, Bi(2)O_6 and Bi(3)O_7	3D	—	Thermally stable up to 370 °C	60
CAU-7-TATB-NH_2	Hpy[Bi(TMC)$_4$(HTMC)] (py = pyridine and HTMC = 2-thiophenecarboxylic acid)	Solution chemistry, H_2O, r.t., and 3 days	Pyridine	Mononuclear 9-coordinated distorted hemidirected polyhedra BiO_9	0D	—	Thermally stable up to 310 °C	30
—	Hpy[Bi$_2$(TMC)$_6$(NO_3)] (py = pyridine and HTMC = 2-thiophenecarboxylic acid)	Solution chemistry, H_2O, r.t., and 3 days	Pyridine	Bi-dimer, 8-coordinated distorted hemidirected polyhedra BiO_8	1D	—	Thermally stable up to 310 °C	30
Bi-BTC	[Bi$_2$(μ_2-η^2-OOCFcCOO-μ_2-η^2)(η^2-OOCFcCOO-η^2)(μ_2-η^2-OOCFcCOO-η^2)]$_2$ (OOCFcCOO = ferrocenedicarboxylic acid)	Solvothermal, dry THF, 130 °C, and 24 h	—	2 Bi centers, 7-coordinated BiO_7 distorted hemidirected polyhedra and 9-coordinated BiO_9, holodirected polyhedra	1D	—	—	62
—	[Bi(μ_2-η^2-FcCOO)(η^2-FcCOO)$_2$]$_n$ (OOCFcCOO = ferrocenedicarboxylic acid)	Reflux, dry toluene 24 h, and recrystallized using DCM	—	7-Coordinated BiO_7, distorted hemidirected polyhedra	Helical 1D	—	—	62
Bi-MMTAA	Bi(MMTAA)2Ph (MMTA = 2-mercapto-4-methyl-5-thiazoleacetic acid)	Reflux method, methylbenzene/MeOH, refluxing at 100 °C, and 24 h	—	5-Coordinated, hemidirected BiS_2O_2Ph (square pyramid)	1D	—	Thermally stable up to 200 °C and stable in water	77

Table 2 Summary of the Bi-based holodirected MOMs, based on their ad hoc name and corresponding formula, synthetic conditions, structures, surface area and stability

Ad hoc name	Formula	Synthesis conditions	Modulating agent	PBU type	Dimension	Topology	Surface area and stability	Ref.
CAU-7	Bi(BTB) (BTB = 4,4′,4″–(benzene-1,3,5-triyl)tribenzoate)	Solvothermal, DMF or MeOH, 120 °C, 12 h or microwave-assisted, 20 min in MeOH	—	9-Coordinated holodirected distorted polyhedra BiO_9	3D	**hcb**	Thermally stable up to 380 °C and surface area 1150 $m^2\ g^{-1}$	61
CAU-17	$[Bi(BTC)(H_2O)]\cdot 2H_2O\cdot MeOH$ (BTC = 1,3,5-benzenetricarboxylate)	Solvothermal, MeOH, microwave at 120 °C, for 20 min, and 600 rpm. Solvothermal, DMF/MeOH, and 120 °C for 12 h	—	9-Coordinated holodirected distorted polyhedra BiO_9	3D featuring an unprecedented topological complexity with 54 unique nodes and 135 edges	**htb**	Surface area 69.5 $m^2\ g^{-1}$	47
—	$[Bi(1,4\text{-}BDC)_2(DMF)]\cdot(DMA)(DMF)_2$ (BDC = 1,4-benzenedicarboxylate)	Solvothermal, DMF, 100 °C, and 3 days	Piperazine	9-Coordinated holodirected distorted polyhedra BiO_9	2D	**sql**	—	90
Bi-BDC	Bi-BDC (BDC = 1,4-benzenedicarboxylate)	Microwave-assisted solvothermal, 100 °C, and 60 min	—	—	—	—	Surface area 38.6 $m^2\ g^{-1}$	73
—	$[Bi_4(1,4\text{-}BDC)_7(HIm)]\cdot(DMA)_2(DMF)_2$ (BDC = 1,4-benzenedicarboxylate and Him = imidazole)	Solvothermal, DMF, 100 °C, and 3 days	Imidazole	Dimeric 9-coordinated holodirected polyhedra $Bi(1)O_9$ and $Bi(2)NO_8$	3D	**dia**	Thermally stable up to 350 °C-450 °C	90
—	$[Bi(1,4\text{-}BDC)_2]\cdot(DMA)$ (BDC = 1,4-benzenedicarboxylate)	Solvothermal, DMF, 100 °C, and 3 days	Imidazole	12- and 9-coordinated holodirected polyhedra $Bi(1)O_{12}$ and $Bi(2)O_9$ trimeric units	3D	**pcu**	Thermally stable up to 415 °C	90
—	$[NaBi(1,4\text{-}BDC)_2(DMF)(H2O)]\cdot(DMF)$ (BDC = 1,4-benzenedicarboxylate)	Solvothermal, DMF, 100 °C, 3 days and exposure to ambient conditions for a few days	NaOH	8-Coordinated and holodirected polyhedra BiO_8	3D	—	—	59
—	Bi-BDC (BDC = 1,4-benzenedicarboxylate)	Hydrothermal, DMF/EtOH, 180 °C, and 3 h	—	7-Coordinated holodirected polyhedra BiO_7	—	—	Surface area is 50.16 $m^2\ g^{-1}$	56
—	$[NaBi(1,3\text{-}BDC)_2(DMF)]$ (1,3-BDC = 1,3-benzenedicarboxylate)	Solvothermal, DMF, 100 °C, and 3 days	NaOH	9-Coordinated holodirected polyhedra BiO_9	3D	—	Thermally stable in the 350–550 °C range and surface area 71.07 $m^2\ g^{-1}$	59
—	$[NaBi(1,3\text{-}BDC)_2(EtOH)]$ (1,3-BDC = 1,3-benzenedicarboxylate)	Solvothermal, EtOH, 100 °C, and 3 days	NaOH	9-Coordinated holodirected polyhedra BiO_9	3D	—	Thermally stable in the 350–450 °C range, less porosity, and surface area 8.28 $m^2\ g^{-1}$	59
—	$K_4Bi(pydc)_3(Hpydc)(H_2O)_{3.3}$ (pydc = pyridine-2,5-dicarboxylate)	Solvothermal, DMF, 100 °C, and 3 days	KOH	8-Coordinated, holodirected polyhedra. BiO_4N_4 with single Bi-center and anionic layer	3D	—	Water unstable	23
—	$(DMA^+)_3Bi(pydc)_2(Hpydc)_2$ (pydc = pyridine-2,5-dicarboxylate)	Solvothermal, DMF, 100 °C, and 3 days	KOH	8-Coordinated, holodirected polyhedra. BiO_4N_4 with single Bi-center and anionic layer	3D	—	—	23
—	BiO-BDC-NH_2 (BDC-NH_2 = 2-aminoterephthalic acid)	Solvothermal, DMF/MeOH, 120 °C, and 48 h	MeOH	JCPDS 35-0939	—	—	Good stability	57
—	BiO-BDC-NH_2@NMCS (BDC-NH_2 = 2-aminoterephthalic acid)	Solvothermal, DMF/MeOH, 120 °C, and 18 h	MeOH	—	—	—	Good stability	46
—	CAU-17 derivative	Solvothermal, DMF/DCM, 155 °C, and @1 h, 4 h, 8 h and 16 h	—	ICSD 00-048-2435	—	—	Surface area 342.7 $m^2\ g^{-1}$	44

Table 2 (*Contd.*)

Ad hoc name	Formula	Synthesis conditions	Modulating agent	PBU type	Dimension	Topology	Surface area and stability	Ref.
Bi-NU-901	$Bi_6(\mu_3OH)_8(HCO_2)_2(TBAPy)_2$ (TBAPy = 1,3,5,8-(p-benzoate)pyrene)	Solvothermal, DMF/EtOH, 100 °C, 8 h, and sonication	Acetic acid	8-Coordinated, holodirected polyhedra BiO_8 with Bi_6 cluster	3D	**scu**	Thermally stable up to 400 °C and surface area is 320 $m^2\ g^{-1}$	101
CAU-31	$[Bi_2(H_2TCPB)(TCPB)(H_2O)_2]\cdot xH_2O$ (TCPB = 1,2,4,5-tetrakis-(4-carboxyphenyl)benzene)	Solvothermal, EtOH, 100–140 ° C, and 12 h	—	8-Coordinated, holodirected polyhedra BiO_8	3D	**bex**	Thermally stable up to 350 °C, chemically unstable in DMF, acetone and THF, and no $N_{2(g)}$ uptake	123
CAU-32	$(NH_2(CH_3)_2)[Bi(TCPB)(H_2O)]\cdot xH_2O$ (TCPB = 1,2,4,5-tetrakis-(4-carboxyphenyl)benzene)	Solvothermal, EtOH/DMF, 100–140 °C, and 12 h	—	9-Coordinated, holodirected polyhedra BiO_9	3D	—	Thermally stable up to 350 °C, unstable in aqueous solution, and no $N_{2(g)}$ uptake	123
Bi-SMOF	$[(Hdma)Bi(1,4\text{-ndc})_2(DMF)]_n\cdot n$DMF (1,4-ndc = 1,4-naphthalenedicarboxylate)	Solvothermal, DMF, 90 °C, and 3 days	Piperazine or imidazole	9-Coordinated holodirected polyhedra BiO_9 and infinite plicate 2D layer	3D	**sql**	Thermally stable up to 380 °C and surface area 1150 $m^2\ g^{-1}$	91
SU-100	$Bi(OH)(H_2BPT)_2(H_2O)_2\cdot H_2O$ (BPT = biphenyl-3,4′,5-tricarboxylate)	Hydrothermal, H_2O, 120 °C, 20 h, and with stirring	—	8-Coordinated holodirected, polyhedra BiO_8 forming Bi-oxo rods	1D	—	—	104
NOTT-220 (α/β)	$[Bi_2(L)_{1.5}(H_2O)_2]\cdot(DMF)_{3.5}(H_2O)_3$; (L = (L = biphenyl-3,3′,5,5′-tetracarboxylate))	Solvothermal, DMF/MeCN, 100 °C, and 10 h	Piperazine/nitric acid	Bi-dimer with 8- and 9-holodirected coordinated polyhedra NOTT-220-α ($Bi(1)O_8$/$Bi(2)O_9$), and NOTT-220-β ($Bi(1)O_9$/$Bi(2)O_8$)	3D	**tfi/pts**	Highly porous and surface area is 1014 $m^2\ g^{-1}$	92
—	$Bi(pydc)_2\cdot(H_3O^+)\cdot(H_2O)_{0.83}$ (pydc = pyridine-2,5-dicarboxylate)	Solvothermal, DMF, 100 °C, and 3 days	—	8-Coordinated holodirected, distorted polyhedra (BiO_6N_2), and layered structure	2D	**kgm**	—	18
—	$[Bi(C_5H_3N_2O_4)(C_5H_2N_2O_4)]$ ($C_5H_3N_2O_4$ = 4,5-imidazoledicarboxylic acid)	Hydrothermal, H_2O, 150 °C, and 3 days	Piperazine	8-Coordinated holodirected, distorted polyhedra (BiO_6N_2), and layered structure	2D	**Brucite**	Thermally stable up to 400 °C	93
CTH-6	$[Bi_2(CPB)(acetato)_2(DMF)_2]\cdot 2$DMF ($H_6$CPB = 1,2,3,4,5,6-hexakis(4-carboxyphenyl)benzene)	Solvothermal, DMF, 120 °C, and 3 days	Acetic acid	9-Coordinated holodirected BiO_9 polyhedra	3D	**rtl**	Thermally stable up to 400 °C and surface area 67.04 $m^2\ g^{-1}$	102
CAU-7-TATB	[Bi(TATB)] (H_3TATB = triazine-2,4,6-triyl-tribenzoic acid)	Microwave-assisted solvothermal, MeOH/DMF, 120 °C, 20 min and with stirring at 600 rpm	—	9-Coord. BiO_{10} holodirected polyhedra forming chains	3D	**Hcb**	Surface area 813 $m^2\ g^{-1}$	122
CAU-7-TATB-NH_2	[Bi(TATB-NH_2)] (H_3TATB = triazine-2,4,6-triyl-tribenzoic acid)	Microwave-assisted solvothermal, MeOH/DMF, 120 °C, 20 min and with stirring at 600 rpm	—	9-Coord. BiO_{10} holodirected polyhedra forming chains	3D	**Hcb**	Surface area 104–627 $m^2\ g^{-1}$	122
—	Hpy[$Bi(TMC)_3NO_3$] (py = pyridine and HTMC = 2-thiophenecarboxylic acid)	Solution chemistry, H_2O, r.t., and 3 days	Pyridine	Bi-dimer, 9-coordinated distorted holodirected polyhedra. BiO_9	0D	—	Thermally stable up to 350 °C	30

Table 2 (*Contd.*)

Ad hoc name	Formula	Synthesis conditions	Modulating agent	PBU type	Dimension	Topology	Surface area and stability	Ref.
—	Hpy[Bi(TMC)$_4$] (py = pyridine and HTMC = 2-thiophenecarboxylic acid)	Solution chemistry, H_2O, r.t., and 3 days	Pyridine	Bi-dimer, 9-coordinated distorted holodirected polyhedra. BiO_9	0D	—	Thermally stable up to 310 °C	30
—	(Hpy)$_2$[Bi$_2$(TMC)$_8$]; (py = pyridine and HTMC = 2-thiophenecarboxylic acid)	Solution chemistry, H_2O, r.t., and 3 days	Pyridine	2 crystallographic bi, each 10-coordinated holodirected polyhedra BiO_{10}	0D	—	—	30
—	Hpy[Bi(TDC)$_2$(H_2O)]·1.5H_2O (py = pyridine and TDC = 2,5-thiophenedicarboxylates)	Solution chemistry, acetic acid/EtOH, r.t., and 5–7 days	Pyridine	Mononuclear sheet 9-coordinated distorted holodirected polyhedra BiO_9	2D	—	—	97
—	(Hpy)$_3$[Bi$_2$(TDC)$_4$(HTDC)(H_2O)]·0.74H_2O (py = pyridine and TDC = 2,5-thiophenedicarboxylates)	Solution chemistry, H_2O/EtOH, r.t., and 5 days	Pyridine	2-Crystallographic Bi with 10- and 9-coordinated holodirected polyhedra	2D	—	—	97
—	(Hpy)$_2$[Bi(TDC)$_2$(HTDC)]·0.36H_2O (py = pyridine and TDC = 2,5-thiophenedicarboxylates)	Solution chemistry, H_2O/EtOH, r.t., and 5 days	Pyridine	10-Coordinated holodirected distorted polyhedra, BiO_{10}	2D	—	—	97
—	[Bi(SB)OH] (H_2SB = 4-sulfobenzoic acid)	Hydrothermal, H_2O, 180 °C, and 48 h	HNO_3	8-Coordinated holodirected distorted polyhedra, BiO_8 inorganic layers	3D	—	—	98
—	[Bi$_4$(ST)$_2$(HST)O$_2$(H_2O)$_2$]·H_2O (H_3ST = 2-sulfoterephthalic acid)	Hydrothermal, H_2O, 180 °C, and 48 h	HNO_3	Tetranuclear Bi center each with 8-coordinated BiO_8 distorted holodirected polyhedra	3D	—	—	98
	[Bi$_4$(ST)$_2$O$_3$(H_2O)$_2$] (H_3ST = 2-sulfoterephthalic acid)	Hydrothermal, H_2O, 180 °C, and 48 h	NaOH	Polynuclear 8 and 7-coordinated distorted polyhedra BiO_8 and BiO_7	3D	—	—	98
Bi-BTC	[Bi(BTC)(DMF)]·DMF (BTC = 1,3,5-benzenetricarboxylate)	Solvothermal, DMF/MeOH, ramp to 120 °C in 45 h, kept for 12 h and cooled to r.t. at 2 °C min^{-1}	—	9-Coordinated holodirected BiO_9, polyhedra connected into a dimeric units Bi_2O_{14}	3D with a very interesting two 1D helix chains along *b* axis	**hcb**	—	149
Bi-BTC	$C_{12}H_{10}BiNO_7$ (BTC = 1,3,5-benzenetricarboxylate)	Microwave-assisted solvothermal,100 °C, and 60 min	—	9-Coordinated holodirected BiO_9, polyhedra connected into a dimeric units Bi_2O_{14}	3D with a very interesting two 1D helix chains along *b* axis	**hcb**	Surface area 16.6 m^2 g^{-1}	73
—	[Bi$_2$(μ_2-η^2-FcCOO)$_2$(η^2-FcCOO)$_4$(H_2O)$_4$]·(2FcCOOH) (OOCFcCOO = ferrocenedicarboxylic acid)	Reflux, dry toluene 24 h, and recrystallized using DCM	—	Binuclear complex, 9-coordinated, BiO_9, distorted holodirected polyhedral	0D	—	—	62
—	(2-apyH)$_2$[Bi(pydc)$_2$(pydcH)]·2H_2O (pydc = 2,6-pyridinedicarboxylate and 2-apy = 2-aminopyridine)	Reflux, H_2O, 6 h, and slow evaporation	2-Amino pyridine	9-Coordinated holodirected BiN_3O_6 polyhedra	0D	—	Thermally stable up to 450 °C	94
—	(4-apyH)$_2$[Bi(pydc)(pydcH)$_2$]·4H_2O (pydc = 2,6-pyridinedicarboxylate and 4-apy = 4-aminopyridine)	Reflux, H_2O, 6 h and slow evaporation	4-Amino pyridine	9-Coordinated holodirected BiN_3O_6 polyhedra	0D	—	Thermally stable up to 460 °C	94
—	(pipzeaH)$_2$[Bi$_2$(pydc)$_3$(pydcH)(H_2O)$_2$]·5H_2O (pydc = 2,6-pyridinedicarboxylate and pipzea = 2-piperazin-1-ylethanamine)	Reflux, H_2O, 6 h, and slow evaporation	2-Piperazine-1-ylethanamine	Bi-dimer, 8-coordinated distorted holodirected BiN_2O_6 polyhedra	0D	—	Thermally stable up to 400 °C	91

Table 2 (*Contd.*)

Ad hoc name	Formula	Synthesis conditions	Modulating agent	PBU type	Dimension	Topology	Surface area and stability	Ref.
—	$[Bi(PTC)(H_2O)_2]$ (H_3PTC = 2,4,6-pyridinetricarboxylic acid)	Hydrothermal, H_2O, 160 °C for 6 h and r.t. in 6 h	NaOH and HNO_3	Layered structure, 9-coordinated holodirected polyhedra $BiNO_8$	2D	—	Thermally stable up to 350 °C	99
—	$(H_3O)[Bi_2(PTC)(HPTC)_2(H_2O)_2]$ (H_3PTC = 2,4,6-pyridinetricarboxylic acid)	Hydrothermal, H_2O, 160 °C for 6 h and r.t. in 6 h	NaOH and HNO_3	Binuclear, 8-coordinated $BiNO_7$ and BiN_2O_6 distorted holodirected polyhedra	2D	—	Thermally stable up to 300 °C	99
—	α[Bi(PTC)] (H_3PTC = 2,4,6-pyridinetricarboxylic acid)	Hydrothermal, H_2O, 180 °C for 48 h and r.t. in 6 h	NaOH and HNO_3	8-Coordinated $BiNO_7$ distorted holodirected polyhedra and dimeric IBU	3D	—	Thermally stable up to 400 °C	99
—	β[Bi(PTC)] (H_3PTC = 2,4,6-pyridinetricarboxylic acid)	Hydrothermal, H_2O, 180 °C for 48 h and r.t. in 6 h	NaOH and HNO_3	9-Coordinated $BiNO_8$ holodirected polyhedra and dimeric IBU	3D	**dia**	Thermally stable up to 400 °C	99
IEF-5	$[Bi_{12}(DTTDC)_{24}]\cdot 23DMA\cdot 4DMF\cdot 2H_2O$ (DTTDC = dithieno[3,2 *b*:2′,3′-*d*]thiophene-2,6-dicarboxylic acid)	Solvothermal, DMF/EtOH, 120 °C, and 72 h	—	Trinuclear, $Bi(1)O_8$, $Bi(2)O_{10}$ and $Bi(3)O_8$, connected holodirected distorted polyhedra	3D	**pcu**	Thermally stable up to 220 °C, chemically stable methanol and acetonitrile, surface area is 30 $m^2\ g^{-1}$	124
—	$(H_2bpy)[Bi(bpy)_2(Hpdc)]\cdot 5H_2O$; (pdc = pyridine-2,6-dicarboxylate and bpy = 4,4′-bipyridine)	Hydrothermal, H_2O, 100 °C and 3 days	Bipyridine	8-Coordinated BiO_5N_3 highly distorted holodirected polyhedra	3D	—	Thermally stable up to 370 °C and moisture stability	95
—	$(Imi)_2[Bi_2(pzdc)_4]\cdot 2H_2O$	Solution chemistry, H_2O/DMF, 48 °C, 10 min, RT and 3 days	Imidazole	9-Coordinated $Bi(1)O_7N_2$ $Bi(2)O_7N_2$ distorted holodirected polyhedra	2D	—	—	136
BiCo-MCP	$Bi_2Co_2C_{42}H_{36}N_6O_{33}$ (2,4-bpa = 2,4-bipyridine dicarboxylic acid)	Hydrothermal, H_2O, 120 °C and 3 days	—	9-Coordinated BiO_9 distorted holodirected polyhedra	2D	—	—	48
CuBi-BPDC	CuBi-BPDC (H_2BPDC = 4,4′-biphenyldicarboxylic acid)	Hydro-solvothermal, H_2O/DMF, 110 °C and 72 h	HNO_3	—	—	—	Surface area 575 $m^2\ g^{-1}$	55
Bi-TDPAT	$(H_3O)\cdot[Bi(TDPAT)_{0.67}]\cdot 3H_2O\cdot 4DMA$ (H_6TDPAT = 2,4,6-tris(3,5-dicarboxylphenylamino)-1,3,5-triazine)	Solvothermal, H_2O/DMA, 90 °C and 4 days	HNO_3	8-Coordinated BiO_8, holodirected (dodecahedra)	3D	**btt**	Thermally stable up to 396 °C and surface area 12.26 $m^2\ g^{-1}$	54

nuclear bismuth-based MOMs were also reported based on hydro- or solvo-thermal methods.[59–67] Solvothermal reactions could also be performed under vacuum inside a sealed borosilicate tube.[68] The branch tube method combines autogenous pressure and thermal gradient with the purpose of dissolving and reacting the reagents in the hot zone, followed by crystallization of the formed compound in the colder zone, which may eliminate the need for slow cooling as in the case of hydro- and solvo-thermal methods. Pyridyl-containing bismuth MOMs were synthesized by adopting this method.[69–72] Nano-sized particles of the compounds were also synthesized using the sonochemical method and the microwave method.[73]

A conventional reflux reaction, followed by slow evaporation, was another successful method for isolating bismuth-based MOMs, although the number of reported compounds is comparatively small.[62,74–77] Examples of hydrothermal followed by slow evaporation are also scarce.[45]

Room-temperature dissolution of the $Bi(NO_3)_3 \cdot 5H_2O$ precursor could also be achieved by gradual addition of concentrated acid.[78–82] Partial dissolution of the precursor and/or the ligand in a common solvent, with which the filtrate was used for slow evaporation, is also a common method. Slow evaporation, precipitation, followed by recrystallization, and layering, either in an inert or ambient atmosphere, have typically been used for other bismuth precursors, *e.g.*, BiX_3 (X = Cl, Br, or I) and triphenylbismuth.[68,83–85]

Solid-state reactions or a solvent-free method, which involved a melt of reagents or thermally stable ligand, followed by slow cooling or sublimation, as well as solution chemistry, both under inert conditions, have been used to synthesize the bismuth carboxylate-based paddle-wheel.[19–22]

Recently, there has been increased interest in exploiting hemi-directed PBU of s^2p^0 main group cations (*e.g.* Bi^{3+}) to direct the formation of polar space groups, either at or below room temperature, for second harmonic generation (SHG) and/or ferroelectric applications. We combined synthetic strategies of ferroelectric oxide (the use of s^2p^0 cations, *e.g.* Bi^{3+}) and a homochiral metal coordination compound (the use of unsymmetrical ligands and a homochiral ligand) to synthesize two homochiral bismuth coordination polymers.[46] The dipole directions from the formed hemidirected bismuth PBU, however, were not parallel to each other; thus, moderate SHG properties were achieved.[46] Mercier and co-workers reported the formation of unparallel and parallel dipoles of the distorted bismuth mixed halides PBU with methyl viologen. The parallel dipoles produced strong polarization, giving true ferroelectric properties with record-breaking spontaneous polarization.[86,87]

An important highlight from the synthetic methods is that despite solvo- and hydro-thermal approaches being commonly used to synthesize Bi-based MOMs due to Bi precursor limited solubility, there are reports in which they were successfully synthesized using a simple, lower temperature dissolution-crystallization route, which may enrich the Bi-based MOMs structural library.

2.2 Modulating agents

2.2.1. Modulation in Bi-based MOM synthesis. The synthesis of Bi-based MOM is often complicated by the high coordination number and irregular coordination flexibility of Bi^{3+}, particularly when flexible multidentate ligands are used. Under these conditions, rapid coordination and uncontrolled aggregation often result in amorphous precipitates or poorly crystalline solids, rather than well-defined architectures. Because Bi^{3+} can coordinate strongly with both hard O-donor and softer N-donor ligands, careful tuning of the reaction environment is essential to obtain crystalline frameworks. Modulated synthesis has therefore become an important strategy for regulating Bi^{3+} coordination chemistry, suppressing undesired precipitation, and promoting the growth of X-ray quality crystals.

2.2.2. General role of modulators. Modulators act by competing with the organic linker for Bi^{3+} coordination, adjusting linker deprotonation, and controlling metal hydrolysis. These effects slow nucleation and moderate crystal growth, thereby improving crystallinity. In addition, solvent composition (discussed *vide infra*) can strongly influence the crystallization pathway. In mixed-solvent systems, the water-to-organic solvent ratio affects hydrolysis and solubility. Excessive water often favors microcrystalline or precipitate products, whereas weaker metal-solvent interactions generally promote crystallinity by limiting solubility and reducing uncontrolled aggregation. Similarly, in some cases, an increased Bi salt-ligand ratio can favor the formation of larger crystals.[53]

2.2.3. Types of modulators used in Bi-based systems. In classical MOF synthesis based on hard Lewis acids, such as Zr^{4+}, Ti^{4+}, or Cr^{3+}, monocarboxylic acids, HF/HBF_4, or dilute mineral acids are commonly used to suppress linker deprotonation and compete with the linker for coordination sites.[88,89] In the Bi^{3+} system, however, modulators are often selected differently. Since Bi^{3+} is a borderline acid, soft or borderline Lewis bases, such as piperazine,[90–94] bipyridine,[23,60,95,96] imidazole,[90,91] and pyridine,[30,94,97] are frequently employed to tune the coordination equilibria and slow down rapid Bi-ligand association. These additives can temporarily coordinate Bi^{3+}, reduce nucleation rates, and facilitate the growth of well-defined crystals. In some cases, inorganic bases or acids, such as NaOH, KOH, LiOH, nitric acid, benzoic acid, or citric acid, have also been used, depending on the desired balance between pH control, linker activation, and metal availability.[59,98–102]

2.2.4. Representative examples and mechanistic insights. A central challenge in Bi^{3+}-based synthesis is to regulate the availability of Bi^{3+} in solution while controlling its hydrolysis reactivity. Excessively fast coordination often leads to dense, non-porous products rather than open frameworks. In one representative example, Yang and co-workers used dilute HNO_3 together with piperazine to synthesize the porous MOCP $[Bi_2(L)_{1.5}(H_2O)_2]\cdot(DMF)_{3.5}(H_2O)_3$ (NOTT-220, L = biphenyl-3,3′,5,5′-tetracarboxylate) from $Bi(NO_3)_3 5H_2O$.[103] In this case, HNO_3 lowered the pH and suppressed excessive linker deprotonation, while piperazine competed with the linker for Bi^{3+} coordination, together slowing nucleation and enabling the growth of high-quality crystals. Similarly, Xin *et al.* showed that pH adjustment with HNO_3 was crucial for the synthesis of crystalline Bi-TDPAT based on 2,4,6-tris(dicarboxylplenylamino)-1,3,5-triazine (TDPAT).[53] At high acidity, only gelatinous material was

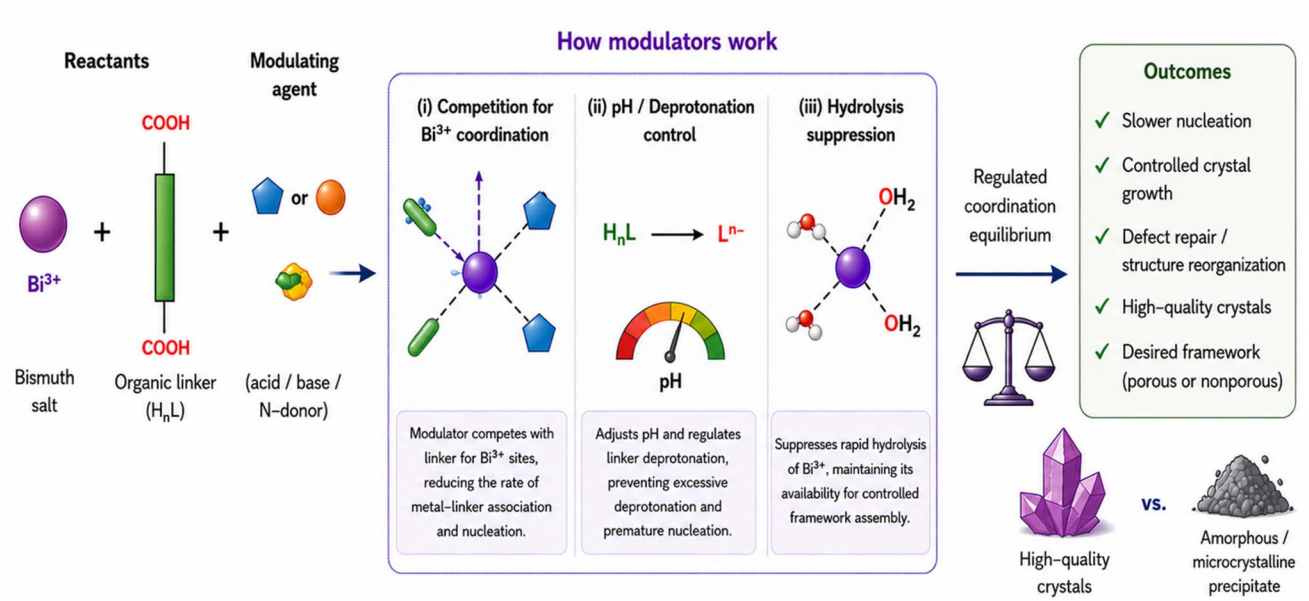

Scheme 1 Roles of modulators in the Bi MOM synthesis.

obtained, whereas at higher pH, rapid precipitation occurred. Optimal acidification with HNO_3 slowed crystallization sufficiently to yield large crystals.

2.2.5. Implications for porous Bi-based MOFs. Interestingly, most porous Bi-based MOFs reported to date, including CAU-7, CAU-17, CAU-33, CAU-35, IEF-5, and Su-101, were synthesized without the intentional use of modulators, whereas only a few, such as Bi-NU-901 and NOTT-220, required additives, such as trifluoroacetic acid or the piperazine/HNO_3 combination. This suggests that modulator-free conditions may sometimes be more favorable for obtaining open Bi-based frameworks, while the presence of organic base modulators may increase Bi^{3+} solubility and promote coordination environments that favor dense or less porous products.

Overall, the role of the modulating agent in forming high-quality single crystals of Bi MOMs is summarized in Scheme 1 and Table 3. From this study, we could gain the insight that the presence of organic base modulators may increase the probability of obtaining an asymmetric and irregular Bi^{3+} geometry. As the pH rises, the rate of linker deprotonation increases and, similarly, the presence of a soft N-donor modulator may also increase the solubility of the bismuth salt; both may create dense and non-porous MOCPs, which is an undesirable synthetic environment for MOF synthesis. Therefore, this may suggest that controlling Bi^{3+} ion availability and its coordination chemistry by securing the perfect ratio of linker deprotonation and bismuth salt dissociation, which may stem from judicial use of appropriate modulator(s) guided by HSAB and

Table 3 Modulating agents in the Bi-based MOMs: types, roles, and representative examples

Modulator type	Typical examples	Main function	Effect on Bi-based synthesis	Representative outcome
Acidic modulators	HNO_3, TFA, benzoic acid, and acetic acid	Lower pH suppresses excessive linker deprotonation and controls hydrolysis	Slows nucleation and can improve crystallinity	Useful when rapid precipitation occurs
Soft/borderline Lewis-base modulators	Piperazine, pyridine, bipyridine, and imidazole	Compete with linker for Bi^{3+} coordination and tune coordination equilibrium	Reduce fast Bi–ligand binding and promotes crystal growth	Effective for growing XRD-quality crystals
Inorganic bases	NaOH, KOH, and LiOH	Increase pH and alter deprotonation and solubility	Can either promote coordination or induce precipitation, depending on conditions	Used selectively for specific linker/metal systems
Mixed acid–base modulation	HNO_3 + piperazine	Combine pH control with coordination competition	Balances deprotonation, Bi^{3+} availability, and nucleation rate	Example: NOTT-220
Modulator-free conditions	None added intentionally	Relies on the intrinsic balance of precursor, linker, and solvent	Sometimes favor open, porous frameworks	Examples: CAU-7, CAU-17, CAU-33, CAU-35, IEF-5, and SU-101

crystallization principles, may enable the isolation of more Bi-based MOFs in the near future. Further, high-quality single crystals of Bi-based MOMs can be isolated by regulating the crystallization process utilizing a proper combination of modulating agent, solvent engineering, and reaction conditions. The last two parameters will be described further in the following section.

2.3 Solvent engineering, reaction conditions and green chemistry

Solvothermal and hydrothermal techniques are widely used synthetic routes for the preparation of bismuth-based MOMs. This is attributed to the solubility concerns regarding the precursor bismuth salts in aqueous and common organic solvents. It is therefore important to meticulously select solvent(s) and a favorable reaction temperature aimed at enhancing the solubility of the precursor salts as well as controlling the hydrolysis of Bi^{3+} in solution. Generally, less attention has been paid to the effects of experimental synthesis parameters, especially temperature and solvents. Solvent is an integral part of MOMs synthesis, playing a role in determining activation energies and reaction thermodynamics. Moreover, depending on their size and polarity, solvents may act as structure-directing agents as well as controlling the crystallinity, morphology, and stability of the MOM products. For the synthesis of Bi^{3+} compounds, dimethylformamide (DMF), methanol (MeOH), ethanol and water are widely used solvents, or mixtures thereof, such as DMF/methanol, DMF/water, DMF/ethanol, water/ethanol or ethanol/acetic acid, DMF/acetonitrile, or DMF/toluene or DMF/nitric acid. This may be connected to their polarities. Among these solvents, only methanol can be used to synthesize bismuth compounds featuring permanent porosity, such as SU-100, CAU-7 and CAU-17. Other solvents are used as mixtures, for instance, DMF with water, DMF with acetonitrile, DMF with ethanol, or DMF with toluene to synthesize CAU-35, NOTT-220, NU-901, or CAU-33, respectively.

Based on that, Nguyen and co-workers studied the impact of different solvent systems, such as DMF, MeOH and DMF/MeOH, on the size, porosity and crystal morphology of the organic decomposition of Bi-BTC. They noticed the crystal structure of Bi-based MOF was highly dependent on solvent selection, where Bi-BTC-DMF/MeOH was isomorphic to CAU-17, while Bi-BTC-DMF and Bi-BTC-MeOH crystals matched the XRD pattern of bismuth carboxylate. Therefore, the effective solvent system to synthesize porous Bi-MOF, in this case, is the mixture of DMF and MeOH. MeOH facilitates the rapid formation of CAU-17 in the initial phase of the solvothermal process, whereas DMF ensures the stability of the CAU-17 structure under extended solvothermal time.[57]

Temperature and reaction time also play vital roles in the synthesis of these materials. Only a few bismuth compounds have been reported to be synthesized at room temperature, with the majority being synthesized at temperatures well above room temperature. Generally, the metal precursor and the organic linker, in the presence or absence of modulators, are typically dissolved/suspended in a suitable solvent(s), depending upon the synthesis route, whether solvothermal, hydrothermal, solution chemistry, microwave-assisted, or, in a few cases, reflux. When H_2O is used as a solvent, mostly higher temperatures ranging from 120–200 °C are required for the synthesis, and reaction times in the range of 3 to 5 days are needed. For instance, in the hydrothermal synthesis of trinuclear Bi_3O_2-$Cu(OH)(pdc)_2$, temperatures up to 200 °C and a 3 days reaction period were required. Similarly, several compounds, such as [Bi(SB)OH], $[Bi_4(ST)_2(HST)O_2(H_2O)_2]\cdot H_2O$, $[Bi_4(ST)_2O_3(H_2O)_2]$,[98] α[Bi(PTC)], β[Bi(PTC)],[99] and $[C_4N_2H_{10}][Bi(C_7H_4NO_4)(C_7H_3NO_4)]\cdot H_2O$ were hydrothermally synthesized at 180 °C in reaction times of 2 to 3 days; also, was Bi-BDC prepared at 180 °C in 3 h. 2D luminescing compounds, $[Bi(PTC)(H_2O)_2]$ and $(H_3O)[Bi_2(PTC)(HPTC)_2(H_2O)_2]$, were both synthesized hydrothermally at 160 °C in 6 hours,[99] while Bi_2-O_2(HBPT) and $Bi_6O_4(H_2TPTC)_5$ were also synthesized at 160 °C.[104] Several other compounds are synthesized hydrothermally using synthesis temperatures between 120 °C and 150 °C. The heterogenous catalysts $[Bi(C_5H_3N_2O_4)(C_5H_2N_2O_4)]$ and $[Bi(\mu_2$-$OH)(C_7H_3NO_4)]$ were both synthesized at 150 °C, while 3D photoactive $[Hbpe][Bi(Hpydc)_2(pydc)]\cdot H_2O$ and Bi(pydc)(Hpydc)(H_2O) were synthesized hydrothermally in 3 days at 140 °C.[23,96] A few other compounds were synthesized hydrothermally at 120 °C, $Bi(OH)(H_2BPT)_2(H_2O)_2\cdot H_2O$ in 20 hours,[104] $Bi_2(HBPT)_3(H_2O)_3\cdot H_3BPT$ in 7 days,[104] and BiCo-MCP in 3 days.[56] Surprisingly, two luminescing MOCPs, Bi-MOF[105] and $(H_2bpy)[Bi(bpy)_2(Hpdc)]\cdot 5H_2O$[95] were both synthesized hydrothermally at 100 °C.

On the other hand, solvothermal synthesis, especially in DMF or a mixture with other solvents, requires lower temperatures, commonly 100 °C, and a 3 days synthesis period. Typically, solvothermal syntheses are carried out at temperatures above the boiling point of the solvent to build the required viscosity and autogenous pressure necessary to allow the desired solubility of the starting material and the stability of the product. However, the boiling point of DMF is 143 °C and the prevalent temperature is 100 °C, this may be related to the solubility of bismuth salt precursors at temperatures below the boiling point of DMF. Other solvents, such as dry THF and dry toluene, have also been used for the synthesis of bismuth-containing ferrocene-based ligands at 130 °C or refluxing for 1 day.[62]

Further, the temperature of the reaction is considered an important parameter for crystalline growth; when the reaction temperature was higher than 140 °C, it became difficult to precipitate the solid product. At 110–130 °C, the product yield was low, and the proportion of microcrystals was small. The crystal quality was somewhat poor at around 100 °C, whereas at 90 °C was significantly better.[53] Moreover, optimizing the reaction temperature is important during synthesis as some of the solvents decompose at high temperatures, affecting the reaction medium and the quality of the final product. Additionally, the stability of some MOF structures is temperature dependent. Excessively high temperatures may lead to framework collapse, while low temperatures can result in incomplete reaction.[106]

In this section, solvent choice is shown to be an integral part of forming the porous network of Bi MOM, like in the case of

CAU-17, where the use of MeOH/DMF was needed. Optimum temperature is also crucial to isolate highly crystalline Bi MOMs and preserve porosity. A move toward a green chemistry route through mechanochemical synthesis has also been reported for Bi MOMs. This method offers solvent-free synthesis of MOF, thereby overcoming the limitations associated with conventional solvent-based methods. Furthermore, products are obtained within minutes in high yield.[107]

2.4 Typical polyhedra and the corresponding structures

A coordination polymer consists of linkers and nodes, which can be PBU (single metal node) or SBU, that repeat to form an extended (one-, two-, or three-dimensional) structure with covalent coordination bonds. The node comprises a single or multiple metal cation centers surrounded by donor atoms, typically O, N, chalcogens, or halogens, of the ligand. A typical bismuth PBU can have a coordination number up to ten,[31] with the possibility of forming asymmetric (hemidirected) or symmetric (holodirected) geometry (Fig. 1), owing to the non-bonding lone pair effects.

2.4.1. Effects of $6s^2$ lone pair activity on Bi^{3+} compounds. The $6s^2$ lone pair on Bi^{3+} is the so-called 'inert pair', exhibiting strong resistance to all kinds of bonding, including covalent or H-bonding, and also inert to removal, a phenomenon that is referred to as the "inert pair effect". Such an effect is also typical of other main groups, such as Pb^{2+}. The stereochemical activity of the lone pairs on the metal center is known to have a strong influence on the macroscopic properties of materials. For example, stereoactive lone pairs are susceptible to second-order Jahn–Teller (SOJT) distortions,[108,109] and favor the formation of acentric materials with noncentrosymmetric (NCS) structures.[108] Solid-state structures crystallizing with the NCS space group are associated with key symmetry-dependent properties, such as ferroelectricity, piezoelectricity, pyroelectricity and second harmonic generation (SHG),[95,108,110] and show atypical optical properties.[95,100,111] On the other hand, cation centers with stereochemically inactive lone pairs of electrons, especially on materials with corner-shared octahedra such as $M(II)X_6$, the so-called perovskites, are fundamental in determining their electronic properties.[112] It is well established that the symmetry in these materials is highly correlated with a smaller band gap, which significantly increases the conductivity properties.[113–116]

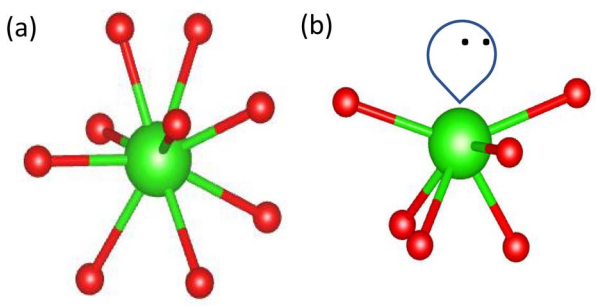

Fig. 1 Effect of lone pair activity: (a) symmetric distribution (holodirected) and (b) asymmetric distribution (hemidirected).

Although the lone electron pair activity of Bi^{3+} and other lone-pair-carrying metals cannot be spectroscopically determined, its manifestation can be detected as structural variances in the coordination network. The manifestation of lone pair activity is seen in the coordination geometry of Bi^{3+} with a varying magnitude of influence. Two distinct structural behaviors indicate the stereochemical activity of lone electron pairs: firstly, strong distortion from the ideal distribution of ligands around the sphere, resulting in visible voids in the geometrical polyhedra, and, secondly, irregular bond distance, with shortening of the M–L bond opposite to the apparent lone pair site. The valence shell electron pair repulsion (VSEPR) model has been explicitly applied to explain the coordination geometry of the heavy main group elements, including Bi^{3+}.[117,118] VSEPR treats non-bonding or bonding valence shell electrons as localized electron pairs distributing themselves within the valence shell to maximize the distance between them. Therefore, the properties and effects of lone pairs (non-bonding electron pairs) on the stereochemistry of the coordination geometry of the lone pair heavy metals can be effectively explained.

During the self-assembly, the Bi^{3+} electron lone pair can either maintain its stereochemical activity with a high asymmetric distribution of ligands (*i.e.* hemidirected polyhedra) or lose its stereochemical activity with a very small distortion in the distribution of ligands around the coordination sphere (*i.e.* holodirected polyhedra). The activity of the lone pair may be influenced by certain factors, including the number of coordination bonds and the nature of coordinating ligands.[119–121] For example, a low coordination number (CN) may lead to a hemidirected mode of ligand distribution, with the lone pair visibly occupying space and actively participating in the structure-directing role, while higher CNs lead to a more uniform ligand distribution with no visible void on the coordination sphere, indicating an inactive lone pair, holodirected polyhedra. However, the nature of the donor groups, in terms of size and polarization, also strongly influences the activity of the lone electron pairs. Large, polarizable and soft Lewis bases largely favor the formation of holodirected polyhedral, even with low coordination number.

2.4.2. Bismuth compounds with asymmetric (hemidirected) polyhedra geometry. Hemidirected Bi^{3+} polyhedra contain stereochemically active lone pairs that occupy one of the apexes, thus forming distorted polyhedra with long and short bonds, from which a dipole direction can be located. Typical observed bond distances between bismuth and the donor atoms are: Bi–O (2.1 to 2.9 Å), Bi–N (2.4 to 2.8 Å), Bi–S (2.6 to 3.1 Å), and Bi–Cl (2.9 to 3.4 Å). The distortion of donor ligands in the coordination sphere is created because of the strong electrostatic repulsions between the lone non-bonding and bonding electron pairs, and the result is displayed as a non-spherical distribution of charge around the Bi^{3+} ion, created by localized electron density of the stereochemically active lone pair.

It is a known phenomenon for $6s^2$ lone-pair containing metals to feature asymmetric geometry when the coordination number is equal to or less than seven. This is especially so for

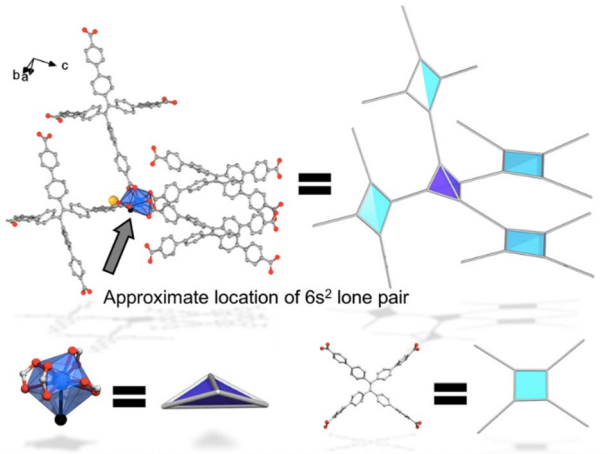

Fig. 2 Lone pair effect on nine-coordinated Bi^{3+} geometry showing the approximate $6s^2$ lone pair location. This figure has been reproduced from ref. 101 with permission from ACS, copyright 2019.

Bi^{3+} when the donating ligands have low polarizability, high electronegativity, and are not readily oxidizable, an archetypal attribute of hard Lewis bases such as O-donor ligands. However, other reports also show that nine-coordinated Bi^{3+} also forms a hemidirected geometry.

2.4.2.1 Porous, hemidirected Bi MOF. A typical example of nine-coordinated hemidirected Bi^{3+} was reported by Li and co-workers, who studied K[Bi(tcbpe)$(DMF)_2$]xDMF (L-MOF-401), in which the Bi^{3+} coordination sphere is surrounded by nine O-donor atoms with stereochemically active lone pairs that cause irregular bond lengths and asymmetric distribution of the ligands.[100] The two-fold interpenetrated anionic 3D net is composed of rectangular tcbpe linkers and a highly distorted hemidirectional tetrahedral Bi^{3+} geometry with respect to linker connectivity (Fig. 2, Table 1). Such nine-coordinated Bi^{3+} hemidirected geometry may be favored because of the surrounding hard, all-O-donating linker geometry with less electron transfer (due to the lone-pair orbital possessing p character) and possible interlinker attractions.

A porous Bi^{3+}-based MOF, Bi(BPT)·2MeOH (SU-100), was the first example of a flexible and breathing bismuth-based MOF capable of separating CO_2 from other gases. It is a thermally stable MOF with a decomposition temperature of 350 °C and a surface area of 473 $m^2\ g^{-1}$. The inorganic building unit (IBU), Bi_2O_{12} dimer, which is related by inversion symmetry, contains two Bi^{3+}, each with seven-coordinated hemidirected polyhedra surrounded by all O-donor atoms from the carboxylate linkers. The Bi–O bond lengths range from 2.3 to 2.7 Å, forming an irregular decahedron coordination geometry around the Bi^{3+} centers (Fig. 3, Table 1).[104]

Isomorphous to SU-100, $Bi_2O(H_2O)_2(C_{14}H_2O_8)\cdot nH_2O$ (SU-101) is a bio-inspired MOF synthesized using common and edible reagents, ellagic acid (a common natural antioxidant) as the linker, and bismuth acetate as the Bi^{3+} precursor, both suspended in aqueous solution and stirred under ambient conditions for 24 hours. The coordination number of Bi^{3+} in SU-101 is six, with hemidirected polyhedra surrounded by 3

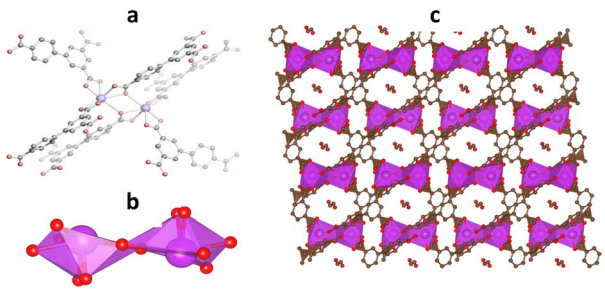

Fig. 3 Structure of SU-100 showing the (a) dimeric unit with three BPT^{3-} bound to each Bi^{3+}, (b) asymmetric Bi^{3+} center with hemi-directed polyhedra and (c) 3D framework with **esg** topology. This figure has been reproduced from ref. 102 with permission from ACS, copyright 2020.

phenolate O atoms, two μ_4-oxygens, and a coordinated terminal water molecule completing the sphere. Given the intermolecular carbon–carbon distance of 3.57 Å, ellagate linkers are in π–π stacking interactions, which further stabilize the structure, with thermal stability up to 250 °C and a surface area of 412 $m^2\ g^{-1}$ (Table 1).

Stock and co-workers reported a microporous bismuth-based MOF, $[Bi_2(O)(OH)(TATB)]\cdot H_2O$ (CAU-35), with 77 $m^2\ g^{-1}$ surface area, containing hemidirected, seven-coordinated, all-O-atom linker surrounded Bi^{3+} spheres. The 3D structure is made of linear IBUs with BiO_7 polyhedra connected into a network similar to a distorted honeycomb topology, with one linker occupying the distorted hexagonal pore (Fig. 4, Table 1).[122]

Another flexible, porous bismuth MOF, $[Bi_4(O)_2(OH)_2(H_2TCPB)(TCPB)(H_2O)_2]\cdot xH_2O$, termed CAU-33, is a similar example of five-coordinated, hemidirected bismuth geometry with an active electron lone pair. The 3D structure is composed of two distinctive Bi^{3+} centers and two TCPB organic linkers, both aligned around the inversion centers. The two distinct Bi^{3+} cations are connected *via* μ-OH and μ_3-oxygen in the rod. Corner-sharing bismuth oxo rods are extended in the *c*-axis and form the IBUs of CAU-33. The rods are linked by

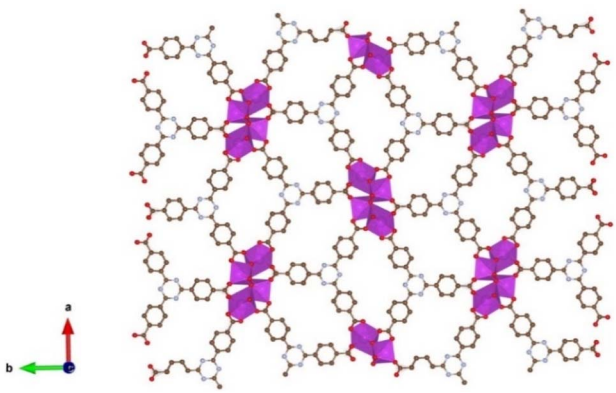

Fig. 4 The crystal structure of CAU-35 view along the *c*-direction. This figure has been reproduced from ref. 119 with permission from ACS, copyright 2002.

H_2TCPB^{2-} and $TCPB^{4-}$ anions into a 3D framework. The compound, having a surface area of 450 $m^2\,g^{-1}$, is stable against common organic solvents, including water at pH 3–11 (Table 1).[123]

2.4.2.2 Non-porous, hemidirected Bi MOMs. There are a large number of reports on the use of non-porous, hemidirected bismuth polyhedra as building blocks. For example, Cheetham and co-workers reported a 3D diamond net, MOCP, [Bi(1,4-BDC)$_2$]·(DMA)(DMF), with a threefold interpenetration.[90] The Bi^{3+} cation is eight-coordinated (BiO_8), surrounded by eight O-atoms from four different BDC linkers. The BiO_8 polyhedra are hemidirected with active lone pairs of electrons. Each Bi^{3+} polyhedron is linked to four other Bi^{3+} polyhedra *via* four different BDC^{2-} anions, leading to an infinite 3D network (Fig. 5).

A dense 3D supramolecular MOCP, Bi(pydc)(Hpydc)(H_2O), reported by us, also features seven-coordinated, hemidirected bismuth (BiO_5N_2) polyhedra.[23] The 3D supramolecular framework is made up of zig–zag 1D chains running along the *c*-axis and connected *via* extensive hydrogen bonds along the *a*- and *b*-axes. The neighboring Bi^{3+} centers within the zig–zag chain are related by 2_1 symmetry along the *c*-axis. O- and N-atoms from $pydc^{2-}$ and $Hpydc^{-}$ anions and one O-atom from the coordinated water molecule complete the coordination sphere, resulting in hemidirected polyhedra around the Bi^{3+} ion in which one of the apexes is taken by the stereochemically active lone pair (Fig. 6).

Besides single-bismuth PBUs, we similarly reported a multi-bismuth IBU cluster bridged by O-atoms, $Bi_3(\mu_3\text{-}O)_2(pydc)(Hpydc)(H_2O)_2$.[44] Using a hydrolytically sensitive bismuth precursor, it decomposed and formed a multinuclear (Bi_6O_4) bismuth-oxo cluster. The centrosymmetric Bi_6O_4 IBU (Fig. 7(a)) consists of Bi_3O_2 repeats that are related by an inversion symmetry, with each made from a BiO_5 distorted hemidirected square bipyramid that shares a common edge with a BiO_5N hemidirected distorted pentagonal pyramid, which, in turn, shares a corner with a BiO_5N_2 hemidirected distorted pentagonal bipyramid. The 2,5-pydc ligands link the Bi_6O_4 IBUs into 2D layers, which are further linked into a supramolecular 3D network *via* extensive H-bonding originating from monoprotonated 2,5-pydc ligands (Fig. 7).

Another multi-bismuth-oxo IBU, Bi_2O_2 cluster containing compound, Bi_2O_2(TA), reported by us, is composed of a planar four-membered Bi_2O_2 ring with bridging μ^2 oxygen (Fig. 8(a)). The whole framework is built around centrosymmetric Bi_2O_2 layers. The asymmetric unit is made of four unique Bi^{3+} cations, four bridging O-atoms, and two independent TA anions. The four unique Bi^{3+} are seven-coordinated, hemidirected $Bi(1)O_7$, $Bi(2)O_7$, $Bi(3)O_7$ and $Bi(4)O_7$, forming a distorted pentagonal bipyramid for Bi(1), Bi(2) and Bi(4), while Bi(3) is a distorted capped octahedra, with a stereochemically active lone pair of electrons (Fig. 8(b)). The Bi_2O_2 are combined into a 2D layer composed of a repeating unit of three different covalently

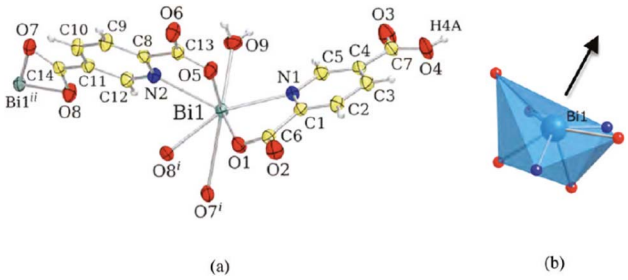

Fig. 6 (a) Bismuth coordination sphere in Bi(pydc)(Hpydc)(H_2O) and (b) distorted hemidirected polyhedron showing the approximate location of the active lone pairs. This figure has been reproduced from ref. 23 with permission from ACS, copyright 2011.

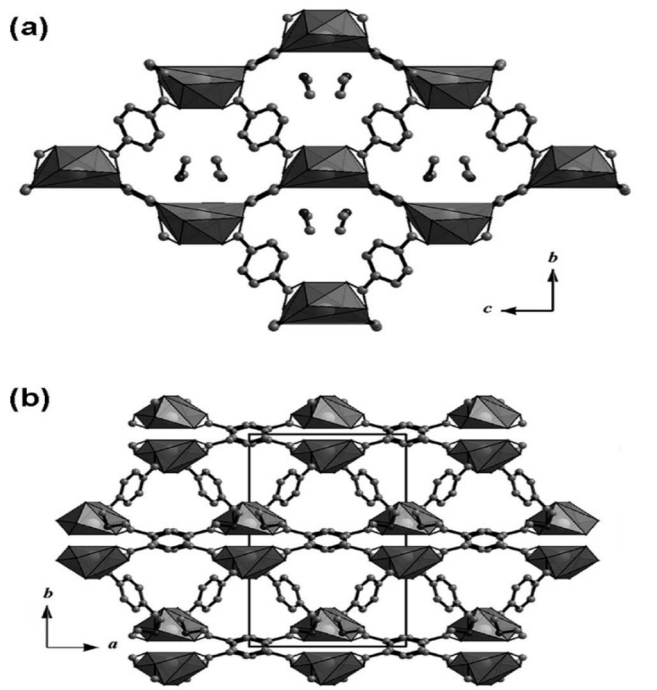

Fig. 5 3D network of [Bi(1,4-BDC)$_2$]·(DMA)(DMF) along the (a) *a*-axis and (b) *c*-axis. This figure has been reproduced from ref. 89 with permission from RSC, copyright 2016.

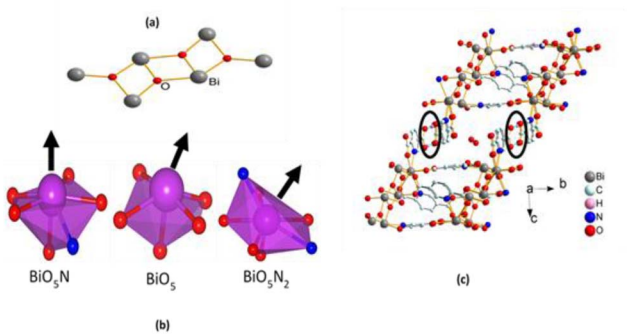

Fig. 7 Centrosymmetric Bi_6O_4 IBU (a), hemidirected polyhedra with the stereochemically active lone pairs (b) and interlinking into a 3D supramolecular compound featuring H-bonds (shown within black circles) (c). This figure has been reproduced from ref. 45 with permission from RSC, copyright 2011.

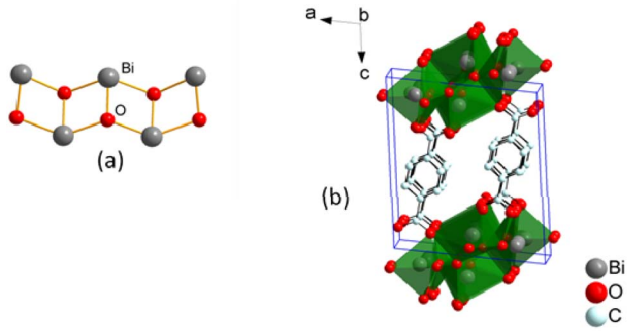

Fig. 8 Bi_2O_2 IBU (a) and covalent bonding into a 2D layer (with green bismuth polyhedra) further pillared by 2,5-pydc ligands (b). This figure has been reproduced from ref. 45 with permission from RSC, copyright 2011.

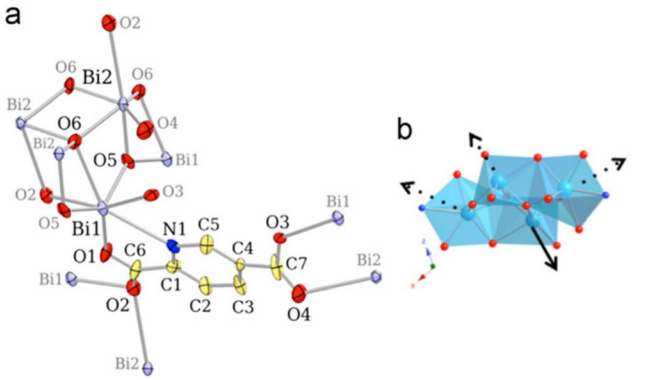

Fig. 9 (a) Labelled asymmetric unit of Bi_2O_2(pydc), depicting the coordination sphere of Bi(1) and Bi(2). (b) Hemidirected distorted polyhedra with arrows indicating the approximate location of the active lone pairs. This figure has been reproduced from ref. 46 with permission from Elsevier, copyright 2012.

bonded chains made from a combination of edge- and corner-sharing distorted bismuth polyhedra. A pillared 3D structure is formed as Bi_2O_2 layers are connected by terephthalate ligands along the *z*-direction.[45]

Using 2-nitro-terephthalic acid (NO_2TA), we reported another multi-bismuth-oxo IBU containing compound, $Bi_4O_3(NO_2TA)_3(H_2O)\cdot(H_2O)_{0.68}$, with an asymmetric unit composed of four unique Bi^{3+} cation centers, three NO_2TA^{2-}, and coordinated and interstitial water molecules. The four unique bismuth cations are surrounded by independent oxo-O-atoms and O-atoms from the NO_2TA^{2-} anions, forming a Bi_4O_3 chain. The four Bi^{3+} centers are $Bi(1)O_7$, a distorted hemi-directed capped octahedron; $Bi(2)O_7$, a hemidirected capped trigonal prism; $Bi(3)O_8$, a distorted capped pentagonal bipyramid; and $Bi(4)O_6$, a hemidirected octahedron. The whole framework is built around a distinct centrosymmetric Bi_4O_3 motif, and the chain of Bi_4O_3 is composed of alternating sequences of Bi(3), Bi(2), Bi(1), and Bi(4) polyhedra that are related by inversion symmetry. The chains are linked to each other by NO_2TA^{2-} linkers along the *ac*-axes, forming a 3D framework.[45]

We further reported another two members, Bi_2O_2 IBU and Bi_2O_2(pydc), mainly composed of Bi_2O_2 chains extended along the *c*-axis, which are linked into a 3D framework by pydc ligands. The N- and O-atoms of the pydc ligands and two oxo-O atoms from thermal degradation of the hydroxo salt surround the coordination sphere of the bismuth ions. The Bi_2O_2 chain contains two unique Bi^{3+} centers, each a six-coordinated hemidirected polyhedron with irregular bond distances. $Bi(1)O_5N$ is a hemidirected pentagonal pyramid, and the $Bi(2)O_6$ is a hemidirected distorted octahedron, all with a stereochemically active lone pair of electrons (Fig. 9). The chains of corner-shared Bi(1)O_5N polyhedra (chain A) and of $Bi(2)O_6$ polyhedra (chain B) are linked *via* edge sharing to form the AB chain. In turn, the AB chain shares edges with the adjacent AB chain, featuring different spatial arrangements (A′B′) to form ABA′B′ chains related by two-fold symmetry along the *a*-direction. The two chains (ABA′B′) are linked into a 2D structure along the *a*-axis and further connected into a chiral 3D framework by pydc ligands.[46] Interestingly, the chirality emerges from an asymmetric binding of the pydc ligands, where the structure is related by 2_1 symmetry in the *c*-axis without an inversion center.

We then presented a mixed metal and mixed valent bismuth-based MOCP using a chiral ligand, 1*R*,3*S*-camphoric acid, $Bi_4Na_4(1R,3S\text{-cam})_8(EtOH)_{3.1}(H_2O)_{3.4}$, a 3D dense MOCP.[46] The framework is built around chains of Bi_2O_2 four-membered IBU extended in the *b*-axis. The Bi_2O_2 is composed of distorted Bi(1)O_6, Bi(2)O_7, Bi(3)O_7 and Bi(4)O_6 polyhedra with the coordination sphere surrounded by O-atoms of the 1*R*,3*S*-cam ligands featuring irregular bond distances. The polyhedra of all the Bi^{3+} centers, Bi(1)O_6, Bi(2)O_7, Bi(3)O_7 and Bi(4)O_6, are hemidirected pentagonal pyramidal, pentagonal bipyramidal, pentagonal bipyramidal, and octahedral, respectively, with a typical stereochemically active lone pair of electrons (Fig. 10). The framework is composed of zig–zag chains that propagate in the *c*-axis. The overall 3D structure has an infinite 2_1 chiral, helical chain stretched in the *c*-axis.

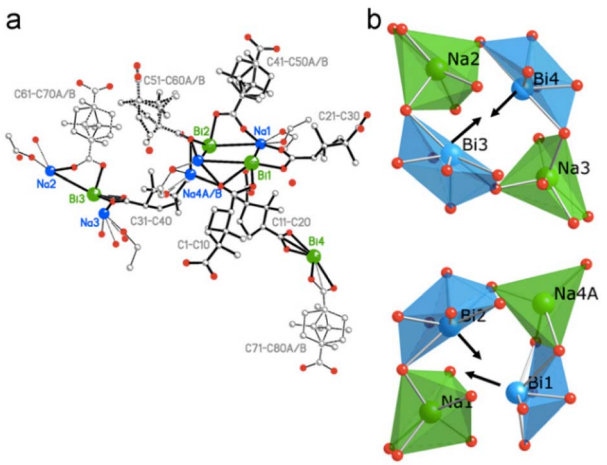

Fig. 10 : Asymmetric unit of $Bi_4Na_4(1R3S\text{-cam})_8(EtOH)_{3.1}(H_2O)_{3.4}$. (b) Hemidirected polyhedra of four unique bismuth atoms with an arrow indicating the lone pair approximate location. This figure has been reproduced from ref. 46 with permission from Elsevier, copyright 2012.

Cheetham and co-workers reported another eight-coordinated, hemidirected (BiO_8) bismuth polyhedra in a mixed metal 3D MOCP ($[NaBi(1,4\text{-}BDC)_2(DMF)_2]$). The 3D structure is composed of alternating BiO_8 and NaO_6 polyhedra linked together into a rhombic 1D channel. The asymmetric unit is composed of one Bi^{3+} and Na^+, two dianion BDC linkers and two DMF molecules. The oxygen atoms in this hemidirected BiO_8 are from four different BDC linkers, with stereochemically active lone pairs of electrons (Fig. 11). The Bi–O bond length is in the range of 2.226(6) to 2.907(4) Å, which further confirms the asymmetric distribution of the ligands around the coordination sphere.[59]

Multivariate, mixed-metal MOCPs are widely used for heterogeneous catalysis. Another multi-metal Bi^{3+}/Cu^{2+} MOCP, $Bi_3O_2Cu(OH)(pdc)_2$, crystallized in the $P\bar{1}$ space group with a 2D inorganic subnetwork featuring an unprecedented structural topology.[60] The asymmetric unit is composed of three unique bismuth centers (Bi(1), Bi(2) and Bi(3)), a single Cu(1), two pdc^{3-} anions, two oxygen atoms (O(9) and O(10)), and one hydroxyl group. The three crystallographically unique Bi^{3+} centers are $Bi(1)N_2O_4$ and $Bi(2)O_6$ in a hemidirected distorted octahedron, and a distorted hemidirected triangular prism, $Bi(3)O_7$, all having an active stereochemical lone pair of electrons (Fig. 12), plus an independent Cu center that connects the PBUs in an infinite inorganic 1D chain. The adjacent inorganic 1D chains are linked by the pyrazole ring of the pdc^{3-} into an infinite inorganic 2D layer.

$Bi_2O_2(HBPT)$ is another dense MOCP with distorted, hemidirected bismuth polyhedra possessing active lone pairs of electrons.[104] The IBU is composed of Bi^{3+} rods connected by six BPT^{3-} anions for each rod sequence. It is composed of two unique bismuth centers having distorted six- and seven-coordinated centers forming hemidirected octahedra and pentagonal bipyramid geometry, respectively, with irregular bond lengths in the range of 2.15 to 2.75 Å. Another non-porous MOCP, described by the same authors, $Bi_6O_4(H_2TPTC)_5$, also features hemidirected bismuth polyhedra with active lone pairs of electrons.[104] A bismuth hexamer cluster connected by four O-atoms makes up the IBU of this compound. There are three distinct hemidirected Bi^{3+} cation centers, two of which are six-coordinated and the other is a seven-coordinated, distorted octahedron with asymmetric bond lengths in the range of 2.0–3.0 Å (Fig. 13).

Natajaran and co-worker reported bismuth carboxylate compounds with brucite- and fluorite-related structures[93] that feature 1D ladder-like chains composed of Bi_2O_2 dimers connected by 2,6-pyridinedicarboxylate anions through μ_3-O, $[C_4N_2H_{10}][Bi(C_7H_4NO_4)(C_7H_3NO_4)]\cdot H_2O$. The seven-coordinated Bi^{3+} (BiO_5N_2) is a distorted capped trigonal prism with a hemidirectional mode of distribution of ligands around the coordination sphere. Such distortion and the irregular bond distances (2.28(4)–2.612(5) Å) around the coordination sphere, with the shortest bond distance (2.28(4) Å) found opposite to the observed gap on the sphere, suggested stereochemically active lone electron pairs. In the same effort, the authors reported another MOCP, $[Bi(\mu_2\text{-}OH)(C_7H_3NO_4)]$, also composed of Bi_2O_2 dimeric units connected into chains by carboxylate groups extended in one dimension. The chains are linked by the N-

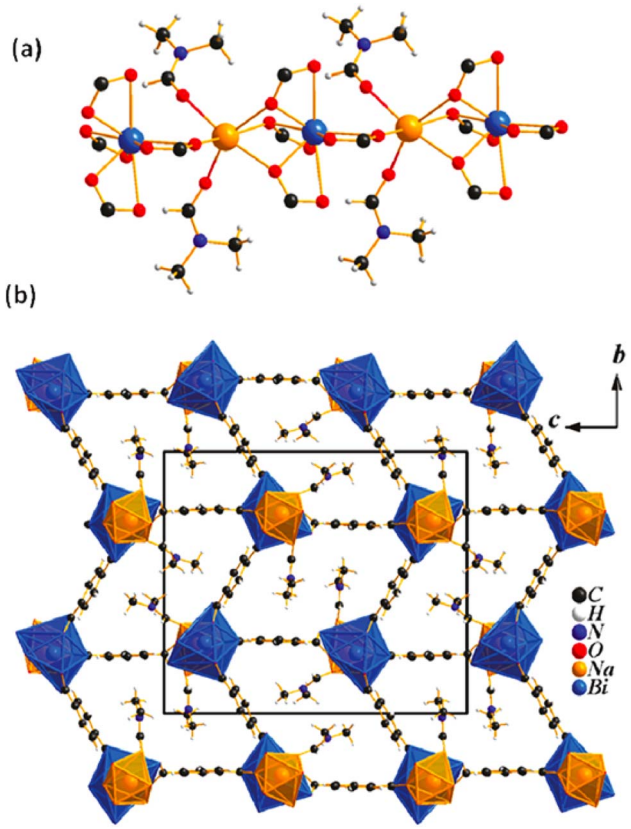

Fig. 11 (a) 1D IBU connectivity of O–Na–O–Bi–O along the *a*-axis and (b) 3D structure showing the 1D rhombic channels along the *a*-axis. This figure has been reproduced from ref. 59 with permission from ACS, copyright 2010.

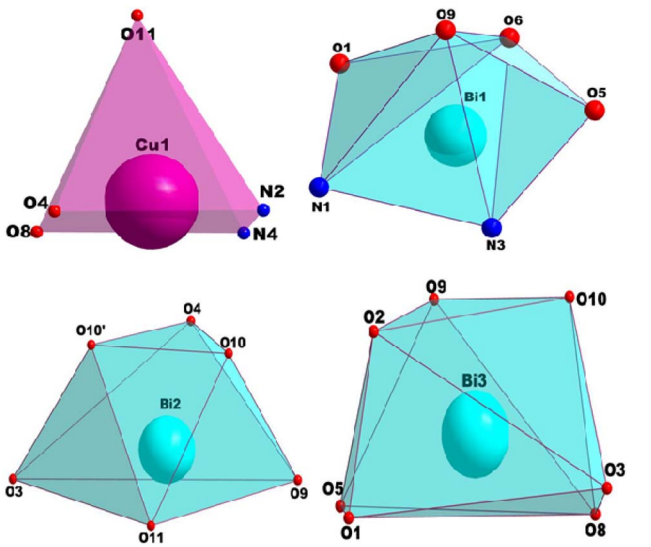

Fig. 12 Geometric representations of the hemidirected octahedra of Bi(1) and Bi(2), capped triangular prism Bi(3) and distorted square pyramid Cu center. This figure has been reproduced from ref. 60 with permission from RSC, copyright 2013.

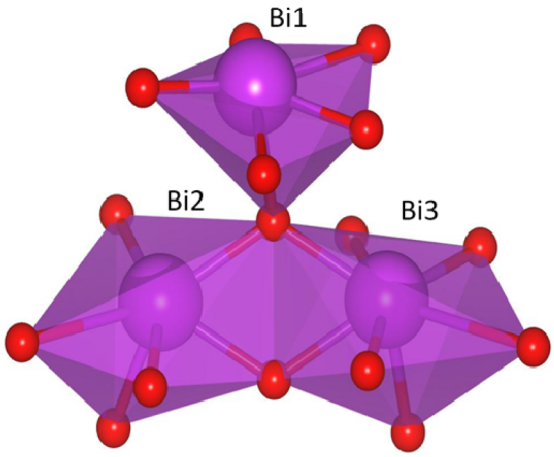

Fig. 13 Hemidirected, distorted polyhedra of Bi1, Bi2 and Bi3 in $Bi_6O_4(H_2TPTC)_5$. This figure has been reproduced from ref. 104 with permission from ACS, copyright 2020.

atom of the pyridine group and an O-atom of the carboxylate group of the 3,4-pyridinedicarboxylate anions. The Bi^{3+} is seven-coordinated ($Bi(OH)_2O_4N$), forming a hemidirected distorted capped octahedra, with asymmetric bond distances and a visible void in the coordination sphere, which is an indication of a stereochemically active lone electron pair.[93] Considering the structure from the perspective of secondary interactions, the Bi^{3+} coordination changes from seven to nine, leading to an infinite Bi–O–Bi connectivity as a 2D layer resembling the so-called Kagomé layer. The Kagomé-related layers are further connected by 3,4-PDC anions into a 3D structure.

Huang and co-workers[96] reported a 1D MOCP with a 3D supramolecular network due to extensive H-bonding. The compound, $[Hbpe][Bi(Hpydc)_2(pydc)]\cdot H_2O$, crystallizes in a triclinic $P\bar{1}$ space group. The Bi^{3+} centers are seven-coordinated, connected by monoprotonated and deprotonated pyridine-2,5-dicarboxylates (Hpydc/pydc) into 1D chains propagated along the crystallographic *b*-axis. The bismuth coordination sphere is surrounded by four O- and three N-atoms of the pydc, forming hemidirected polyhedra with irregular bond distances, with the shortest bond distance opposite the identified void space, an indication of a stereochemically active lone pair of electrons (Fig. 14).

In a one-dimensional bismuth-thiophenemonocarboxylate (TMC) based MOCP, $Hpy[Bi_2(TMC)_6(NO_3)]$,[30] the asymmetric unit is composed of one distinct Bi^{3+} center, three TMC anions, one coordinated nitrate ion, and one pyridinium cation. Adjacent metal centers are connected by the carboxylate group to form a dimer $[Bi_2(TMC)_6]$, which is further connected by nitrate ions into the anionic 1D MOCP, with pyridinium ions located between the 1D chains balancing the charge (Fig. 15(a)). Each bismuth center is surrounded by eight O-atoms from four TMC anions and one nitrate ion. The geometry around the Bi^{3+} center is a distorted hemidirected polyhedron with significant lone pair activity manifested by the identifiable gap in the coordination sphere and irregular bond distances in the range of 2.209(2) to 3.057(4) Å (Fig. 15(b)).

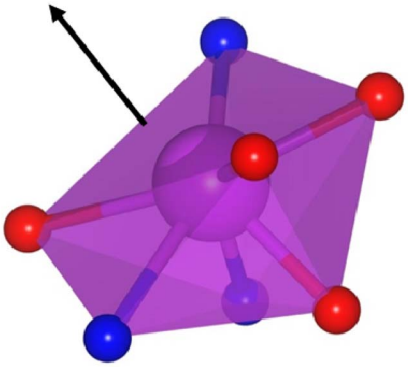

Fig. 14 Hemidirected polyhedra found in $[Hbpe][Bi(Hpydc)_2(pydc)]\cdot H_2O$. This figure has been reproduced from ref. 96 with permission from Elsevier, copyright 2017.

In a typical example of a ferrocene-dicarboxylate based bismuth MOCP, 1D $[Bi_2(\mu_2\text{-}\eta^2\text{-}OOCFcCOO\text{-}\mu_2\text{-}\eta^2)(\eta^2\text{-}OOCFcCOO\text{-}\eta^2)(\mu_2\text{-}\eta^2\text{-}OOCFcCOO\text{-}\eta^2)]_2$,[62] is built from a bismuth dimer, Bi_2O_2, containing two distinct Bi^{3+} centers, Bi(1) and Bi(2), with seven- and eight-coordinated geometry, respectively. Both Bi(1) and Bi(2) have hemidirected distorted polyhedra surrounded by O-atoms from the ferrocene-dicarboxylate ions (Fig. 16(a)). Three different ferrocene-dicarboxylate coordination modes, $\mu_2\text{-}\eta^2\text{-}OOCFcCOO\text{-}\mu_2\text{-}\eta^2$, $\eta^2\text{-}OOCFcCOO\text{-}\eta^2$, and $\mu_2\text{-}\eta^2\text{-}OOCFcCOO\text{-}\eta^2$, connect the Bi(1) and Bi(1) into two dimer motifs as well as linking them into a 1D chain (Fig. 16(b)). One of the linkages results in an extended sixteen-membered heterobimetallic Bi_2Fe_2 macrocycle (Fig. 16(c)).

Another example of ferrocene-based 1D bismuth coordination polymer is a helical $[Bi(\mu_2\text{-}\eta^2\text{-}FcCOO)(\eta^2\text{-}FcCOO)_2]_n$, with the monomeric repeating motif $[Bi(\mu_2\text{-}\eta^2\text{-}FcCOO)(\eta^2\text{-}FcCOO)_2]$. The bismuth is seven-coordinated with hemidirected distorted polyhedra having irregular bond lengths. Three ferrocene-dicarboxylates bind the central bismuth ion, two of which bind in an anisobidentate chelation mode η^2-FcCOO, while the

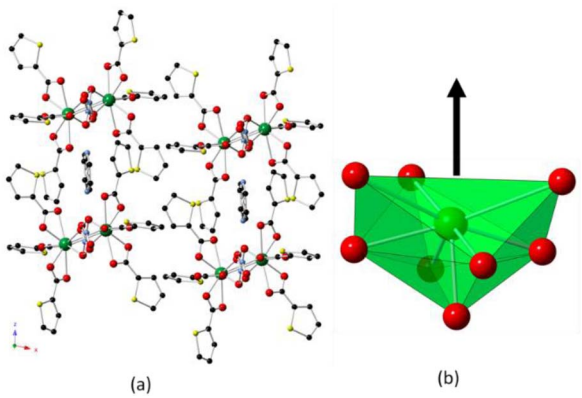

Fig. 15 Structure of 1D $Hpy[Bi_2(TMC)_6(NO_3)]$ showing the (a) chains of anionic $[Bi(TMC)_3(NO_3)]^-$ extended along the *b*-axis with pyridinium cations occupying the interchain space and balancing the charge and (b) distorted, hemidirected polyhedra showing the approximate lone pair location. This figure has been reproduced from ref. 30 with permission from Wiley, copyright 2017.

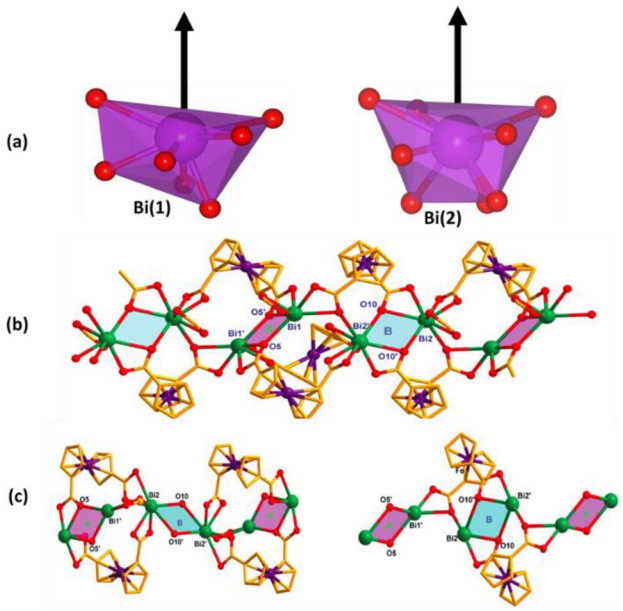

Fig. 16 (a) Hemidirected coordination sphere of Bi(1) and Bi(2), showing the approximate location of the lone pairs of electrons. 1D extended chain showing (b) Bi dimers and (c) alternative repeating motifs found in the compound. This figure has been reproduced from ref. 62 with permission from RSC, copyright 2012.

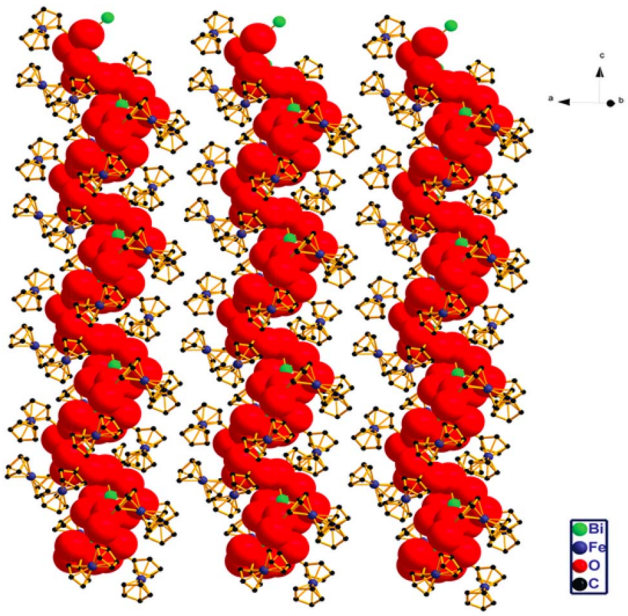

Fig. 18 1D helical chain conformations wrapped with an outer sheath of ferrocene-dicarboxylate in $[Bi(\mu_2\text{-}\eta_2\text{-}FcCOO)(\eta_2\text{-}FcCOO)_2]_n$. This figure has been reproduced from ref. 62 with permission from RSC, copyright 2012.

last one binds in both anisobidentate chelation and bridging modes, μ_2-η^2-FcCOO (Fig. 17). The 1D MOCP adopts a right-handed helical conformation, where the Bi^{3+} PBU chain is wrapped with an outer sheath of ferrocene-dicarboxylate ligands (Fig. 18). Interestingly, this compound showed the absence of a common Bi_2O_2 core commonly present in bismuth-carboxylate-based CPs.[62]

In summary, the hemidirected coordination geometry of Bi^{3+} rises from the stereochemically active $6s^2$ lone pair, which leads to asymmetric ligand distribution and forms distorted polyhedra. This anisotropic electron density creates irregular coordination environments. Although hemidirected polyhedra typically lead to comparably irregular extension with denser structures, there are, however, porous Bi MOFs with good chemical (*e.g.* CAU-33) and thermal stability (up to 350 °C) and medium surface area (up to ~400 $m^2\ g^{-1}$) reported that possess such asymmetric polyhedra geometry.

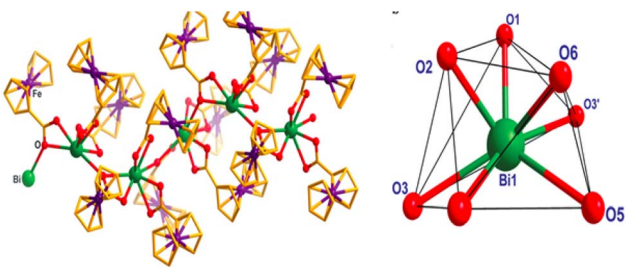

Fig. 17 (a) 1D structure of $[Bi(\mu_2\text{-}\eta_2\text{-}FcCOO)(\eta_2\text{-}FcCOO)_2]_n$ and (b) hemidirected bismuth coordination sphere. This figure has been reproduced from ref. 62 with permission from RSC, copyright 2012.

2.4.3. Bismuth compounds with symmetric (holodirected) polyhedral geometry

2.4.3.1 Porous, holodirected Bi MOFs. The first Bi-based MOF was reported by Stock and co-workers, who used conventional solvothermal and microwave-assisted reactions. The compound, Bi(BTB) (CAU-7, BTB = 1,3,5-benzenetrisbenzoate), was constructed from chains of face-sharing BiO_9 tricapped trigonal prisms with holodirected geometry that were linked into a porous, slightly distorted honeycomb structure *via* BTB ligands.[61] The structure was solved by using a combination of Rietveld refinement, electron diffraction and DFT calculations. It exhibited thermal stability up to 380 °C with a surface area of 1150 $m^2\ g^{-1}$, the highest surface area for Bi MOF to date (Table 2). Another porous and conductive MOF that exhibits enhanced cathode-ray scintillation, termed Bi–SMOF, presents an unconventional strategy for designing phosphors for field emission displays. The Bi–SMOF, $[(Hdma)Bi(1,4\text{-}ndc)_2(\text{-}DMF)]_n \cdot n(DMF)$, was solvothermally synthesized and structurally characterized using single-crystal X-ray diffraction. The asymmetric unit contains one unique Bi^{3+} center coordinated by nine oxygen atoms forming a holodirected, slightly distorted tricapped trigonal prism geometry (Fig. 19). The two 1,4-ndc^{2-} in the asymmetric unit each exhibits a μ_2-coordination mode, connecting other Bi^{3+} centers into an infinite 2D layer along the *ac*-plane. The stack of 2D layers along the *b*-direction held by hydrogen bonding further formed a 3D supramolecular compound.

Topological complexity, but not to a greater extent like those in TM-based MOFs, is common among bismuth-based compounds; in fact, large inorganic IBUs, including layers and rods, are archetypal among bismuth-containing organic–

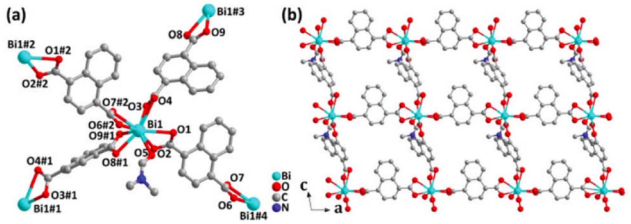

Fig. 19 Structure of Bi-SMOF showing the (a) Bi^{3+} center and the coordination environment of the 1,4-ndc ligands and (b) 2D layer along the *ac*-plane. This figure has been reproduced from ref. 61 with permission from Wiley, copyright 2012.

inorganic compounds. For instance, CAU-17, $[Bi(BTC)(H_2O)]\cdot 2H_2O\cdot MeOH$[12] (Fig. 20 and Table 2), with a surface area of 69.5 $m^2\ g^{-1}$, is an unusually complex bismuth-containing porous 3D extended structure, featuring helical Bi–O rods cross-linked by BTC^{3-} anions. The asymmetric unit is composed of nine Bi^{3+}, nine BTC^{3-}, and nine coordinated water molecules. Each Bi^{3+} is coordinated with nine O-atoms, eight of which are from BTC ligands, and an O-atom from coordinated water completing the coordination sphere to give BiO_9 holodirected polyhedra. Along the *c*-direction, each Bi^{3+} shares four O-atoms with two adjacent Bi^{3+}, forming helical rods made of regular octahedra, with each rod further connected to four other rods.

Another porous Bi^{3+}-based MOF with an interesting structural intricacy is Bi-BTC, $[Bi(BTC)(DMF)]\cdot DMF(CH_3OH)_2$. Synthesized solvothermally using DMF and MeOH, the structure was refined using single-crystal XRD data.[32] The Bi^{3+} center is nine-coordinated by carboxylate O-atoms to give BiO_9 holodirected polyhedra. Five different BTC^{3-} anions and one coordinated DMF complete the coordination sphere. Various coordination modes, including bidentate chelation and monodentate bridging BTC^{3-} anion carboxylates, led to the formation of centrosymmetric Bi_2O_{14} dimeric units. Six BTC^{3-} anions further connect the dimers into a 3D structure that is composed of two distinct 1D helical chains, with right-handed and left-handed chains arranged alternately along the *b*-direction. Ying Bai and his coworkers reported a similar 1,3,5-benzenetricarboxylate-based MOF, $[Bi(BTC)(H_2O)]\cdot H_2O$ (Bi-MOF), which was synthesized solvothermally and characterized using single-crystal XRD data. Bi-MOF features an interesting white-light emission and enables sensing of Fe^{3+} and $Cr_2O_7^{2-}$ ions in water.[105] The asymmetric unit is composed of one unique Bi^{3+} center, coordinated by nine O-atoms, BiO_9, from five BTC^{3-} anions having both monodentate and bidentate chelate coordination mode, further arranged into a symmetric dimer of Bi_2O_{18}. The individual Bi^{3+} center is holodirected, with a stereochemically inactive lone electron pair. The neighboring co-dimers (Bi_2O_{18}) are linked by the BTC^{3-} anions into a 3D network with two distinct types of pore channels.[105]

The Stock group reported a series of bismuth-based porous MOFs, *i.e.* CAU-7-TATB, CAU-7-TATB-NH_2, CAU-31 and CAU-32, all of which possess holodirected Bi^{3+} polyhedra, with surface areas ranging from 104 to 813 $m^2\ g^{-1}$ and thermal stability up to 350 °C (Table 2). Both CAU-7-TATB and its analog, CAU-7-TATB-NH_2, were synthesized using a microwave-assisted reaction at 120 °C and 600 rpm for only 20 minutes and characterized using high-resolution PXRD data and Rietveld refinement.[122] The bismuth centers in these MOFs are ten-coordinated with O-atoms from the TATB anions, forming holodirected polyhedra, BiO_{10}. Face-sharing of the bismuth polyhedra leads to the formation of Bi^{3+} IBUs chains in the *c*-direction. $TATB^{3-}$ anions further linked the chains into a somewhat distorted 3D honeycomb network featuring a 1D channel along the *c*-direction. CAU-31 and CAU-32 were synthesized solvothermally in methanol and a mixture of methanol and DMF, respectively. The CAU-31 structure, $[Bi_2(TCPB)(H_2TCPB)(H_2O)]\cdot xH_2O$, was resolved using Rietveld refinement against data obtained from continuous rotation electron diffraction. The Bi^{3+} center in CAU-31 is composed of holodirected, eight-coordinated O-atoms, in which six O-atoms are chelated from three TCPB carboxylates and coordinated water molecules complete the coordination sphere to give BiO_8 polyhedra. $TCPB^{4-}$ and H_2TCPB^{2-} connectivity lead to a 2D layer with **bex** topology. Inclined interpenetration in the 2D layers results in a 3D interlocked structure.[123] On the other hand, in CAU-32, $(NH_2(CH_3)_2)[Bi(TCPB)(H_2O)]\cdot xH_2O$, the structure was solved using single-crystal XRD data. The Bi^{3+} center in CAU-32 is nine-coordinated holodirected polyhedral BiO_9, with four $TCPB^{4-}$ chelation and one water molecule completing the coordination sphere. Four carboxylate groups are linked to each Bi^{3+}, resulting in a 3D structure featuring 3D channels.[123] The second-highest reported Bi MOF surface area (1014 $m^2\ g^{-1}$) was observed for NOTT-220, with holodirected Bi polyhedra (Table 2). It consists of Bi-dimers with 8- and 9-holodirected coordinated polyhedra with two polymorphs, NOTT-220-α ($Bi(1)O_8$/$Bi(2)O_9$) and NOTT-220-β ($Bi(1)O_9$/$Bi(2)O_8$). The topology of the compound can be represented as **tfi** or **pts** when the ligand is considered as 3- or 4-connected nodes, respectively.[92]

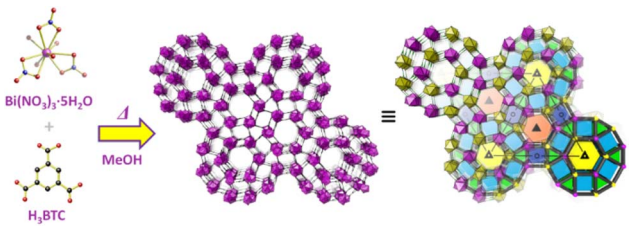

Fig. 20 Structural depiction of CAU-17, showing the bismuth polyhedra in purple and the two periodic htb nets. This figure has been reproduced from ref. 12 with permission from ACS, copyright 2016.

2.4.3.2 Non-porous, holodirected Bi MOMs. Besides the hemidirected, stereochemically active lone pair of Bi^{3+} polyhedra, there exists the non-stereochemically active one. Bi^{3+} polyhedra with non-stereochemically active lone pairs, or so-called holodirected polyhedra, possess slightly distorted, if not regular, polyhedra. As a result, many Bi^{3+}-based MOCPs of this category are reported to have the well-known TM-based MOCP structures. For instance, we reported the first 2D bismuth-based Kagomé lattice motif, featuring slightly distorted bicapped octahedra, holodirected, BiO_6N_2 PBU, with

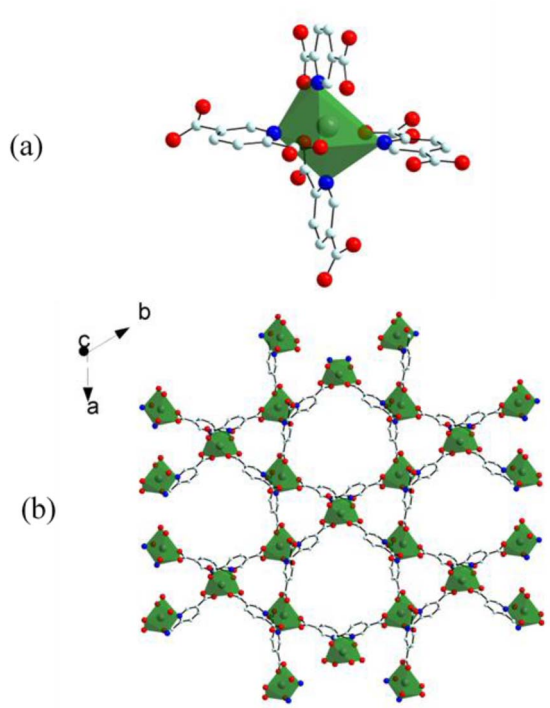

Fig. 21 Four-connected node (2 up and 2 down) of holodirected (green) bismuth polyhedra (a), forming a 2D Kagome lattice (b). This figure has been reproduced from ref. 18 with permission from RSC, copyright 2011.

four 2,5-pydc ligands (two up and two down) that formed a four-connected node (Fig. 21(a)),[18] forming three- and six-membered rings with the overall structure of a 2D polymer with the renowned Kagomé Lattice motif (Fig. 21(b)). This was the first report of bismuth-based CPs, while there are ample examples of TM-based CPs.

We also reported two other four-connected bismuth node, supramolecular coordination compounds, with three "up", one "down" 2,5-pydc ligand arrangements.[23] An interesting anionic layered structure, $K_4Bi(pydc)_3(Hpydc)(H_2O)_{3.3}$, consisting of one $[Bi(pydc)_3(Hpydc)]^{4-}$ complex, four K^- ion positions, and one ordered and five fractionally occupied water molecules. The bismuth coordination sphere is surrounded by four O and four N atoms from pydc and Hpydc ligands, forming a slightly distorted holodirected bicapped-octahedral BiO_4N_4 polyhedron. Three pydc ligands occupied the "up" position, and one Hpydc ligand occupied the "down" position of the bismuth polyhedra viewed along the *b*-axis. The other 1D supramolecular compound, $(DMA^+)_3Bi(pydc)_2(Hpydc)_2$, also shows an interesting three "up", one "down" pydc arrangement. The asymmetric unit comprises one anionic bismuth complex, $[Bi(pydc)_2(Hpydc)_2]^{3-}$, and three dimethylammonium cations (Fig. 22(a)). The coordination geometry around the bismuth is also a holodirected, slightly distorted bicapped octahedron, BiO_4N_4 (Fig. 22(b)), with Bi–O and Bi–N bond distances in the range of 2.362(2)–2.479(2) Å and 2.562(2)–2.610(2) Å, respectively. The bismuth cationic complex is arranged into 1D supramolecular chains extended along the *x*-axis through H-bonding from the monoprotonated Hpydc, which is further balanced by DMA^+ residing in the interchain spaces.

Natarajan and coworker[93] reported Bi^{3+}-carboxylate compounds with interesting brucite- and fluorite-related structures. In Bi(4,5-IDC)(4,5-IDCH) (where 4,5-$IDCH_2$ is 4,5-imidazoledicarboxylic acid), the Bi^{3+} center is eight-fold coordinated with distorted holodirected bicapped trigonal prismatic polyhedra (Fig. 23(a)). The coordination sphere is surrounded by six O-atoms and two N-atoms, BiO_6N_2. The Bi^{3+} centers are linked together by 4,5-IDC anions through the μ_3-oxygen atom (O(3)), forming a 2D bilayer along the *ab*-planes (Fig. 23(b)). Structurally, each 4,5-IDC ligand is bound to three Bi_2O_2 centers, and each center is linked to six 4,5-IDC anions; if the Bi_2O_2 dimer and 4,5-IDC are simplified as single nodes, then the resulting framework mimics the classical inorganic structure, the brucite topology (Fig. 23(c)) commonly observed in CdI_2, $CdCl_2$, or $Mg(OH)_2$.[93]

Another Bi^{3+}-based MOF featuring rutile (**rtl**) topology, a CTH-6, $[Bi_2(cpb)(HOAc)_2(DMF)_4]$ (cpb = 1,2,3,4,5,6-hexakis(4-carboxyphenyl) benzene), reported by the Öhrström group, was also found to have a Bi^{3+} center with holodirected polyhedra, BiO_9 (Fig. 24). Nine O-atoms complete the Bi^{3+} coordination sphere, six O-atoms from three cpb carboxylate groups, two O-atoms from DMF, and one O-atom from acetic acid. The overall structure formed a 3,6-connection in a well-known 3D rutile framework topology.[102]

Using thiophenemonocarboxylic (TMC) acid as a ligand, the Knope group prepared a series of Bi^{3+}-thiophenemonocarboxylate compounds, three of which possess a bismuth center with holodirected polyhedra.[30] $Hpy[Bi(TMC)_3(NO_3)]$ is composed of nitrato bridged anionic dimers, $[Bi(TMC)_3(NO_3)]^-$, balanced by pyridinium cations. Each Bi^{3+} center is a nine-coordinated BiO_9 polyhedron surrounded by all O-atom from three chelating

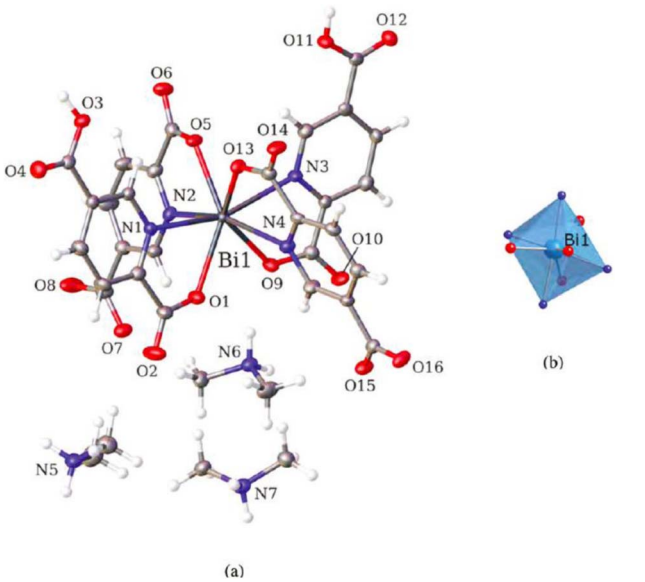

Fig. 22 (a) Asymmetric unit and (b) bismuth coordination geometry in $(DMA^+)_3Bi(pydc)_2(Hpydc)_2$. This figure has been reproduced from ref. 23 with permission from ACS, copyright 2011.

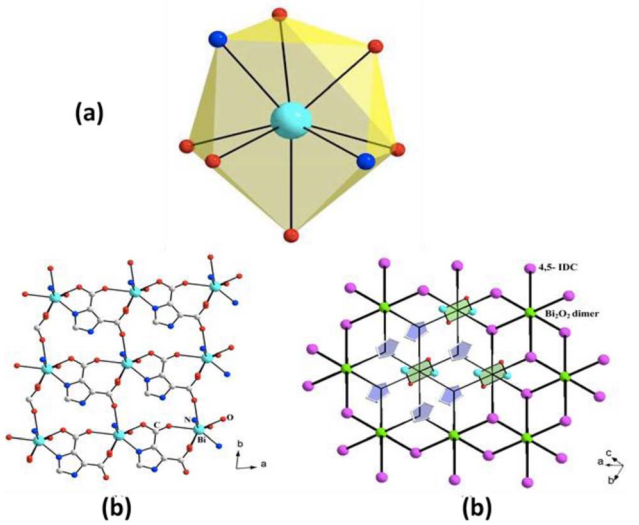

Fig. 23 Structure of Bi(4,5-IDC)(4,5-IDCH) showing the (a) holodirected Bi^{3+} polyhedra, (b) view of the single layer and (c) topological presentation of the (6, 3) net. This figure has been reproduced from ref. 93 with permission from ACS, copyright 2013.

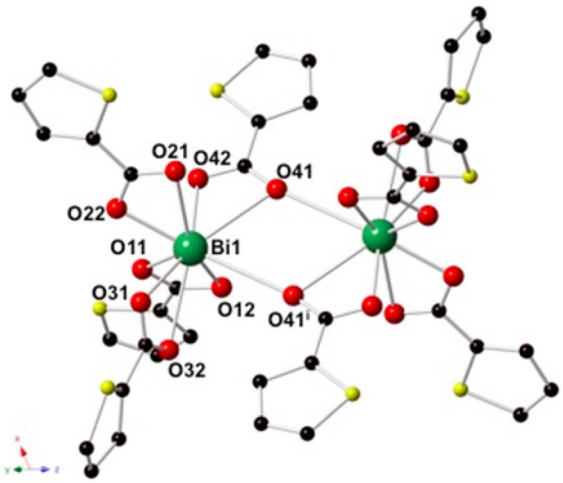

Fig. 25 Anionic dimer of $[Bi_2(TMC)_8]^{2-}$ showing the holodirected BiO_9 polyhedra. This figure has been reproduced from ref. 30 with permission from Wiley, copyright 2017.

TMC anions and two nitrate groups in mono- and bi-dentate fashion. Two Bi^{3+} centers are further bridged into dimers through nitrato groups and through intermolecular forces, including H-bonding and π–π stacking interactions, from which the dimers are stabilized in the structure. The second structure, $Hpy[Bi(TMC)_4]$, comprises an asymmetric unit made of one unique Bi^{3+} center, four TMC ions and a pyridinium cation. All Bi^{3+} centers are similarly nine coordinated O-atoms from five TMC anions to form holodirected BiO_9 polyhedra. Each two BiO_9 polyhedra are bridged by TMC's carboxylate O-atoms to form a binuclear anionic unit, $[Bi_2(TMC)_8]^{2-}$ (Fig. 25). H-bonding between the H-atom of the pyridinium cations and a carboxylate O-atom further stabilizes the structure.

In the third structure, $Hpy[Bi(TMC)_4]$, the asymmetric unit is composed of two unique Bi^{3+} centers, eight TMC anions and two pyridinium cations. Each Bi^{3+} center is holodirected with ten- and eight-coordinated $Bi(1)O_{10}$ and $Bi(2)O_8$ polyhedra, respectively. Similarly, TMC carboxylate O-atoms link two Bi^{3+} polyhedra into a dimeric unit; H-bonding between pyridinium cations and TMC anions further stabilizes the structure.[30]

Using thiophenedicarboxylic acid (H_2TDC), synthesized at room temperature in aqueous solution, the Knope group also reported a series of Bi^{3+}-based CPs featuring holodirected polyhedra.[97] $Hpy[Bi(TDC)_2(H_2O)]\cdot 1.5H_2O$ comprises a unique Bi^{3+} center, two TDC^{2-} anions, one H_2O and one pyridinium cation. The Bi^{3+} center is a holodirected, nine coordinated, in which all O-atoms form the BiO_9 polyhedra (Fig. 26(a)). Bi^{3+} centers are bridged by TDC anions forming zig–zag chains (Fig. 26(c)), further linked into an anionic 2D sheet through TDC anions, charge balanced by pyridinium cations (Fig. 26(b)). These chains combine with other chains (related by inversion symmetry), resulting in an interpenetrated network (Fig. 26(d)). The sheets are stacked together with coordinated water molecules located in the interlayer. H-bonding and strong π–π stacking interactions between proximal thiophene rings across the interlayers further stabilize the structure.

$[Hpy]_3[Bi_2(TDC)_4(HTDC)H_2O]\cdot xH_2O$ possesses an asymmetric unit of two distinct Bi^{3+} centers, four TDC^{2-} anions, one protonated TDC anion, three disordered pyridinium cations and one bound water molecule. The anionic framework is charged-balanced by pyridinium cations. The two Bi^{3+} centers

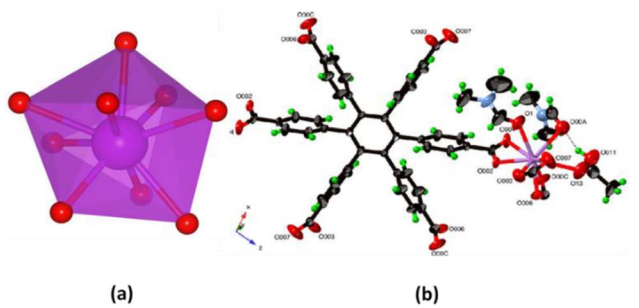

Fig. 24 Structure of CTH-6 showing the (a) holodirected Bi^{3+} polyhedra and (b) asymmetric unit of CTH-6. This figure has been reproduced from ref. 102 with permission from ACS, copyright 2020.

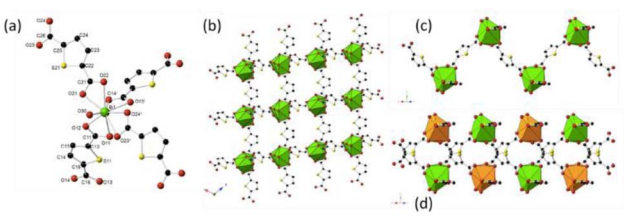

Fig. 26 Structure of $Hpy[Bi(TDC)_2(H_2O)]\cdot 1.5H_2O$ showing the (a) asymmetric unit and coordination sphere, (b) one sheet, (c) single zig–zag chain and (d) interpenetrated chains. This figure has been reproduced from ref. 97 with permission from RSC, copyright 2018.

(Bi(1) and Bi(2)) are ten and nine coordinated O-atoms from the TDC anions to form holodirected $Bi(1)O_{10}$ and $Bi(2)O_9$ polyhedra, respectively. One TDC^{2-} ligand bridges Bi(1) and Bi(2) to give a similar zig–zag chain propagating along the *ab*-plane. TDC ligands further linked the zig–zag chains into interpenetrated 2D sheets packed along the *c*-axis. In $(Hpy)_2[Bi(TDC)_2(HTDC)]\cdot 0.36H_2O$, however, the asymmetric unit is composed of one unique Bi^{3+} center coordinated by ten O-atoms from four chelating TDC^{2-} anions and one monoprotonated $HTDC^-$ anion to give holodirected BiO_{10} polyhedra. TDC^{2-} anions further connect the polyhedra into zig–zag chains that are further connected by TDC^{2-} anions into a thick 2D sheet. These sheets are stacked together through H-bonding between the terminal $HTDC^-$ ligand and a partially occupied water molecule and display π–π stacking interactions between proximal thiophene rings.[97]

The Cheetham group reported four anionic bismuth-based MOCPs, three of which feature holodirected Bi^{3+} polyhedra.[90] In the first MOCP, a two-dimensional $[Bi(1,4\text{-}BDC)_2(DMF)]\cdot(DMA)(DMF)_2$, the asymmetric unit comprises one bismuth cation, two BDC anions, three DMF molecules and one DMA cation. The Bi^{3+} cation possesses a non-stereochemical lone pair, leading to a holodirected, nine-coordinated BiO_9 polyhedron. It is coordinated with eight O-atoms from the BDC ligands and one O-atom from a terminal water molecule. The BDC anions connect each Bi^{3+} cation with four other proximate Bi^{3+} cations, creating a 2D corrugated layered structure. The DMA cations are located between the stacked layers, and the non-coordinated DMF are located both within and between the layers. The second MOCP, $[Bi_4(1,4\text{-}BDC)_7(Him)](DMA)_2(DMF)_2$, is a 3D diamondoid net (**dia**) with two-fold interpenetration. The asymmetric unit comprises two Bi^{3+} cations, three and a half BDC anions, one DMF and one DMA molecule, and a half imidazole molecule. Two distinct Bi^{3+} cation centers are found, each with nine coordinated and holodirected polyhedra. $Bi(1)NO_8$ is coordinated by one N-atom from the terminal imidazole molecules and eight O-atoms from four different BDC anions. While $Bi(2)O_9$ is a nine-coordinated polyhedron surrounded by O-atoms from six unique BDC ligands. Face sharing between $Bi(1)NO_8$ and $Bi(2)O_9$ polyhedra results in dimeric IBU formation, and seven BDC anions connect each dimer with four other proximal dimers to form an infinite 3D structure, with a twofold interpenetrated **dia** topology.[90]

The third MOCP, $[Bi(1,4\text{-}BDC)_2]\cdot(DMA)$, is also a 3D compound featuring two unique Bi^{3+} centers, $Bi(1)O_{12}$ and $Bi(2)O_9$. Both Bi(1) and Bi(2) are holodirected with stereochemically inactive lone electron pairs.[90] Through face sharing, the $Bi(1)O_{12}$ polyhedra connect with two different $Bi(2)O_9$ *via* three carboxylate O-atoms, forming a trimeric IBU, with each trimer linked to six analogous trimers through twelve BDC ions, resulting in the formation of an infinite 3D structure (Fig. 27), featuring twofold interpenetrated primitive cubic packing (**pcu**) topology. The DMA cations are disordered and occupy the spaces between the BDC ions.

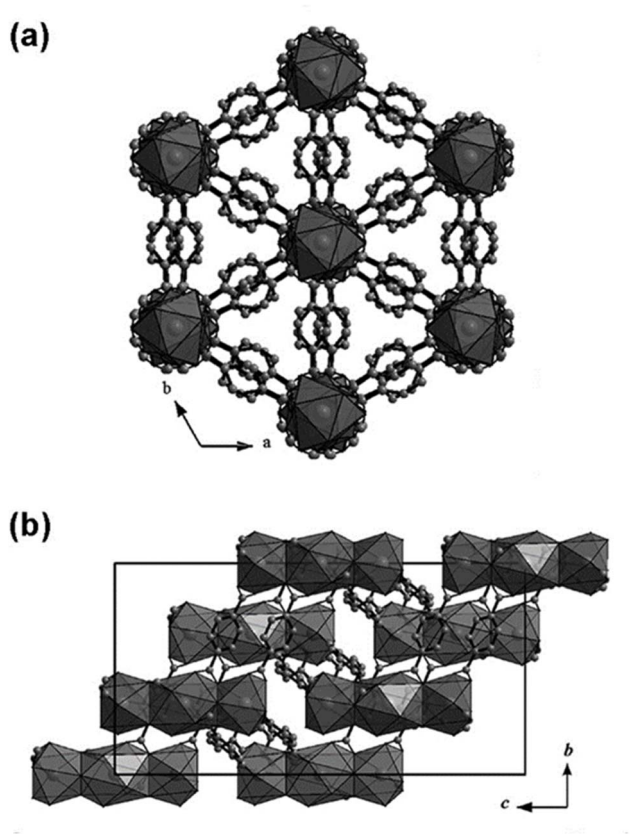

Fig. 27 Structural representation of the 3D $[Bi(1,4\text{-}BDC)_2]\cdot(DMA)$ along the (a) *c*-axis and (b) *a*-axis. This figure has been reproduced from ref. 90 with permission from Wiley, copyright 2010.

A typical example of a heterometallic bismuth-containing 3D MOCP with holodirected bismuth polyhedra was also reported by the Cheetham group.[59] The 3D heterometallic $NaBi[(1,4\text{-}BDC)_2(DMF)(H_2O)]\cdot(DMF)$, contains chains of alternating BiO_8 and NaO_6 polyhedra, which are further linked to each other through BDC ligands into a 3D framework featuring 1D rhombic channels. The Bi^{3+} cation center is eight-coordinated with seven O-atoms from the BDC anions and one coordinated water molecule. The geometry has a symmetrical distribution of ligands with an inactive stereochemical lone pair of electrons. The Bi^{3+} and Na^+ are connected by the BDC anions in the asymmetric unit, leading to the formation of 1D inorganic chains of O–Na–O–Bi–O along the *a*-direction (Fig. 28). The alternating edge- and face-sharing polyhedra of BiO_8 and NaO_6 are further linked by other proximal chains in a 3D framework featuring two types of rhombic 1D channels.

The other heterometallic 3D framework, $NaBi[(1,3\text{-}BDC)_2(DMF)]$, has an asymmetric unit containing one Bi^{3+}, one Na^+, two 1,3-BDC anions and one DMF molecule. The Bi^{3+} cation has nine coordinated O-atoms from five distinct BDC anions, giving a holodirected BiO_9 coordination geometry with a characteristic inactive stereochemical lone pair of electrons. BDC anions connect the Bi^{3+} and Na^+ cations as an infinite 1D IBU chain of alternating Bi^{3+} and Na^+ edge- and face-sharing polyhedra O–Na–O–Bi–O. The chains are further linked through edge-shared Bi^{3+} polyhedra into a 2D inorganic framework. BDC anions bridge the 2D layers into a 3D framework.[59]

Similarly, $Bi_2Co_2C_{42}H_{36}N_6O_{33}$ (BiCo-MCP) is another typical example of heterometallic bismuth-based 2D compounds with

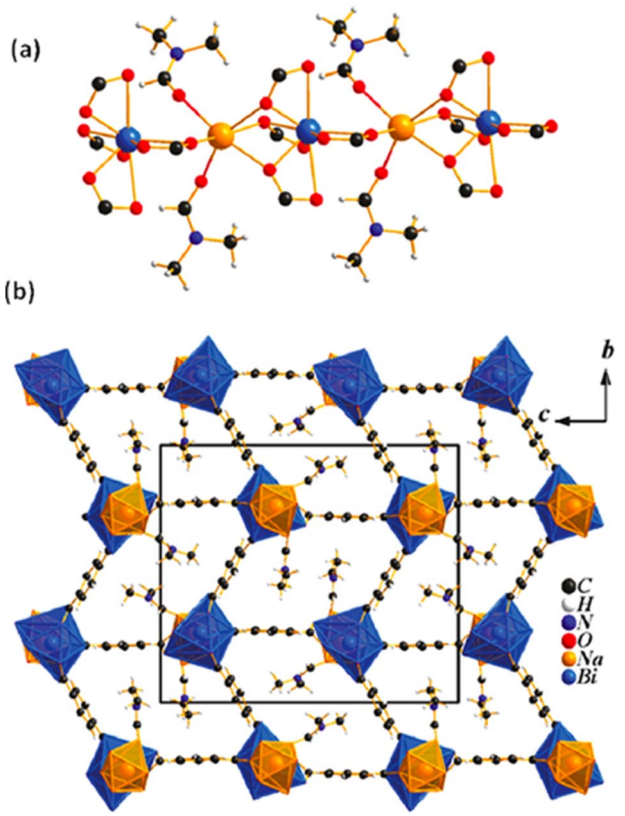

Fig. 28 The structural representation of NaBi[(1,4-BDC)$_2$(-DMF)(H2O)]·(DMF) showing the (a) infinite O–Na–O–Bi–O IBU chains (b) the 3D view of the framework showing the 1D rhombic channels along the *a*-direction. This figure has been reproduced from ref. 59 with permission from ACS, copyright 2010.

holodirected Bi^{3+} polyhedra, synthesized solvothermally with a photocatalytic activity towards the degradation of imidacloprid pesticide in wastewater.[56] The asymmetric unit is composed of two distinct, nine-coordinated Bi^{3+} centers, bound by three distinct 2,4-bipyridine dicarboxylate (2,4-pda^{2-}) anions donating six O-atoms and three coordinated water molecules to give holodirected polyhedra, $Bi(1)O_9$ and $Bi(2)O_9$. On the other hand, the Co^{2+} is a six-coordinated, slightly distorted CoN_3O_3 octahedron in which 2,4-pda ligands act as bridging ligands by chelating Co^{2+} and connecting Bi^{3+} centers to form a 2D layer along the *b*-direction with a staggered arrangement between the Co^{2+} and Bi^{3+} centers.[56]

Ferrocene-dicarboxylic acid-based bismuth CPs are also found to have very interesting structures. For instance, the solvothermal reaction of ferrocene-dicarboxylic acid and triphenyl-bismuth afforded a 1D polymer, $[Bi_2(\mu_2\text{-}\eta^2\text{-}OOCFc\text{-}COO\text{-}\mu_2\text{-}\eta^2)(\eta^2\text{-}OOCFcCOO\text{-}\eta^2)(\mu_2\text{-}\eta^2\text{-}OOCFcCOO\text{-}\eta^2)]_2$, the structure of which was solved from single-crystal XRD data.[62] The asymmetric unit contains two unique Bi^{3+} centers (Bi(1) and Bi(2)), while Bi(1) is a seven-coordinated BiO_7 hemidirected polyhedron, Bi(2) is an eight-coordinated BiO_8 featuring a holodirected square antiprism. Three unique ferrocene-dicarboxylates with different coordination modes surround the coordination sphere of the Bi^{3+} centers and connect them into a 1D CP. The 1D CP features two types of Bi_2O_2 IBUs and their interconnections give rise to a 1D chain (Fig. 29).

The second described compound, $[Bi_2(\mu_2\text{-}\eta^2\text{-}FcCOO)_2(\eta^2\text{-}FcCOO)_4(H_2O)_4]\cdot(2FcCOOH)$, is a dimeric complex. Each bismuth is bound to three ferrocene carboxylate anions in chelating and bridging modes, giving rise to a Bi_2O_2 moiety. The two Bi^{3+} centers are nine-coordinated, holodirected, tricapped trigonal prisms (Fig. 29(c)).

Hakimi and coworkers reported an example of 0D discrete bismuth-pyridine dicarboxylate based compounds, possessing holodirected polyhedra.[94] An anionic complex, $(2\text{-apyH})_2[Bi(pydc)_2(Hpydc)]\cdot 2H_2O$, has an asymmetric unit comprising one distinct Bi^{3+} cation, two unprotonated and one protonated pydc ligands, two H_2O molecules and two 2-$apyH^+$ cations. The Bi^{3+} center is a nine-coordinated, holodirected polyhedron surrounded by six O-atoms and three N-atoms, BiO_6N_3. Through H-bonding between the 2-$apyH^+$ cation, carbonyl groups and H_2O molecules, the anionic monomers are linked into a 3D supramolecular compound. Similarly, $(4\text{-apyH})_2[Bi(pydc)(Hpydc)_2]\cdot 4H_2O$ is also a discrete 0D anionic complex balanced by 4-$apyH^+$ cations. The asymmetric unit is composed of one unique Bi^{3+} center coordinated by nine atoms, six O-atoms and three N-atoms from one $pydc^{2-}$ and two $Hpydc^-$ to give rise to holodirected BiO_6N_3 polyhedra with stereochemically inactive lone electron pairs. All the pyridine carboxylates adopt similar coordination modes, forming anionic monomeric units. Through H-bonding between carboxylate and 4-apyH, each monomeric unit is connected to three 4-$apyH^+$ cations, resulting in an interesting 3D supramolecular structure. Another compound, $(pipzeaH)_2[Bi_2(pydc)_3(pydcH)(H_2O)_2]\cdot 5H_2O$, features two types of dimeric units, one

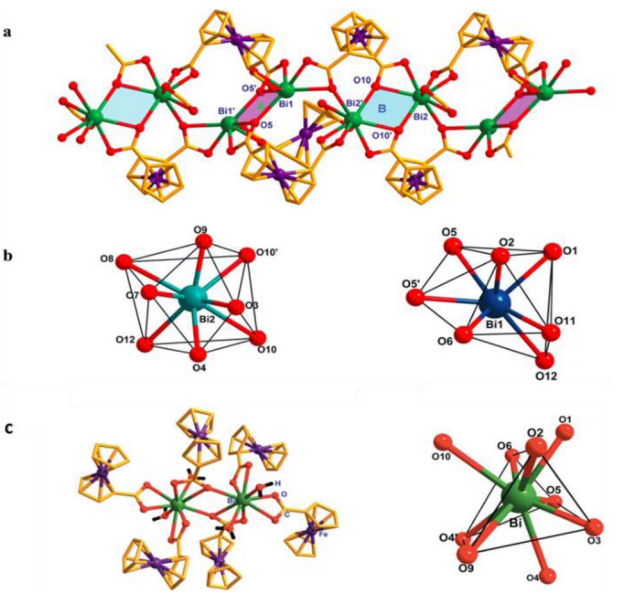

Fig. 29 (a) One-dimensional structure showing the alternating Bi_2O_2 four-membered rings (ring A and B). (b) Bi(1) and Bi(2) polyhedra showing the coordination environments. (c) Dimeric unit of $[Bi_2(\mu_2\text{-}\eta_2\text{-}FcCOO)_2(\eta_2\text{-}FcCOO)_4(H_2O)_4]\cdot(2FcCOOH)$ and the corresponding geometry. This figure has been reproduced from ref. 62 with permission from RSC, copyright 2012.

neutral $[Bi_2(pydc)_2(pydcH)_2]$ and one anionic $[Bi_2(pydc)_4]^{2-}$ complex. The asymmetric unit of this complex is composed of two distinct Bi^{3+} eight coordination centers, bound by six O-atoms and two N-atoms to give holodirected bicapped octahedra with a slight effect of the lone electron pair activity. Both the neutral and the anionic dimeric units are disposed through alternating rows along the [010] plane, giving rise to a 3D supramolecular structure parallel to the *c*-axis. The structure is further stabilized through H-bonding and π–π stacking interactions.[94]

In a similar way, using pyridine-tricarboxylic acid through high-throughput investigation, four novel Bi^{3+}-based MOCPs featuring holodirected polyhedra were reported by the Stock group. Through varying the molar ratios of the starting materials, Bi^{3+} salt, 2,4,6-pyridinetricarboxylic acid (H_3PTC), NaOH, HNO_3 and H_2O, and the reaction time, four MOCPs, *i.e.* $[Bi(PTC)(H_2O)_2]$, $(H_3O)[Bi_2(PTC)(HPTC)_2(H_2O)_2]$, α[Bi(PTC)] and β[Bi(PTC)] were synthesized. $[Bi(PTC)(H_2O)_2]$ features a 2D layered framework and the asymmetric unit contains one unique Bi^{3+} cation center, one PTC anion and two coordinated H_2O molecules. The Bi^{3+} cation center is a nine-coordinated, holodirected, monocapped square antiprism, $BiNO_8$, surrounded by three PTC^{3-} and H_2O molecules. Fully deprotonated PTC^{3-} anions link the $BiNO_8$ polyhedra into an edge-sharing IBU chain. The IBU chains are further connected into layers by PTC^{3-} anions, and H-bonding between carboxylate O-atoms and coordinated H_2O molecules connect the layers to each other. Similarly, $(H_3O^+)[Bi_2(PTC)(HPTC)_2(H_2O)_2]$ is also a 2D layered structure with two unique Bi^{3+} centers, each is an eight-coordinated, holodirected, slightly distorted square antiprism bound by O- and N-atoms from PTC^{3-} anions. The coordination sphere of the $Bi(1)NO_7$ polyhedron is surrounded by four $HPTC^{2-}$, while $Bi(2)N_2O_6$ polyhedra are bound by two $HPTC^{2-}$ and one PTC^{3-} anions. The IBU is made of an alternating chain of edge and corner-sharing $Bi(1)NO_7$ and $Bi(2)N_2O_6$ polyhedra linked by PTC^{3-} anions into a 2D layer. The 2D layers are joined by a network of H-bonding between H_3O^+ residing in the interlayer space and O-atoms from the proximal carboxylate. On the other hand, α[Bi(PTC)] is a 3D framework and the asymmetric unit comprises one unique Bi^{3+} cation center and one PTC^{3-} anion. The Bi^{3+} cation center is bound to six PTC^{3-} molecules, leading to a coordination number of eight, $BiNO_7$, a holodirected, marginally distorted square antiprism. In this compound, the IBU unit is composed of a dimeric unit of edge-sharing $BiNO_7$ polyhedra linked by PTC^{3-} anions. Each dimer is surrounded by ten PTC^{3-} molecules, which further link 24 more dimers. β[Bi(PTC)] is a polymorph of α[Bi(PTC)], also a 3D MOCP, however the Bi^{3+} cation center is bound with five PTC^{3-} anions, leading to a nine coordination number. The polyhedron is a holodirected, monocapped square antiprism, $BiNO_8$. The IBU unit also consists of a dimeric unit formed by edge-sharing polyhedra, further connected into a 1D chain along the *z*-axis. The chains are further linked into a 3D framework through PTC^{3-} anions.[99]

Using heterocyclic dicarboxylate ligands, dithieno[3,2-*b*:2′,3-*d*′]thiophene-2,6-dicarboxylic acid (DTTDC), García-Sánchez and coworkers prepared a porous Bi^{3+}-based MOF, $[Bi_{12}(DTTDC)_{24}]\cdot 23DMA\cdot 4DMF\cdot 2H_2O$ (IEF-5).[124] The PBU in IEF-5 is composed of three Bi^{3+} centers $[Bi_3(-COO)_{12}]^{3-}$ linearly arranged and connected by twelve carboxylate groups from $DTTDC^{2-}$ anions. Two parallel $DTTDC^{2-}$ ligands linked each PBU with six proximal PBUs into an anionic **pcu** topology, charge-balanced by DMA cations. The three distinct Bi^{3+} centers in the trinuclear $[Bi_3(-COO)_{12}]^{3-}$ are all holodirected eight-, ten- and eight-coordinated polyhedra for Bi(1), Bi(2) and Bi(3), respectively.[124]

Our group also reported a highly water-stable and proton-conducting MOCP that was also synthesized by using a heterocyclic dicarboxylate ligand, pyrazine-2,3-dicarboxylate (pzdc).[125] The 2D MOCP, $(Imi)_2[Bi_2(pzdc)_4]\cdot 2H_2O$, is composed of two distinct Bi^{3+} centers in the asymmetric unit, each with a coordination number of nine. Five $pzdc^{2-}$ bound the coordination sphere donating both N- and O-atoms to give holodirected, marginally distorted bicapped pentagonal bipyramids, $Bi(1)N_2O_7$ and $Bi(2)N_2O_7$, featuring a symmetric coordination environment with no lone pair spectrochemical activity (Fig. 30). The 2D layer is made from chains of Bi(1) and Bi(2) polyhedra bridged by pzdc ligands. The adjacent 2D layers are linked by H-bonding between imidazolium cations and the $pzdc^{2-}$ anions.[125]

From this subsection, we can conclude that, unlike structures built from hemidirected polyhedra, holodirected polyhedra with more symmetrical building blocks, in general, self-assemble into less dense structures adopting prototypical topologies that are well-known in reticular chemistry-guided transition-metal-based MOMs. Several Bi MOFs were reported that possess holodirected PBU geometry, such as Bi-SMOF, CAU-7-TATB, CAU-17, CAU-31, CAU-33, and NOTT-220, with surface area reaching 1150 $m^2\ g^{-1}$ and remaining thermally stable up to 380 °C.

2.5 Bi MOMs derivatives

Bi MOMs derivatives, especially bismuth oxide and sulfide, have attracted considerable interest due to their improved structure

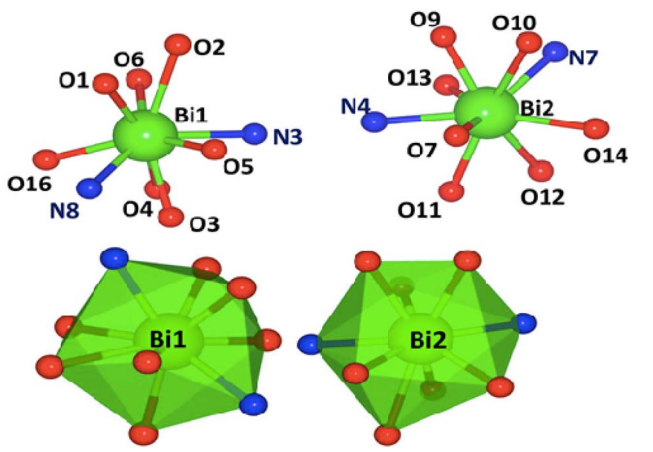

Fig. 30 Holodirected and bicapped pentagonal bipyramids of the Bi(1) N_2O_7 and $Bi(2)N_2O_7$ polyhedra of 2D $(Imi)_2[Bi_2(pzdc)_4]\cdot 2H_2O$, respectively. This figure has been reproduced from ref. 125 with permission from Taylor & Francis, copyright 2021.

stability, large surface area, tunable morphology, and improved physicochemical properties. Typically, these derivatives are obtained through sulfurization or thermal treatment (calcination) of Bi-based MOMs. Bismuth oxides have been widely used for applications in gas sensing, photocatalysis, and energy storage because of their visible light activity and suitable band structure. Bismuth sulfides exhibit excellent catalytic performance and electrical conductivity, making them attractive for environmental and electrochemical applications. Moreover, employing Bi MOMs as a precursor provides a prefabricated template that can form porous structured materials with controlled size, porosity, shape, and phase through a facile calcination process.[126–128] Bi_2O_3@C microrods, for example, were synthesized from Bi-BTC CAU-17 by calcination at 500 °C under N_2 atmosphere for 2 h.[129] An example of Bi_2S_3-derived Bi MOM, with nanorod morphology, was reported by Tianran Hao and coworkers wherein they used a bismuth coordination polymer of trithiocyanuric acid as the precursor for the hydrothermal reaction at 160 °C for 12 h.[130] A single atom site can also be made from MOF precursors using similar, but controlled, calcination methods. One example was reported by Erhuan Zhang *et al.*, who used Bi-BTC MOF (CAU-17) as a precursor to synthesize single-atom Bi by pyrolysis at 600 °C under 1.45 mbar Ar pressure in the presence of dicyandiamide as an N source to form Bi–N_4 sites on porous carbon.[131] Single-atom site catalysts are known to be highly regio- and site-selective for hydroformylation, hydrosilylation, hydroboration, hydrophosphinylation, hydrogenation, azide–alkyne click chemistry, carbenoid insertion, hydrogen–deuterium exchange, and difunctionalization of alkenes.[132]

3. Potential applications

3.1 Electrochemical sensors

In sensing applications, bismuth-based MOFs (Bi MOFs) have gained increasing interest owing to the distinctive characteristics of bismuth, including its environmentally benign nature, stereochemically active $6s^2$ lone pair of electrons, and versatile coordination behavior. These features make Bi MOFs promising platforms for a wide range of applications, from electrochemical and fluorescent sensing to photocatalysis, gas detection, and biomedical diagnostics.[133,134] In particular, Bi-MOFs have been widely explored for electrochemical,[134] photoluminescent,[135] colorimetric,[50] and photoelectrochemical sensing,[136] attributed to their excellent redox-active centres, and compatibility with nanomaterial composites, as summarized in Table 4.

In most cases, MOF-based electrochemical sensors operate as illustrated in Fig. 31.[134] The diagram depicts the fundamental working principle of a nanomaterial-modified electrochemical sensor designed for analyte detection in complex matrices such as food and water. The system comprises three primary components: the analyte, the receptor, and the transducer. The analyte (*e.g.*, H_2O_2, glucose, urea, ethanol, or heavy metal ions) interacts with a specific receptor immobilized on the sensor interface. These receptors, which may include enzymes, carbon nanotubes, graphene, or MOF-based nanomaterials, are tailored to selectively recognize and bind the target analyte. Following analyte recognition, the resulting physicochemical change is transformed into an electrical signal by a transducer, commonly an electrode or thermistor. This signal is then amplified to improve sensitivity and resolution, yielding distinct electrochemical outputs for analysis.

The incorporation of MOFs and other nanomaterials enhances sensor performance by providing high surface area, tunable porosity, and excellent conductivity. These characteristics contribute to improved sensitivity, selectivity, and lower detection limits, making MOF-based electrochemical sensors highly effective for monitoring trace contaminants in food and environmental samples.[134,135]

Another important class of electrochemical sensors includes gas sensors, which are widely used for the detection of hazardous gases and volatile organic compounds in environmental and industrial monitoring applications. A novel electrochemical sensor for detecting lead (Pb^{2+}) ions in water was developed utilizing a nanocomposite of bismuth oxide (Bi_2O_3) nanoparticles and carbonized UiO-66-NH_2 metal–organic framework (MOF). The sensor was fabricated through a one-step calcination process, resulting in a material with enhanced surface area and active sites conducive to Pb^{2+} ion detection. Characterization techniques, such as scanning electron microscopy (SEM), transmission electron microscopy (TEM), and X-ray photoelectron spectroscopy (XPS), confirmed the successful synthesis and structural integrity of the nanocomposite. Electrochemical testing demonstrated that the sensor exhibited a wide linear detection range from 2 to 130 μg L^{-1} and a low detection limit of 0.05 μg L^{-1} for Pb^{2+} ions. The sensor also showed excellent stability, repeatability, and resistance to interference from other ions, making it suitable for practical applications, such as monitoring lead contamination in water environments.[137]

In addition, Bi-MOFs gas sensors have shown great promise in detecting gases, such as NO_2, acetone, and triethylamine, at room temperature.[138] Studies using Bi_2Se_3 and ZnO–Bi_2O_3 heterojunctions have enabled highly selective and sensitive detection platforms, with quick response and recovery times, making them suitable for environmental monitoring. M. Xu *et al.* developed a triethylamine (TEA) gas sensor using bismuth molybdate (Bi_2MoO_6) nanorods derived from a metal–organic framework (MOF). The sensor exhibited high sensitivity and selectivity towards TEA, with rapid response and recovery times. The enhanced performance is attributed to the unique nanorod morphology and the high surface area provided by the MOF-derived structure. This study demonstrates the potential of MOF-derived Bi_2MoO_6 nanorods in developing efficient gas sensors for environmental monitoring applications.[139]

3.2 Colorimetric sensors

Bismuth-based metal–organic frameworks (Bi MOFs) have shown considerable promise as colorimetric sensors due to their peroxidase-mimicking nanozyme activity, high surface area, and chemical tunability. These properties allow Bi MOFs to catalyze chromogenic reactions, enabling rapid, visual

Table 4 Application summary of some important Bi MOMs and their derivatives

Ad hoc name	Bi-(S or O)	Conversion	Application area	Advantages	Limitations	Ref
UiO-66-NH_2	—	—	Electrochemical sensors	Good reproducibility, high efficiency, good selectivity, and environmentally friendly alternative	High cost, less scalability, and limited long-term validation	137
CAU-17-derived Bi_2MoO_6	Oxide	Annealed at 450 °C		High sensitivity, low detection limit, fast response, good selectivity, and low-cost sensor	High operating temperature	139
Bi-BDC-NH_2@Au	—	—	Colorimetric sensors	Very strong innovation, high sensitivity, good stability, low-cost, and easy to use	Depending on external device and complex sensing mechanism	141
CAU-17-derived Bi_2S_3	Sulfide	*In situ* ion-exchange	Photoelectrochemical sensors	Good biocompatibility and selectivity, good stability, and high reproducibility	Less scalability and complex synthesis	142
Bi-BTC-Cu-TCPP	—	—		Good selectivity, high reproducibility, and low detection limit	Narrow detection range, high cost, and limited scalability	134
—	—	—	Photoluminescence sensors	High luminescence efficiency and high sensitivity	Complex synthesis	135
Bi-MOF	—	—		Good performance in real samples and high selectivity	Stability	145
NOTT-220	—	—		Good fluorescence stability and high sensitivity and repeatability	Less stable in biological environment and high cost for lanthanide elements	144
Bi-TCBPE ($[Bi(TCBPE)(H_2O)]\cdot(Me_2NH_2^+)$)	—	—		High sensitivity and selectivity toward Fe^{3+}	Less stable in biological environments, high cost, and scalability	133
$[Bi(BTC)(DMF)]\cdot DMF$	—	—	Photocatalytic activity	High porosity and good adsorption ability	Moisture sensitivity, poor electrical conductor, and low stability	149
$Bi_2O_2CO_3$/g-C_3N_4	Oxide	Calcination at 550 °C		Low cost, environmentally friendly, and recyclability	Scalability and complex synthesis	150
BiOBr/$Bi_{24}O_{31}Br_{10}$	Oxide	Annealed at 450 °C		Good pH adaptability, stability and recyclability	High cost and scalability	151
Bi-TATB and Bi-BTC	—	—		Good selectivity	Moisture sensitivity and high cost	152
Bi SAs/NC	—	—	Electrocatalytic reduction	Good selectivity and environmentally friendly	High cost and limited long-term validation	131
Bi_2O_3@C	Oxide	Annealed to 500 °C	Supercapacitor	High energy storage performance, long lifetime, and environmentally friendly	Incomplete real device testing	129
MOF-836	—	—		Low cost, renewable energy integration, and good long-cycle performance	Synthesis complexity	156
Bi_2Se_3@NC	—	—		Long lifetime and fast charging capability	High cost and not tested for high energy-density applications	157 and 158
BiI_3Cl_2	—	—	Ferroelectricity	Large spontaneous polarization, low cost, and room temperature operation	Low stability and scalability	86
$NaBi(1,4\text{-}BDC)_2(DMF)_2$	—	—	Photoluminescence	Good selectivity	High cost and low stability	59

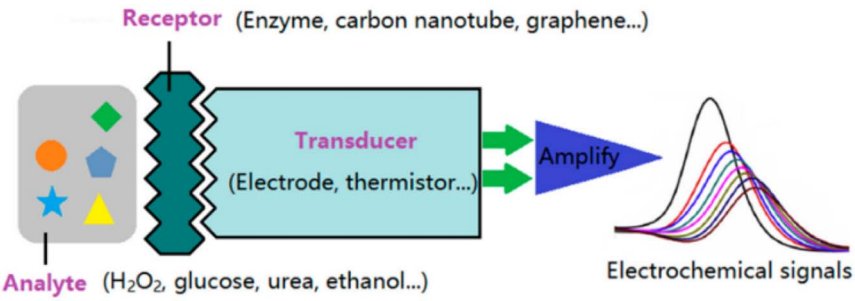

Fig. 31 Schematic of a Bi-MOF based electrochemical sensor platform. This figure has been reproduced from ref. 134 with permission from Elsevier, copyright 2024.

detection of various analytes in environmental and biomedical samples.

Q. Y. Yang *et al.* synthesized a Bi MOF nanozyme capable of catalyzing the oxidation of 3,3′,5,5′-tetramethylbenzidine (TMB) in the presence of hydrogen peroxide, with the help of Cr^{6+} as both promoter and analyte. The system produced a blue-colored product whose intensity decreased linearly with increasing concentrations of Cr^{6+}, enabling sensitive and selective colorimetric detection of chromium ions.[50] In a separate study, El-Sewify *et al.* developed a dual-mode detection platform based on Zr MOFs for the detection of Bi^{3+} ions. Although the MOF used was not bismuth-based, the interaction of Bi^{3+} with the MOF induced a distinct color change from colorless to yellow, complemented by fluorescence quenching. This dual-mode strategy enhanced sensitivity and allowed both visual and spectroscopic detection routes.[140] Further advancing practical applications, C. Jin and co-workers reported a paper-based, triple-readout biosensor for point-of-care detection of glucose in urine. The system incorporated a Bi-MOF nanozyme that catalyzed a glucose oxidation cascade, producing a measurable colorimetric signal alongside fluorometric and photothermal outputs. The platform enabled rapid, low-cost, and non-invasive glucose monitoring, demonstrating the utility of Bi-MOFs in integrated diagnostic devices.[141]

Overall, these studies show that Bi-MOFs are versatile and effective for colorimetric sensing, making them suitable for portable and easy-to-use sensors in real-world applications.

3.3 Photoelectrochemical sensors

Bi MOFs have recently gained attention as effective components in photoelectrochemical (PEC) sensing platforms, owing to their light-responsive semiconducting properties, structural tunability, and ability to promote charge separation. For example, a visible-light-driven PEC aptasensor using a Ce-UiO-66/Mn:Bi_2S_3 heterojunction was constructed for the detection of ofloxacin. In this system, Bi_2S_3 acted as a photosensitizer, enhancing photocurrent generation and overall sensitivity.[136] Similarly, S. Wang and colleagues developed a self-screening PEC biosensor based on a CAU-17-derived Bi_2WO_6/Bi_2S_3 heterojunction for the detection of quorum-sensing molecules. The heterojunction improved visible-light absorption and charge transfer, while the inclusion of aptamer-bound MoS_2 quantum dots modulated the photocurrent through a dual-inhibition mechanism.[142] In another example, a PEC sensor was devised based on a Bi-MOF nanosheet electrode functionalized with copper porphyrinic ligands, which significantly enhanced photoactivity and sensitivity for the detection of hydrogen peroxide.[143]

These studies collectively demonstrate the potential of Bi-MOFs as efficient photoactive materials in photoelectrochemical sensors, where they enhance light harvesting, charge transport, and photocurrent response for the ultrasensitive detection of a wide range of analytes. Importantly, the sensing mechanisms underlying these systems are based on the generation of photocurrent upon light irradiation, which fundamentally differentiates photoelectrochemical sensors from colorimetric sensors that rely on visible color changes for analyte detection.

3.4 Photoluminescence sensors

Unlike photoelectrochemical sensors, which rely on light-induced photocurrent responses, luminescence-based sensors detect target analytes by measuring changes in emitted light intensity, typically through fluorescence or phosphorescence. Bi-MOFs have shown considerable promise in luminescence sensing due to their structural tunability, strong coordination with lanthanide ions, and intrinsic fluorescence or quenching properties. When doped with luminescent rare-earth ions, such as Eu^{3+} or Tb^{3+}, or designed to interact with analytes that modulate emission intensity, Bi-MOFs offer highly sensitive, selective, and real-time optical detection of a wide range of molecules. For example, L. Xu *et al.* developed a Bi-MOF functionalized with Eu^{3+} and Tb^{3+} ions for the ratiometric fluorescence detection of dipicolinic acid (DPA), a key biomarker of bacterial spores. In this system, DPA selectively enhanced Eu^{3+} emission while quenching Tb^{3+} fluorescence, enabling accurate quantification based on the fluorescence intensity ratio. This dual-lanthanide strategy improved signal reliability by mitigating the influence of environmental variability and background interference.[135]

Similarly, L. Song and co-workers constructed an Eu^{3+}-doped Bi-MOF for the selective detection of serotonin (5-HT). The presence of 5-HT resulted in a clear fluorescence quenching response, enabling quantitative analysis with high specificity,

even in complex biological samples.[144] L. Peng *et al.* reported a Bi-MOF nanozyme that mimicked peroxidase activity and catalyzed a fluorescent reaction in the presence of hydrogen peroxide (H_2O_2). The system not only allowed for sensitive H_2O_2 detection but also distinguished between phenylenediamine isomers based on differential fluorescence output.[145] Further, Q. L. Guan *et al.* designed a Bi-MOF incorporating a tetraphenylethylene-based ligand with strong aggregation-induced emission (AIE) characteristics for Fe^{3+} sensing. This system exhibited fluorescence quenching upon Fe^{3+} binding and a fluorescence "turn-on" response to cysteine, enabling dual-mode detection in environmental and biological samples.[133] These examples highlight the versatility of Bi-MOFs as photoluminescence sensors, leveraging metal–ligand interactions and optical tunability for effective and selective detection of ions, biomolecules, and reactive species.

3.5 Other potential applications

Bismuth-based MOMs have, to date, been shown to have potential in multivarious applications. For decades, Bi^{3+}-based compounds, owing to their biocompatibility and low accumulation in cells, have been exploited as drugs and as nanocarriers for biomedical imaging and drug delivery.[13–17,146–148]

This is attributable to the simultaneous intrinsic insolubility in neutral aqueous media and efficient inhibition of pathogenic bacteria. A typical example, Bi-NU-901, has been proven to be an efficient computed tomography (CT) contrasting agent for CT imaging, which allows visualization of human internal organs and more. Heavy atoms are desired for the attenuation of X-rays because they improve the contrast. This is conventionally done using elements such as iodine and barium. Bi-NU-901 was proven to have a higher attenuation factor compared to the commercially available iodixanol.[101] Similarly, CAU-7 has a demonstrated propensity as an ideal platform for drug delivery with higher therapeutic efficiency compared to the free drug approach.[17] This MOF has been used to deliver two cancer drugs, sodium dichloroacetate and α-cyano-4-hydroxycinnamic acid, with loading capacities of 33 and 9 wt%, respectively, achieving a slow rate of drug release of up to 17 days and 33 days for sodium dichloroacetate and α-cyano-4-hydroxycinnamic acid, respectively.

Bi^{3+}-based MOCPs have also shown outstanding performance in photocatalysis, where solar energy is converted into renewable energy. Bi-BTC, ([Bi(BTC)(DMF)]·DMF), a 3D MOF with a very interesting 1D helical chains along the *b*-axis,[149] shows a remarkable photocatalytic activity towards O_2 evolution (up to 880 μL h^{-1}) under UV-Vis radiation. However, the structure collapsed due to photo-corrosion after photocatalysis. To overcome the issue of photo-corrosion, ligands with high electron density and a rigid core must be used to improve stability and hole-transport ability. In this regard, IEF-5 ($[Bi_{12}(DTTDC)_{24}]\cdot 23DMA\cdot 4DMF\cdot 2H_2O$), with the DTTDC ligand, is proven to be more efficient for photo-electrocatalytic activity production of H_2 gas.[124] Another photocatalyst with a promising potential as a green photocatalyst is BiCo-MCP ($BiCo(2,4\text{-}pda)_3(H_2O)\cdot 1.5H_2O$). The 2D layered bimetallic shows an interesting photocatalytic degradation of imidacloprid and rhodamine B in wastewater of up to 81% and >94%, respectively, within 120 minutes under acidic conditions.

Another efficient way of photodegradation is the use of Bi^{3+}-based MOCP derivatives, owing to their high stability, exceptional electron–hole separation and ample active sites. Nanoscale $Bi_2O_2CO_3$ nanoparticles, derived from Bi^{3+}-based MOCP, CAU-17/melamine for the construction of $Bi_2O_2CO_3$/porous g-C_3N_4 *Z*-scheme heterojunction display a superior performance over $Bi_2O_2CO_3$ made by the conventional method.[150] In another example, a bromination-annealing process of Bi-BTC MOCP creates a hierarchical $BiOBr/Bi_{24}O_{31}Br_{10}$ heterojunction with rhodamine B removal of 92.4% at 60 minutes illumination, displaying good activity, pH adaptability, and reusability.[151]

In the photocatalytic field, two bismuth-based MOCPs, Bi–BTC and Bi–TATB, were explored to study the effects of metal dots on their excitonic behavior.[152] Although both the BTC and TATB ligands show strong fluorescence emissions, the corresponding Bi–BTC and Bi–TATB MOFs display a strong phosphorescence emission, which can be ascribed to a more efficient singlet-to-triplet intersystem crossing in Bi–BTC and Bi–TATB MOFs. As a result, highly selective photo-oxidation of benzyl alcohol to benzaldehyde using Bi–BTC and Bi–TATB MOFs under UV-Vis irradiation was reported. The intersystem crossing induces the $^3O_2 \rightarrow {}^1O_2$ conversion and subsequently the singlet $^1O_2$ oxidizes benzyl alcohol to benzaldehyde with high selectivity.[152]

Derivatives of monometallic and heterometallic bismuth-based MOMs have potential catalytic applications in organic reactions. $Bi_3O_2Cu(OH)(pdc)_2$ was thermally stable under air and could be used as a precursor to form Bi_2CuO_4 with high selectivity and diastereoselectivity (>99%) for the synthesis of (*E*)-2-benzylidenecyclohexanone.[60]

Pristine Bi-based MOMs were also reported to be active catalysts. The Bi-based heterometallic paddle-wheel complexes were found to be comparable in terms of reactivity and selectivity for metal carbenoid catalysis reaction, although in the cyclopropanation reaction with styrene it was found that the Bi–Rh heterometallic carboxylate paddle-wheel, namely $BiRh(O_2CCF_3)_3(O_2CCH_3)$, was less reactive compared to the original homometallic dirhodium-carboxylate paddle-wheel counterpart.[153] A robust Bi–Pd carboxylate paddle-wheel was synthesized and used as a precursor for a carbon-supported bimetallic catalyst in the conversion of glucose into gluconic acid with high catalytic activity.[19] The first truly porous Bi-based MOF, synthesized solvothermally using $Bi(NO_3)_3\cdot 5H_2O$ and BTB (BTB = 1,3,5-benzenetrisbenzoate) ligand in methanol, was reported to have high catalytic activity for solvent-free hydroxymethylation of hemicellulose-derived 2-methylfuran to give 5-methylfurfuryl alcohol.[61]

Single-atom and dual-atom site catalysts (SAC and DAC) are state-of-the-art compounds that can drastically enhance catalytic regio- and site-selectivity and activity. There is only one paper that reported Bi SAC made from calcined Bi-MOF; the others were made using Bi salt. Zhang *et al.* reported a Bi SAC that could promote global carbon balance and mitigate climate change. The resulting $Bi\text{–}N_4$ electrocatalyst showed an

exceptionally high activity and selectivity for the electrocatalytic reduction reaction of CO_2 with high faradaic efficiency up to 97% and high turnover frequency of 5535 h^{-1} at a low overpotential of 0.39 V *versus* the hydrogen electrode.[131]

The Mo–O–Bi compound, $[Cp^*(O)_2–Mo–O–Bi(o\text{-tolyl})_2]_n$, was decomposed in the presence of polyol hydrolyzing agent into biphasic bismuth molybdates, $Bi_2Mo_2O_9$ and Bi_2MoO_6, whose ratio can be determined by the choice of the hydrolyzing reagent.[154] Such a bismuth molybdate mixture was proven to be capable of sensing EtOH selectively at elevated temperatures.[155]

Supercapacitors and batteries as energy storage technologies are another potential application for Bi MOM derivatives due to their intrinsic high porosity, large surface area, and high energy density and specific capacitance. CAU-17 derived Bi_2O_3 microrods were explored as a negative electrode supercapacitor and demonstrated an interesting long-term retention of 93% after 4000 cycles with 1378 C g^{-1} at 0.5 A g^{-1}, outperforming all other Bi_2O_3-based materials.[129]

A novel way to engineer Bi–Sb alloy nanoparticles for sodium ion batteries was reported by the Deng group.[156] Using MOF-836 as a precursor, they prepared Bi–Sb alloy nanoparticles ($Bi_{1-x}Sb_x$) using nanoscale laser metallurgy with a uniform particle size, exhibiting a specific capacity of 259.8 mA h g^{-1} at 200 mA h g^{-1} after 500 cycles and a capacity retention of 180.9 mA h g^{-1} at 1 A g^{-1} over 1000 cycles.

Selenylation of Bi-MOF was also reported as another novel method to prepare bismuth selenide nanosheet/nitrogen-doped nanocarbon (Bi_2Se_3@NC) for lithium-ion battery anodes with enhanced cyclic performance.[157] Bi_2Se_3@NC prepared at a post-treatment temperature of 400 °C was found to have a large specific capacity of 410.6 mA h g^{-1} at 100 mA h g^{-1} after 50 cycles, and 500 and 335.8 mA h g^{-1} were also achieved after 400 cycles, an indication of the excellent lithium storage feature, which can be credited to the synergistic effects between Bi_2Se_3 nanosheet and N-doped nanocarbon. Similarly, using Bi-BTC MOF as a precursor, another composite material, Bi_2Te_3@C, featured uniform particle size and, interestingly, retained the morphology of Bi–BTC MOF. It displayed a reversible specific capacity of 236.4 mA h g^{-1} after 100 cycles at 100 mA h g^{-1}.[158] Another bismuth-based coordination compound was also used as a precursor to form Bi-based nanomaterials. Highly crystalline Bi_2O_3 nanoparticles were obtained from the decompositions of several single-source precursors, such as $((4\text{-Hmapy})[(\mu\text{-}2,3\text{-pydc})(2,3\text{-Hpydc})Bi(NO_3)]\cdot 2H_2O)_n$ (4-mapy = 2-amino-4-methylpyridine),[103] $[Bi_2(\mu\text{-}4,4'\text{-bipy})Cl_{10}]\cdot 2(4,4'\text{-Hbipy})\cdot(4,4'\text{-}H_2bipy)\cdot 2H_2O$,[59] and Bi(2,6-pydc)$(H_2O)$F.[66] Decompositions of $[Bi(2\text{-bpmp})Br_{2.06}Cl_{0.94}]$ and $[Bi(4\text{-}H_2bpmp)Br_{4.29}Cl_{0.71}]\cdot H_2O$ in air yielded agglomerated BiOBr nanoparticles with 35 to 70 nm in size. Calcination of the supramolecular nanoparticles of $[Bi_2(4,4'\text{-Hbipy})_{1.678}(4,4'\text{-Hbipy})_{0.332}(\mu\text{-I})_2I_{5.678}](4,4'\text{-bipy})$ under nitrogen resulted in BiI_3 nanowires, whereas Bi_2O_3 nanorods were obtained when they were decomposed under air.[159] These nanoparticles were thermally unstable compared to their single-crystal counterparts due to the large surface area of the former. Tiekink and co-workers reported the formation of crystalline Bi_2S_3 nanorods, nanotapes, and nanocrystals, depending on the nature of the Bi-thiolate ligand used (xanthate *vs.* dithiocarbamate), and the resulting structural motif (dimeric or polymeric), as well as the method conducted (solvothermal *vs.* CVD).[80]

Photoluminescence property, which may be attributed to intra-ligand $\pi \rightarrow \pi^*$ and/or $n \rightarrow \pi^*$ transitions, and ligand-to-metal-charge transfer (LMCT), was also observed in Bi-based coordination compounds.[18,23,45,63,76] The photoluminescence properties of luminescing pristine compounds can also be tuned by, in this case, doping of rare-earth elements into Bi sites.

A heterometallic Na–Bi with bdc ligands, which exhibited blue photoluminescence, was doped with trivalent Eu and Tb (2 mol% each) to establish red and green ligand-sensitized photoluminescence, respectively, indicating a successful energy transfer.[59] Another successful energy transfer by rare-earth doping was established by Cheetham *et al.* in the Bi-2,6-pydc system. Further, Cheng and co-workers reported a heterometallic Bi–Cd-2,6-pydc system in which the pristine compound, originally exhibiting blue photoluminescence, was tuned in terms of photoluminescence color by 5 mol% rare-earth doping. Dy-doped, Eu-doped, Tb-doped, and Sm-doped compounds led to white, red, green, and blue photoluminescence, respectively.[65]

An interesting single-component white-light-emitting phosphor, $Bi_3(\mu_3\text{-O})_2(2,5\text{-pydc})_2(2,5\text{-Hpydc})(H_2O)_2$, was reported by us, featuring a pristine bismuth coordination polymer exhibiting white composite photoluminescence without the addition of any dopant.[44] Although some other mononuclear, non-bismuth coordination compounds also exhibited white-light emission,[20,131,160–163] the exact reasoning for this is still elusive. Tuning the white-light emission from a single-source phosphor to obtain the desired chromaticity coordinate (CIE) remains a great pursuit.

Bismuth-based MOMs, which crystallized in non-centrosymmetric and, more importantly, polar space groups, gained increased attention due to their technologically important applications, such as SHG and ferroelectricity. We reported the first polar Bi-based coordination polymer that exhibited SHG properties.[46] Mercier and co-workers reported a genuine ferroelectric Bi-based coordination compound with the highest spontaneous polarization in a Bi-based coordination compound to date.[86]

The development of energetic materials was reported as another potential application of Bi-based coordination compounds. The impact and flame-stimulus studies of $[Bi(tza)]_n$ showed that it had potential for energetic materials and may be used as a catalyst for solid propellants.[76] A thermal study showed that Bi-containing bipy, $[4,4'\text{-Hbipy}]_n^{n+}[Bi(4,4'\text{-bipy})Br_4]_n^{n-}$, was an energetic compound as it was highly exothermic at ~350 °C, which was believed to be due to the presence of cationic bipy.[69]

Applications in gas adsorption and separation have also been reported as another potential use of bismuth-based coordination compounds. $[LiBi(2,6\text{-pydc})_3(H_2O)]\cdot 2(dma)$ was observed to have appreciable H_2 adsorption selectivity, whereas CO_2 sorption was observed in $Li_5Bi(2,6\text{-pydc})_4(H_2O)_2$, regardless of the lack of porosity of the two compounds.[164]

4. Conclusion and future outlook

Bi-based compounds' gain popularity in the realm of materials chemistry is two-fold: their biocompatibility and, more importantly, Bi^{3+} dual stereochemical activities that generate two structural libraries, one based on hemidirected polyhedra and a second based on holodirected ones. Several key conclusions and future works can be summarized as follows:

• To this end, an accurate and precise method to synthesize either polyhedral geometry is still elusive. However, recent developments suggest that the presence of an organic base modulator has the propensity to form asymmetric and irregular Bi^{3+} polyhedral (hemidirected), especially when combined with a hard donor ligand. Holodirected polyhedra possessing more symmetric building blocks typically yield less dense structures, adopting well-known topologies similar to those of reticular chemistry-guided transition-metal-based MOFs.

• In terms of isolating the Bi-based MOF structure, one may need to avoid using high pH in combination with a soft donor modulator. Nevertheless, Bi MOFs synthesized from both polyhedral geometries were reported.

• Therefore, a question arises: What governs the formation of permanent porosity in Bi MOMs? In transition-metal-based MOFs, as a comparison, symmetric SBUs are interconnected without or with minimum interpenetration among the nets, leading to the formation of extended pores, which is accomplished by using a supermolecular building layer (SBL)[165,166] or a supermolecular building block (SBB) approach.[166,167]

• In Bi MOMs, however, an example of structural complexity having a high connectivity node/cluster, hence robustness, while chiefly controlling porosity, is yet to be reported. Can one, then, adopt an SBL (or SBB) strategy to build a robust (high degree of connectivity) Bi MOF with tunable pore size? This is another question to be resolved in the near future to advance Bi MOFs to levels on a par with those of transition metal-based MOFs.

• In terms of synthetic procedures, solvo- and hydro-thermal routes are currently dominating, while simpler and greener approaches, like dissolution-crystallization and mechano(-chemical) synthesis, are starting to gain traction.

• A proper formula of modulating agent, solvent engineering, and reaction conditions becomes a fundamental recipe to isolate high-quality single crystal Bi MOMs.

• Macroscopic properties of Bi-based compounds are strongly dependent on the stereochemical activity of Bi^{3+}. A noncentrosymmetric structure, resulting from a stereochemically active lone pair of electrons, typically displays ferroelectricity, piezoelectricity, pyroelectricity, and non-linear optical activity. The stereochemically inactive ones often present tunable electrical conductivity.

• In terms of coordination number (CN), Bi^{3+} is susceptible to both low and high CN, as one of the attributes of being a borderline acid. Such privilege means that its Lewis acidity can be fine-tuned for various catalytic processes. Reports on precisely adjusting the Lewis acidity to address a specific catalytic process are still in the infant stage, especially for Bi MOM with extended structures.

• Single- and dual-atom site catalysts containing bismuth are expected to further improve the regio- and site-selectivity and activity for (electro)catalytic processes, *e.g.* CO_2 reduction.

• Bi-based MOMs and their (nano-sized) derivatives are also applicable for multiprobe sensing technologies, offering a versatile and sustainable platform. Overall, their high performance arises from the unique chemical and structural properties of bismuth as one of the lone pair-containing heavy metals with low toxicity.

• As research continues to advance in the design and functionalization of Bi-based MOMs using a combination of high throughput and machine learning, these materials are well-positioned to play a pivotal role in addressing urgent technological and environmental challenges. Such a combination of high-throughput (HT) synthesis coupled with machine learning (ML) offers a powerful and efficient technique to synthesize MOF specifically crafted for a certain application. Unlike trial-and-error experiments and computational insights that would take years to design and develop a product, "HT-ML duo" requires weeks to accomplish the same outcomes, including reduced manufacturing cost.[168] Prof. Norbert Stock's group reported a HT approach to Bi MOMs, investigating the crystallization and transformation of six new bismuth coordination polymers. The combination of HT and *in situ* PXRD measurements demonstrated how the solution to the complexity of the reactions and the role of the reaction time and temperature, as well as metal-to-linker molar ratio, could be fast-forwarded to achieve a shorter timeline.[169]

• Research on Bi MOMs is still developing compared with the more mature field of transition-metal MOMs (MOFs). Cost, stability, and scalability remain key barriers to their commercialisation, as summarized in Table 4.

Author contributions

A. C. W. proposed the topic of the review. All authors wrote and discussed the manuscript.

Conflicts of interest

There are no conflicts to declare.

Data availability

No primary research results, software or code have been included, and no new data were generated or analysed as part of this review.

Acknowledgements

The authors would like to acknowledge the Block Funding Program, Ministry of Higher Education, Oman, grant no. RC/RG/SCI/C/24/219, for the financial support.

Notes and references

1 J. J. Perry IV, J. A. Perman and M. J. Zaworotko, *Chem. Soc. Rev.*, 2009, **38**, 1400–1417.

2 O. M. Yaghi, D. A. Richardson, G. Li, C. E. Davis and T. L. Groy, *Mater. Res. Soc. Symp. Proc.*, 1995, **371**, 15–19.
3 M. Yaghi and H. Li, *J. Am. Chem. Soc.*, 1995, **117**, 10401–10402.
4 S. I. Noro Kitagawa, M. Kondo and K. Seki, *Angew. Chem. Int. Ed.*, 2000, **39**, 2081–2084.
5 S. Shimomura, S. Horike and S. Kitagawa, *Chemistry and Application of Porous Coordination Polymers*, Elsevier B.V., 2007, vol. 170.
6 M. O. Omar, M. Yaghi Nathan, W. Ockwig, H. K. Chae, M. Eddaoudi and J. Kim, *Nature*, 2003, **423**, 705–714.
7 M. Eddaoudi, D. B. Moler, H. Li, B. Chen, T. M. Reineke, M. O. Keeffe and O. M. Yaghi, *Acc. Chem. Res.*, 2001, **34**, 319–330.
8 A. F. WELLS, *Acta Crystallogr.*, 1954, **7**, 535.
9 A. F. Wells, *Three-dimensional Nets and Polyhedra*, 1978, J. Wiley, New York.
10 A. F. Wells, *Structural Inorganic Chemistry*, Oxford University Press, London, 1984.
11 A. Walsh and G. W. W. Ã, *J. Solid State Chem.*, 2005, **178**, 1422–1428.
12 A. K. Inge, M. Ko, J. Su, M. Feyand, H. Xu, X. Zou, M. O. Kee and N. Stock, *J. Am. Chem. Soc.*, 2016, **138**, 1970–1976.
13 Y. Yang, R. Ouyang, L. Xu, N. Guo, W. Li, K. Feng, Z. Yang, S. Zhou and Y. Miao, *J. Coord. Chem.*, 2015, **68**, 379–397.
14 K. Krüger, *Die romanischen Westbauten in Burgund und Cluny : Untersuchungen zur Funktion einer Bauform*, Gebr. Mann Verlag, 2003.
15 H. Suzuki N. Komatsu, T. Ogawa, T. Murafuji, T. Ikegami, and Y. Matano, *Organobismuth Chemistry*, Elsevier, 2001.
16 E. R. T. Tiekink, *Crit. Rev. Oncol. Hematol.*, 2002, **42**, 217–224.
17 C. Orellana-tavra, M. Ko, A. Li, N. Stock and D. Fairen-jimenez, *ACS Appl. Mater. Interfaces*, 2020, **12**, 5633–5641.
18 A. C. Wibowo, M. D. Smith and H. Loye, *Commun. Chem.*, 2011, **47**, 7371–7373.
19 B. Li, H. Zhang, L. Huynh, C. Diverchy, S. Hermans, M. Devillers, E. V. Dikarev, C. De Louvain, P. Louis and C. Hill, *Inorg. Chem.*, 2009, **48**, 6152–6158.
20 A. S. Filatov, M. Napier, V. D. Vreshch, N. J. Sumner, E. V Dikarev and M. A. Petrukhina, *Inorg. Chem.*, 2012, **51**, 566–571.
21 E. V Dikarev and B. Li, *Inorg. Chem.*, 2004, **43**, 3461–3466.
22 T. G. G. Evgeny, V. Dikarev and B. Li, *Angew. Chem. Int. Ed.*, 2005, **44**, 1721–1724.
23 A. C. Wibowo, M. D. Smith and H. Loye, *Cryst. Growth Des.*, 2011, **11**, 4449–4457.
24 A. M. Hamisu, A. Ariffin and A. C. Wibowo, *Inorg. Chim. Acta*, 2020, **511**, 119801.
25 S. Barbara, A. Introduction and C. Dawnofthenewera, *Coord. Chem. Rev.*, 1990, **100**, 403–425.
26 R. G. Pearson, *J. Chem. Educ.*, 1987, **64**, 561–567.
27 R. G. Pearson, *J. Am. Chem. Soc.*, 1963, **85**, 3533–3539.
28 R. G. Pearson, *Inorg. Chim. Acta*, 1995, **240**, 93–98.
29 Z. Wang, Z. Zeng, H. Wang, G. Zeng, P. Xu, R. Xiao, D. Huang, S. Chen, Y. He, C. Zhou, M. Cheng and H. Qin, *Coord. Chem. Rev.*, 2021, **439**, 213902.
30 A. K. Adcock, R. J. Batrice, J. A. Bertke and K. E. Knope, *Eur. J. Inorg. Chem.*, 2017, 1435–1445.
31 V. Stavila, R. L. Davidovich, A. Gulea and K. H. Whitmire, *Coord. Chem. Rev.*, 2006, **250**, 2782–2810.
32 M. Schlesinger, A. Pathak, S. Richter, D. Sattler, A. Seifert, T. Rüffer, P. C. Andrews, C. A. Schalley, H. Lang and M. Mehring, *Eur. J. Inorg. Chem.*, 2014, 4218–4227.
33 H. Wullens, B. Tinant and J. Declercq, *Inorg. Chim. Acta*, 2003, **343**, 335–342.
34 V. Stavila, J. C. Fettinger and K. H. Whitmire, *Organometallics*, 2007, **26**, 3321–3328.
35 P. C. Andrews, G. B. Deacon, C. M. Forsyth, P. C. Junk, I. Kumar and M. Maguire, *Angew. Chem.*, 2006, **118**, 5766–5770.
36 W. Levason and G. Reid, *J. Chem. Soc., Dalt. Trans.*, 2001, 2953–2960.
37 B. Barszcz, J. Masternak and M. Kowalik, *Coord. Chem. Rev.*, 2021, **443**, 213935.
38 K. Wang, Y. Ren, F. Yang and J. Wang, *Inorg. Chem. Commun.*, 2026, **183**, 115796.
39 Y. Wang, H. Sun, Z. Yang, Y. Zhu and Y. Xia, *Carbon Neutralization*, 2024, **3**, 737–767.
40 W. Wang, D. Zeng, J. Wang, Y. Zhang, L. Zhang, W. Wang, W. Wang, D. Zeng, J. Wang, Y. Zhang, L. Zhang and W. Wang, *Prog. Chem.*, 2022, **34**, 2405–2416.
41 Q. X. Wang and G. Li, *Inorg. Chem. Front.*, 2021, **8**, 572–589.
42 M. Y. K. Byrappa, *Handbook of Hydrothermal Technology*, William Andrew, 2012.
43 D. J. Chesnut, D. Hagrman, P. J. Zapf, R. P. Hammond, R. Laduca, R. C. Haushalter and J. Zubieta, *Coord. Chem. Rev.*, 1999, **192**, 737–769.
44 A. C. Wibowo, S. A. Vaughn, M. D. Smith and H. Loye, *Inorg. Chem.*, 2010, **49**, 11001–11008.
45 A. C. Wibowo, M. D. Smith and H. Loye, *CrystEngComm*, 2011, (13), 426–429.
46 A. C. Wibowo, M. D. Smith, J. Yeon, P. S. Halasyamani, H. Loye and H. C. Zur Loye, *J. Solid State Chem.*, 2012, **195**, 94–100.
47 J. Abdi, A. Jamal, M. Hadipoor and A. Khataee, *J. Hazard. Mater.*, 2022, **424**, 127558.
48 M. Kang, Y. Yao, B. Yuan, S. Zhang and O. Oderinde, *Food Chem.*, 2024, **437**, 137827.
49 B. Zhang, H. Xu, M. Wang, L. Su, S. Zhang, Y. Zhang and Q. Wang, *J. Environ. Chem. Eng.*, 2022, **10**, 108469.
50 Q. Y. Yang, C. Q. Wan, Y. X. Wang, X. F. Shen and Y. H. Pang, *J. Hazard. Mater.*, 2023, **451**, 131148.
51 Y. Li, Y. Han, H. Li, X. Niu, D. Zhang, H. Fan and K. Wang, *Int. J. Biol. Macromol.*, 2024, **265**, 130797.
52 H. Ai, L. Pham, V. Huu, T. Lee and V. C. Nguyen, *Chemosphere*, 2024, **357**, 142114.
53 Z. You, Y. Xiao, Q. Guan, Y. Xing, F. Bai and F. Xu, *Inorg. Chem.*, 2022, **61**, 13893–13914.
54 Q. Yang, X. Sun, Y. Sun, X. Shen and Y. Pang, *ACS Appl. Nano Mater.*, 2023, **6**, 7901–7909.
55 L. Wang, Q. He, F. Xiao, L. Yang, Y. Jiang, R. Su, P. He, H. Lei, B. Jia and B. Tang, *Electrochim. Acta*, 2024, **484**, 144082.

56 F. Liang, M. Lu, Y. Zhang, Q. Shi and F. Shi, *J. Mol. Struct.*, 2021, **1230**, 129636.
57 V. Huu, L. Van Tan, T. Lee and T. Duy, *Sustain. Chem. Pharm.*, 2021, **20**, 100385.
58 Y. Xiong, P. Zhang, W. Ren, S. Li and C. Jin, *J. Environ. Chem. Eng.*, 2024, **12**, 111906.
59 A. Thirumurugan, J. Tan and A. K. Cheetham, *Cryst. Growth Des.*, 2010, **10**, 1736–1741.
60 F. Shi, A. R. Silva and T. Yang, *CrystEngComm*, 2013, **15**, 3776–3779.
61 M. Feyand, E. Mugnaioli, F. Vermoortele, B. Bueken, J. M. Dieterich, T. Reimer, U. Kolb, D. De Vos and N. Stock, *Angew. Chem. Int. Ed.*, 2012, **51**, 1–5.
62 V. Chandrasekhar and R. K. Metre, *Dalton Trans.*, 2012, **41**, 11684.
63 X. Zhang, H. Tian, G. Yan, Y. Su, Y. Feng and J. Cheng, *Dalton Trans.*, 2013, **42**, 1088–1093.
64 H. Gao and X.-M. Zhang, *Dalton Trans.*, 2012, **2012**(41), 1562–1567.
65 X. Zhang, D. Wang, Y. Su, H. Tian, J. Lin, Y. Feng and J. Cheng, *Dalton Trans.*, 2013, **42**, 10384–10387.
66 H. Rim, D. Woo and K. Min, *J. Solid State Chem.*, 2012, **187**, 83–88.
67 X. Chen, Y. Cao, H. Zhang, Y. Chen, X. Chen and X. Chai, *J. Solid State Chem.*, 2008, **181**, 1133–1140.
68 G. Huang, Y. Sun, Z. Xu and A. D. Hunter, *Dalton Trans.*, 2009, 5083–5093.
69 A. Morsali, *Solid State Sci.*, 2006, **8**, 82–85.
70 S. Khanjani, N. Soltanzadeh, R. Sabahi and A. Morsali, *J. Coord. Chem.*, 2013, **66**, 3391–3401.
71 N. Soltanzadeh and A. Morsali, *Polyhedron*, 2009, **28**, 1343–1347.
72 N. Soltanzadeh and A. Morsali, *Polyhedron*, 2009, **28**, 703–710.
73 V. Huu, A. Le, H. Pham, V. Nguyen, T. Lee and T. Duy, *Chem. Eng. Res. Des.*, 2021, **177**, 321–330.
74 O. Anjaneyulu, T. K. Prasad and K. C. K. Swamy, *Dalton Trans.*, 2010, **39**, 1935–1940.
75 P. C. Andrews, G. B. Deacon, P. C. Junk and M. Silberstein, *Dalton Trans.*, 2006, 4852–4858.
76 S. Wang, L. Yang, T. Zhang, G. Zhang and J. Zhang, *J. Coord. Chem.*, 2011, **64**, 2583–2591.
77 L. Lei, Y. Liu, F. Tong, G. Zhai, H. Zhang, C. Zhang, Z. Wang, P. Wang, Z. Zheng, H. Cheng, Y. Dai and B. Huang, *Inorg. Chem.*, 2022, **61**, 11110–11117.
78 E. R. T. Tiekink, *Main Group Metal Chemistry*, 1994, vol. 17, pp. 727–736.
79 M. R. Snow and R. T. Edward, *Aust. J. Chem.*, 1987, **40**, 743–750.
80 Y. W. Koh, C. S. Lai, A. Y. Du and E. R. T. Tiekink, *Chem. Mater.*, 2003, **15**, 4544–4554.
81 B. F. Hoskins, E. R. T. Tiekink and G. Winter, *Inorg. Chim. Acta*, 1985, **99**, 177–182.
82 I. Chimica, *Inorg. Chim. Acta*, 1984, **84**, 13–14.
83 H. Yin, F. Li, F. Li and D. Wang, *J. Inorg. Organomet. Polym. Mater.*, 2007, **17**, 331–331.
84 H. W. Yim, K. Lam, A. L. R. U and D. R. U, *Polyhedron*, 2000, **19**, 849–853.
85 V. Stavila, Y. A. Simonov and J. Lipkowski, *Inorg. Chem. Commun.*, 2004, **7**, 634–637.
86 N. Leblanc, N. Mercier, L. Zorina, S. Simonov, P. Auban-senzier and C. Pasquier, *J. Am. Chem. Soc.*, 2011, **133**, 14924–14927.
87 N. Leblanc, N. Mercier, M. Allain, O. Toma, P. Auban-senzier and C. Pasquier, *J. Solid State Chem.*, 2012, **195**, 140–148.
88 X. Zhang, B. Wang, A. Alsalme, S. Xiang, Z. Zhang and B. Chen, *Coord. Chem. Rev.*, 2020, **423**, 213507.
89 Y. Bai, Y. Dou, L. Xie, W. Rutledge, J. Li and H. Zhou, *Chem. Soc. Rev.*, 2016, **45**, 2327–2367.
90 A. Thirumurugan and A. K. Cheetham, *Eur. J. Inorg. Chem.*, 2010, 3823–3828.
91 J. Lu, X. Zhao, B. Bai, F. Zheng and G. Guo, *J. Mater. Chem. C*, 2019, **7**(36), 11099–11103.
92 M. Savage, S. Yang, M. Suyetin, E. Bichoutskaia, W. Lewis, A. J. Blake, S. A. Barnett and M. Schrçder, *Chem. – Eur. J.*, 2014, **20**, 8024–8029.
93 S. R. Sushrutha and S. Natarajan, *Cryst. Growth Des.*, 2013, **13**, 1743–1751.
94 M. Hakimi, E. Motieiyan, F. Bertolotti, D. Marabello, V. Hugo and N. Rodrigues, *J. Mol. Struct.*, 2015, **1099**, 523–533.
95 H. Qi, H. Jo, X. Chen, J. Hong and K. M. Ok, *Inorg. Chem.*, 2020, 11554–11561.
96 Y. Huang, Y. Zheng, J. Wang and L. Zhou, *J. Solid State Chem.*, 2017, **246**, 42–47.
97 K. E. K. Alyssa, K. Adcock, J. D. Einkauf, J. A. Bertke, J. Faye Rubinson and D. T. de Lill, *Dalton Trans.*, 2018, **47**, 13419–13433.
98 M. Albat, A. K. Inge and N. Stock, *Z. Kristallogr. Cryst. Mater.*, 2017, **232**, 245–253.
99 C. dos, S. C. Timo Rhauderwiek Huayna Terraschke and N. Stock, *Eur. J. Inorg. Chem.*, 2018, **2018**, 3232–3240.
100 B. J. Deibert, E. Velasco, W. Liu, S. J. Teat, W. P. Lustig and J. Li, *Cryst. Growth Des.*, 2016, **16**, 4178–4182.
101 L. Robison, L. Zhang, R. J. Drout, P. Li, C. R. Haney, A. Brikha, H. Noh, B. L. Mehdi, N. D. Browning, V. P. Dravid, Q. Cui, T. Islamoglu and O. K. Farha, *ACS Appl. Bio Mater.*, 2019, **2**, 1197–1203.
102 O. Lars, A. K. Inge, C. J. Mckenzie and J. Ma, *J. Am. Chem. Soc.*, 2020, **142**, 9471–9481.
103 M. Tabatabaee, S. Amjad, S. Tabatabaei, M. Tabatabaee, S. Amjad and S. Tabatabaei, *Synth. Inorg. Met.-Org. Chem.*, 2014, **44**, 507–513.
104 E. S. Grape, H. Xu, O. Cheung, M. Calmels, J. Zhao, C. Dejoie, D. M. Proserpio, X. Zou and A. K. Inge, *Cryst. Growth Des.*, 2020, **20**, 320–329.
105 N. Z. Ying Sun Qing Lin Guan, C. H. Liu, B. Li, K. Y. Zhang, G. Hua Li, Y. H. Xing, F. Ying Bai and Li X. Sun, *Cryst. Growth Des.*, 2019, **19**, 7217–7229.
106 O. M. Y. Hong-Cai Zhou and J. R. Long, *Chem. Rev.*, 2012, **112**, 673–674.

107 L. Tröbs, M. Wilke, W. Szczerba, U. Reinholz and F. Emmerling, *CrystEngComm*, 2014, **16**, 5560–5565.
108 K. M. Ok, *Acc. Chem. Res.*, 2016, **49**, 2774–2785.
109 R. A. Wheeler, M. Whangbo, T. Hughbanks, R. Hoffmann, J. K. Burdett and T. A. Albrightll, *J. Am. Chem. Soc.*, 1986, **108**, 2222–2236.
110 K. M. Ok, E. O. Chi and P. S. Halasyamani, *Chem. Soc. Rev.*, 2006, **35**, 710–717.
111 B. W. Bi, N. Louvain, N. Mercier, J. Luc, I. Rau and F. Kajzar, *Adv. Mater.*, 2008, **20**, 1013–1017.
112 A. M. GLAZER, *Acta Crystallogr., Sect. A*, 1975, **31**, 756–762.
113 Y. Takahashi, R. Obara, K. Nakagawa, M. Nakano, J. Tokita and T. Inabe, *Chem. Mater.*, 2007, **19**, 6312–6316.
114 D. Barrit, P. Cheng, K. Darabi, M. Tang, D. Smilgies, S. F. Liu, T. D. Anthopoulos, K. Zhao and A. Amassian, *Adv. Funct. Mater.*, 2020, **30**, 1907442.
115 S. Sourisseau, N. Louvain, W. Bi, N. Mercier, D. Rondeau, F. Boucher, J. Buzare, C. Legein, L. De Chimie, B. La V, I. Mate, J. Rouxel, A. V Oli, V. Messiaen, L. M. Cedex and R. V October, *Chem. Mater.*, 2007, **19**, 600–607.
116 B. A. Connor, R. Biega, L. Leppert and H. I. Karunadasa, *Chem. Sci.*, 2020, **11**, 7708–7715.
117 I. H. Ronald, and J. Gillespie, *The VSEPR Model of Molecular Geometry*, Courier Corporation, 2013.
118 R. J. Gillespie, *Chem. Soc. Rev.*, 1992, **21**(1), 59–69.
119 M. Atanasov and D. Reinen, *J. Am. Chem. Soc.*, 2002, **124**, 6693–6705.
120 G. A. Fisher and N. C. Norman, *Adv. Inorg. Chem.*, 1994, **41**, 233–271.
121 C. Lode, *Z. Anorg. Allg. Chem.*, 2001, **627**, 841–846.
122 N. S. M. Köppen, S. Wuttke and U. Lüningb, *Dalton Trans.*, 2017, **46**, 8658–8663.
123 M. Köppen, V. Meyer, J. Ångström, A. K. Inge, N. Stock, M. Köppen, V. Meyer, J. Ångström, A. K. Inge and N. Stock, *Cryst. Growth Des.*, 2018, **18**, 4060–4067.
124 M. Gomez-mendoza, M. Barawi, I. J. Villar-garcia, A. De Pen, O. Shea, M. Liras and F. Ga, *J. Am. Chem. Soc.*, 2020, **142**, 318–326.
125 M. A. A. Al-nubi, A. M. Hamisu, A. Ariffin, J. Zhang, K. H. Shimizu, H. Jo, K. M. Ok, A. C. Wibowo, A. M. Hamisu, A. Ariffin and J. Zhang, *J. Coord. Chem.*, 2021, **74**, 1810–1822.
126 A. F. Payam, S. Khalil and S. Chakrabarti, *Small*, 2024, **20**, 2310348.
127 T. De Villenoisy, X. Zheng, V. Wong, S. S. Mofarah, H. Arandiyan, Y. Yamauchi, P. Koshy and C. C. Sorrell, *Adv. Mater.*, 2023, **35**, 2210166.
128 Z. Wang, Z. Zeng, H. Wang, G. Zeng, P. Xu, R. Xiao, D. Huang, S. Chen, Y. He, C. Zhou, M. Cheng and H. Qin, *Coord. Chem. Rev.*, 2021, **439**, 213902.
129 X. Yu, J. Sun, W. Zhao, S. Zhao, H. Chen, K. Tao, Y. Hu and L. Han, *RSC Adv.*, 2020, **10**, 14107–14112.
130 T. Hao, H. Xu, H. Yu, M. Li, B. Song, G. Shao, B. Fan, H. Wang, H. Lu and R. Zhang, *Sep. Purif. Technol.*, 2025, **360**, 131072.
131 E. Zhang, T. Wang, K. Yu, J. Liu, W. Chen, A. Li, H. Rong, D. Wang, J. Zhang and Y. Li, *J. Am. Chem. Soc.*, 2019, **141**, 16569–16573.
132 X. Shang, B. Yu, X.-T. Min, X. Su, B. Qiao and Y. Huang, *Angew. Chem. Int. Ed.*, 2026, e5513543.
133 Q. L. Guan, C. Han, F. Y. Bai, J. Liu, Y. H. Xing, Z. Shi and L. X. Sun, *Sens. Actuators, B*, 2020, **325**, 128767.
134 B. Li, X. Xie, T. Meng, X. Guo, Q. Li, Y. Yang, H. Jin, C. Jin, X. Meng and H. Pang, *Food Chem.*, 2024, **440**, 138213.
135 L. Xu, Y. Xu, X. Li, Z. Wang, T. Sun and X. Zhang, *Dalton Trans.*, 2018, **47**, 16696–16703.
136 R. Feng, X. Zhang, X. Xue, Y. Xu, H. Ding, T. Yan, L. Yan and Q. Wei, *ACS Appl. Bio Mater.*, 2021, **4**, 7186–7194.
137 C. Chang, Q. Xue, R. Wang, Z. Liu, Y. Liu, L. He, F. Liu and H. Xie, *Appl. Surf. Sci.*, 2023, **616**, 156510.
138 J. Fan, L. Jiang, H. Lv, F. Qin, Y. Fan, J. Wang, M. Ikram and K. Shi, *J. Mater. Chem. A*, 2023, **11**, 15370–15379.
139 M. Xu, P. L. Tremblay and T. Zhang, *ACS Appl. Nano Mater.*, 2023, **6**, 13466–13474.
140 I. M. El-Sewify, M. A. Shenashen, A. Shahat, H. Yamaguchi, M. M. Selim, M. M. H. Khalil and S. A. El-Safty, *J. Lumin.*, 2018, **198**, 438–448.
141 C. Jin, S. Yang, J. Zheng, F. Chai and M. Tian, *Biosens. Bioelectron.*, 2025, **269**, 116931.
142 S. Wang, P. Ju, W. Liu, J. Chi, T. Jiang, Z. Chi, S. Wang, R. Qiu and C. Sun, *Anal. Chim. Acta*, 2024, **1304**, 342558.
143 N. G. Balasubramaniyan and P. Perumal, *Anal. Methods*, 2024, **16**, 624–638.
144 L. Song, F. Tian and Z. Liu, *J. Solid State Chem.*, 2022, **312**, 123231.
145 L. Peng, H. Guo, N. Wu, M. Wang, Y. Hui, H. Ren, B. Ren and W. Yang, *Talanta*, 2024, **272**, 125753.
146 J. Della Rocca, D. Liu and W. Lin, *Acc. Chem. Res.*, 2011, **44**, 957–968.
147 Q. Qiu, H. Chen, Y. Wang and Y. Ying, *Coord. Chem. Rev.*, 2019, **387**, 60–78.
148 Y. Sun, L. Zheng, Y. Yang, X. Qian, T. Fu and X. Li, *Nano-Micro Lett.*, 2020, **12**, 1–29.
149 G. Wang, Y. Liu, B. Huang, X. Qin, X. Zhang and Y. Dai, *Dalton Trans.*, 2015, **44**, 16238–16241.
150 Z. Wang, H. Wang, Z. Zeng, G. Zeng, P. Xu, R. Xiao, D. Huang, X. Chen, L. He, C. Zhou, Y. Yang, Z. Wang, W. Wang and W. Xiong, *Appl. Catal., B*, 2020, **267**, 118700.
151 Z. L. Ganghong Huang Kun Liu, X. Tang, J. Huanga and G. Zhang, *Catal. Sci. Technol.*, 2020, **10**, 4645–4654.
152 R. Zhang, Y. Liu, Z. Wang, P. Wang, Z. Zheng and X. Qin, *Appl. Catal., B*, 2019, **254**, 463–470.
153 J. Hansen, B. Li, E. Dikarev, J. Autschbach and H. M. L. Davies, *J. Org. Chem.*, 2009, **74**, 6564–6571.
154 S. Roggan, C. Limberg and B. Ziemer, *Angew. Chem. Int. Ed.*, 2005, **44**, 5259–5262.
155 S. Roggan, C. Limberg, B. Ziemer, M. Siemons, U. Simon, V. Humboldt-uni, R. Aachen and A. Chemie, *Inorg. Chem.*, 2006, **45**, 9020–9031.
156 W. Zhang, W. Yan, H. Jiang, C. Wang, Y. Zhou, F. Ke, H. Cong and H. Deng, *ACS Sustainable Chem. Eng.*, 2020, **8**, 335–342.

157 Z. Li, H. Pan, W. Wei, A. Dong, K. Zhang, H. Lv and X. He, *Ceram. Int.*, 2019, **45**, 11861–11867.
158 S. Wen, J. Zhao, Y. Zhu, J. Mao, H. Wang and J. Xu, *J. Alloys Compd.*, 2020, **837**, 155536.
159 X. W. Yan, E. Haji-Hasani and A. Morsali, *Ultrason. Sonochem.*, 2016, **31**, 129–134.
160 A. C. Wibowo, S. A. Vaughn, M. D. Smith and H.-C. Zur Loye, *Inorg. Chem.*, 2010, **49**, 11001–11008.
161 M. Wang, S. Guo, Y. Li, L. Cai, J. Zou, G. Xu and W. Zhou, *J. Am. Chem. Soc.*, 2009, **131**, 13572–13573.
162 J. He, M. Zeller, A. D. Hunter and Z. Xu, *J. Am. Chem. Soc.*, 2012, **134**, 1553–1559.
163 E. R. Dohner, E. T. Hoke and H. I. Karunadasa, *J. Am. Chem. Soc.*, 2014, **136**, 1718–1721.
164 A. Alzamly, S. H. Ahmed and M. Bakiro, *ACS Symp. Ser.*, 2021, **1393**, 53–82.
165 J. F. Eubank, H. Mouttaki, A. J. Cairns, Y. Belmabkhout, L. Wojtas, R. Luebke, M. Alkordi and M. Eddaoudi, *J. Am. Chem. Soc.*, 2011, **133**, 14204–14207.
166 V. Guillerm, H. Jiang, D. Alezi, N. Alsadun and M. Eddaoudi, *Adv. Mater.*, 2025, **37**, 2414153.
167 J. F. Eubank, F. Nouar, R. Luebke, A. J. Cairns, L. Wojtas, M. Alkordi, T. Bousquet, M. R. Hight, J. Eckert, J. P. Embs, P. A. Georgiev and M. Eddaoudi, *Angew. Chem. Int. Ed.*, 2012, **51**, 10099–10103.
168 A. Ramirez, E. Lam, D. P. Gutierrez, Y. Hou, H. Tribukait, L. M. Roch, C. Copéret and P. Laveille, *Chem Catal.*, 2024, **4**, 100888.
169 M. Albat and N. Stock, *Inorg. Chem.*, 2018, **57**, 10352–10363.